12-2001

An investigation of bicomponent polypropylene/poly(ethylene terephthalate) melt blown microfiber nonwovens

Rongguo Zhao
University of Tennessee

To the Graduate Council:

I am submitting herewith a dissertation written by Rongguo Zhao entitled "An investigation of bicomponent polypropylene/poly(ethylene terephthalate) melt blown microfiber nonwovens." I have examined the final electronic copy of this dissertation for form and content and recommend that it be accepted in partial fulfillment of the requirements for the degree of Doctor of Philosophy, with a major in Human Ecology.

Larry C. Wadsworth, Major Professor

We have read this dissertation and recommend its acceptance:

John Collier, Gajanan Bhat, Kermit Duckett, Christine Sun, Dong Zhang

Accepted for the Council:

Carolyn R. Hodges

Vice Provost and Dean of the Graduate School

(Original signatures are on file with official student records.)

To the Graduate Council:

I am submitting herewith a dissertation written by Rongguo Zhao entitled "An Investigation of Bicomponent Polypropylene/Poly(Ethylene Terephthalate) Melt Blown Microfiber Nonwovens". I have examined the final paper copy of this dissertation for form and content and recommend that it be accepted in partial fulfillment of the requirements for the degree of Doctor of Philosophy, with a major in Human Ecology.

Larry C. Wadsworth, Major Professor

We have read this dissertation and recommend its acceptance:

Accepted for the Council:

Vice Provost and Dean of

The Graduate School

AN INVESTIGATION OF BICOMPONENT POLYPROPYLENE/POLY(ETHYLENE TEREPHTHALATE) MELT BLOWN MICROFIBER NONWOVENS

A Dissertation

Presented for the Doctor of Philosophy Degree

The University of Tennessee, Knoxville

Rongguo Zhao

December 2001

DEDICATION

To

my parents

Mr. Rubin Zhao and Mrs. Xiuling Sun

my daughter Amanda,

my son Davey,

and

my wife Xinmin,

ACKNOWLEDGMENTS

My gratitude can never be expressed enough to the people I met here in the University of Tennessee, Knoxville, especially those in the textile program and in Textiles and Nonwovens Development Center (TANDEC).

I would like to express my deepest appreciation to my major professor Dr. Larry C. Wadsworth for his guidance and encouragement in the past three years. I feel indebted to Dr. John Collier, Dr. Gajanan Bhat, Dr. Kermit Duckett, Dr. Christine Sun and Dr. Dong Zhang for taking the time to serve on my committee and the helpful suggestions they made during this work.

I am very thankful to the following TANDEC faculty and engineers for their precious assistances and suggestions: Dr. Billie Collier, Dr. David Garner, Dr. Allen Stahl, Dr. Peter Tsai, Dr. Charlie Hassenboheler, Dr. Molly Dever, Mr. Van Brantley, Mrs. Lisa Salamie, Mr. Anthony Whaley, Mr. Gary Wynn, and Mr. Stanley Gredig. I would like to give special thanks to Mr. Douglas Fielden, Dr. David Joy, and Dr. John Dunlap for their assistances in experiments. The financial supports from Reifenhauser Co., Germany and the University of Tennessee are most greatly appreciated.

Finally, I would like to thank my wife and closest friend whole-heartedly for her unselfish support, sacrifices and understanding. Without her special encouragement, this work would have taken a substantially longer time for completion.

ABSTRACT

As mono-component melt blown (MB) nonwovens are finding more applications in filtration, absorbency, hygiene, and apparel, bicomponent (bico) MB nonwovens with side-by-side (S/S) cross-sectional fiber geometry are attracting significant attention from both industries and academic institutions. The S/S bico fiber provides the possibility to combine the advantages of the two polymers to produce unique fiber and web properties, such as greater fiber crimp, when the two polymers provide different shrinking behavior under heat.

This work studied polypropylene/poly(ethylene terephthalate) (PP/PET) bico MB microfiber nonwovens, including the effects of processing conditions on fiber and web properties, process/structure/property relationships, and spinline dynamics. It was conducted in the 24-inch Reicofil® MB pilot line with bicomponent MB capability.

The Response Surface Methodology was employed for experimental design and statistical analysis. It remarkably reduced number of runs for the most important information, investigated all selected factors as a whole, and predicted their effects on the properties of interest (responses).

Phase 1 concentrated on the preliminary determination of the processing conditions of 100% PP and 100% PET. The fiber diameter of $PP_{1200MFR}$ is significantly affected by throughput and airflow rate. Comparatively, the effects of melt temperature (Tm), air temperature (Ta), and DCD on the $PP_{1200MFR}$ fiber

diameter are less significant, although a temperature in the range of 230°C to 300°C was recommended. The fiber diameter of PET is significantly affected by melt temperature and airflow rate. The effect of throughput is much less important than that for $PP_{1200MFR}$. The effects of air temperature and DCD are minimal. PET and $PP_{1200MFR}$ behave differently. Melt blowing $PP_{1200MFR}$ and PET on the Reicofil® MB pilot line to produce bico microfiber nonwovens requires a careful consideration of the properties of the two polymers. Thermal analysis and rheological measurements suggest that PP_{35MFR} /PET is a better pair for bico melt blowing. The bico filaments possess a side-by-side cross-sectional geometry.

Phase 2 focused on the processing of PP/PET bico MB nonwovens and the process-structure-property relationships. After considering the processability, the thermal stability of the polymer pair, the temperature window is quite narrow. Both melt and air temperatures were set at 599°F (315°C). Throughput, airflow rate, DCD, and weight percentage of PP affected the final fiber diameter; airflow rate was the most significant parameter. The effect of throughput on the fiber diameter was much less important due to the PET component. The interaction between throughput and airflow rate was minimal. The effect of PP percentage on the fiber diameter of bico filament varied with the airflow rate. This effect was more important at a lower airflow rate, and was minimal as the air rate increased. The effect of DCD on the fiber diameter of the bico filaments depended on the ratio of the two polymers. The fiber diameter distribution at different locations in the spinline varied accordingly. It was very broad at a location near the die and

became narrower as the position moves further from the die. The ratio of average fiber diameter and the packing density highly correlated to the average circular-capillary-equivalent pore size. As this ratio increases, the average pore size decreases. This ratio also highly correlates to web performance properties, such as latex filtration efficiency, air permeability and water penetration resistance. It is a relative measure of the web structure and is very useful in MB web design for a particular final application.

Phase 3 focused on spinline dynamics to develop a fundamental understanding of the PP/PET bico MB process. It was found that both airflow rate and DCD have an effect on the air jet temperature decay profile. The MB filaments attenuated from several hundred micrometers to a few micrometers in the first two inches from the die. PP filaments continuously decrease in diameter at a much slower rate. PET filaments shows a slowly increased trend in fiber diameter after reaching the lowest point in the fiber diameter profiles. The diameters of bico MB filaments were between that of 100% PP and 100% PET filaments. The PET component in bico filament controls the final fiber diameter. The filaments increased their average velocities almost linearly before they reach a maximum point. Then, their velocities decreased accordingly. Under the same processing condition, 100% PP filaments have a much higher maximum velocity than 100% PET filaments. The maximum velocity of bico filaments lies between that of PP and PET single component filaments. The fiber velocity relative to the surrounding air stream varies with the component and the distance from the die. By taking the high-speed melt spinning model and giving special consideration of

the heat transfer coefficient, the filament temperature profile was estimated. It changes dramatically in the first two inches and then decays slowly. The temperature profiles for single component and bico filament are nearly identical in trend. At a certain location in the spin-line, temperature of PP filament was a few degrees centigrade higher than in PET filament. The temperature profiles of bico filaments were between that of PP and PET. The elongational viscosities of the filaments were estimated based on the calculated filament temperature profile. Under the processing conditions, the elongation viscosity of PET filament was 5 to 10 times higher than that of PP. The elongation viscosity of bico filament was also estimated by using the simple rule of mixtures. These results provide fundamental information to explain the observations of fiber attenuation and web structure development.

Based on the findings of this study and the literature review, several recommendations were also made for further investigation of bico MB microfiber nonwovens.

TABLE OF CONTENTS

LIST OF TABLES

LIST OF FIGURES

CHAPTER 1

INTRODUCTION

The Background

Melt blowing is one of the most popular processes to make ultra-fine fibers on the micrometer or sub-micrometer scale. It is a "one-step process in which high velocity fluid, normally air blows molten thermoplastic resin from an extruder die tip onto a conveyor, or take-up screen, or substrate to form a fine fibered, self-bonded web" [Staff report, 1989]. The concept of melt blowing thermoplastics was first introduced to the public in 1956 through a Naval Research Laboratory project initiated by Wente [1956]. Since then, the melt blowing process and a variety of melt blown products have been recognized, developed, and commercialized. Over 320 US patents have been granted to the technologies and products related to melt blowing in the past 50 years. Only 20 patents were granted from the 1950s to the 1970s; it increased to 64 patents in the 80s and jumped to 236 patents in the 90s. It is clear that the melt blown technology is finding its application in an increasing number of fields, such as filtration, absorbency, hygiene and apparel.

Although there are many different designs of melt blown (MB) lines, the following basic components are quite common to almost all MB processes [Khan, 1993]

1. A polymer feed system, generally a hopper fed screw extruder (two extruders for bicomponent MB system).

2. A metering pump system to vary the polymer throughput rate (and/or ratio).
3. A die assembly that consists of a polymer feed distribution system, such as a coat-hunger, to provide even polymer flow and residence time across the width of the MB die, a nose tip, and air manifolds.
4. An air assembly to provide air streams with different temperatures and velocity.
5. A collection device for collecting the attenuated filament streams thus forming a web with an almost random network of fibers, and
6. A winding system to wind the formed MB web into a cylindrical package for easier subsequent handling.

McCulloch (1999) gave a brief history of melt blown technology development. He noted that ExxonMobil, Accurate Products, Reifenhauser, Kimberly-Clark and J&M Laboratories are among the biggest players in melt blown technology.

Melt blown technology requires precisely engineered and user-friendly equipment for successful new product development. Many significant efforts have been made to fully understand the technology and to improve the equipment by researchers and engineers around the world. The die assembly itself has always been the key innovation spot in the history of melt blown technology developments. Among more than 210 US Patents related to melt blowing technology, approximately one third are about hardware equipment and

over 30 patents are on the MB die assembly [Zhao, 2001].

Theoretically, all thermoplastics may be processed by MB technology, although polypropylene (PP), polyethylene (PE), poly(ethylene terephthalate) (PET), poly [butylene terephthalate] (PBT), poly [cyclohexane-dimethylene terephthalate] (PCT), co-polyesters and polyamides are among the preferred polymers. Currently, PP shares about 90% of all the MB nonwovens market because of its low cost, ease of processing, good mechanical properties, negligible shrinkage and chemical inertness. However, bicomponent (bico) MB nonwovens with side-by-side (S/S) cross-sectional fiber geometry are attracting significant attention from both industries and academic institutions. The S/S bico fiber provides the possibility to combine the advantages of the two polymers to produce unique fiber and web properties, such as greater fiber crimp when the two polymers provide different shrinking behavior under heat.

Figure 1.1 shows the state-of the-art new 24-inch Reicofil® MB bico fiber pilot line which was commissioned at the Textiles and Nonwovens Development Center (TANDEC) of The University of Tennessee, in March 1999. Since then, several polymer pairs have been successfully processed to investigate bico MB webs. The preliminary trial runs of the PP/PET bico pair resulted in interesting MB web properties, such as thermal dimensional stability, finer fiber, and improved barrier properties; and has demonstrated the production of very uniform, high quality webs in both bico and mono-component (M/C) operating modes. In the M/C mode, 100% of either polymer was processed for comparison to the bico PP/PET webs.

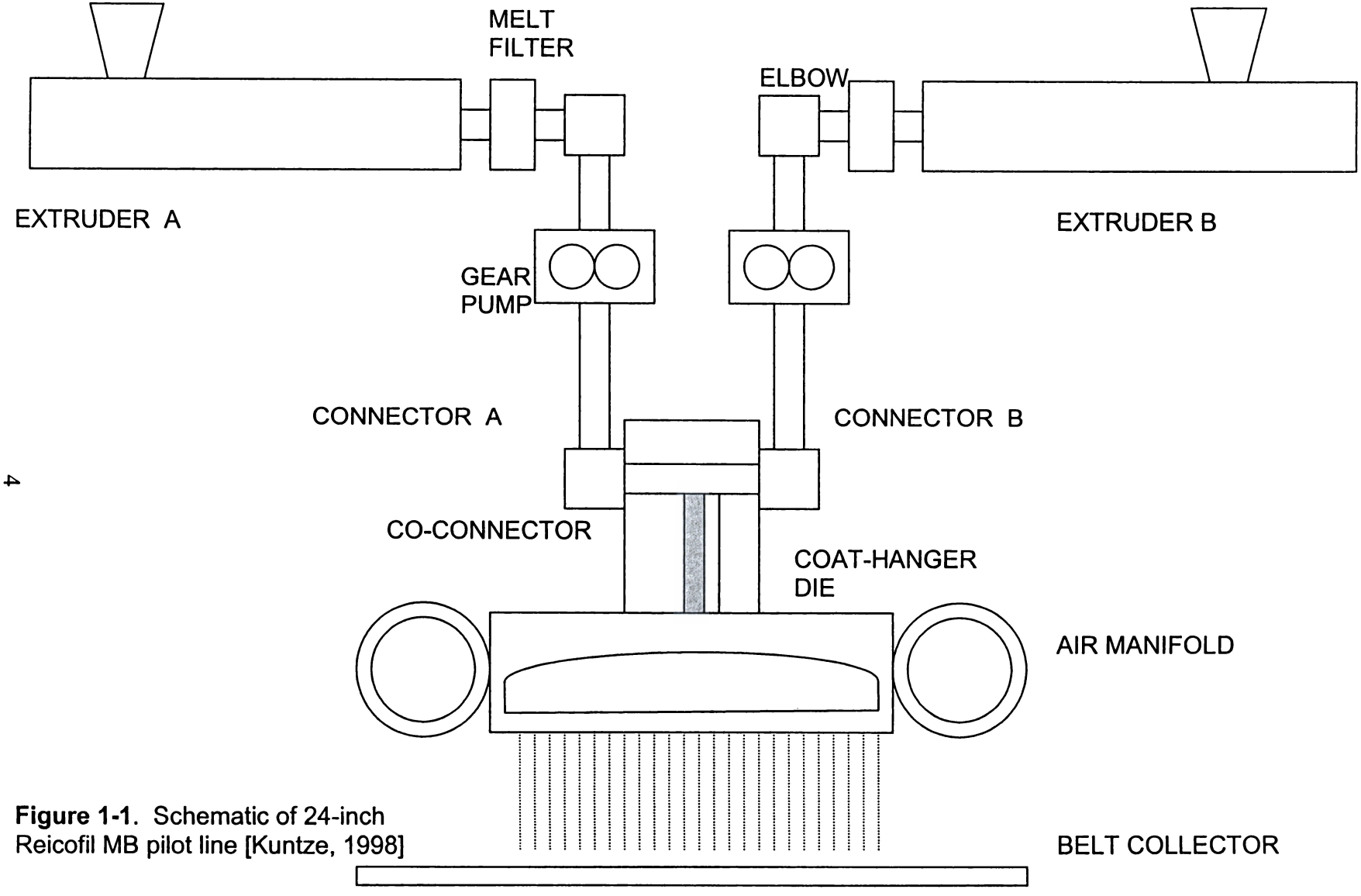

Figure 1-1. Schematic of 24-inch Reicofil MB pilot line [Kuntze, 1998]

The goals of this research

Since melt blowing technology involves many factors, such as melt/die temperatures, throughput, die geometry, air flow rate and its temperature, die-to-collector distance and collector speed, a statistical experimental design methodology is essential for success in determining the significant parameters with less expensive experimental operations.

Processing two polymers together to produce bico fiber melt blown fabric is even more complex because of the differences between the two components, e.g., rheological properties such as melt viscosity (elongational and shear viscosity), melt density and crystallization rates. Furthermore, notable differences may exist between the bicomponent fiber components in terms of thermal stability and response, fiber densities, and chemical and physical properties of the two components. In addition to controlling processing parameters for the most efficient melt blowing operation, it may also be possible to manipulate the process parameters to produce specific web products. For example the use of a polymer with a very low melt viscosity may allow sufficient flow around a high viscosity component to produce a core-sheath type of fiber cross-section with a side-by-side MB spinneret die geometry.

Response Surface Methodology (RSM) has proven a good choice for multi-factorial research. Based on the experimental design of RSM, the trends of parameters affecting fiber and web properties can be determined. Then follow-up MB trial studies of these key factors may be conducted so that processing

conditions may be optimized for the desired fiber and web properties with a high degree of confidence.

Nevertheless, production of the finest MB fibers was one of the main goals; therefore, fiber diameter was selected as a response in the RSM analysis, and the processing conditions will be optimized. However, the optimized conditions for fiber diameter may not always be the best for the web properties, even though they are significantly affected by fiber size. Therefore, additional MB process optimization was required for the desired web properties, depending on the end applications.

Furthermore, because of the significant difference in rheological properties, polymer distribution in the bico web should be carefully controlled. It was expected that the less viscous component has a tendency to move toward the edges of the bico web and that the extent of this behavior depends on the types of polymers in the bico pairs and on their weight ratios. Methods to control the polymer distribution were considered in the process optimization.

As in a more conventional M/C melt blown process, a wide variety of bicomponent (bico) MB fabrics can be produced by manipulating the processing conditions. With the growing interests and demands from the industry, bico MB fabrics show great potential as unique products. It is essential to investigate the processing/web-structure/property relationships to gain knowledge and a better understanding on the fundamentals of the bico MB process.

As a part of the joint "Bicomponent MB Nonwovens" project funded by the University of Tennessee, and Reifenhäuser GmbH & Co. Troisdorf, Germany, this dissertation focuses on the polymer pair of PP/PET to develop a fundamental understanding of process and web characteristics, which involves two polymers with very different properties.

The primary objectives of this dissertation are:

1. To investigate the effects of operating conditions on MB fiber and web properties.
2. To develop interrelationships between web properties and processing conditions.
3. To study the MB spinline dynamics to achieve a fundamental knowledge of the bicomponent MB process.

CHAPTER 2

LITERATURE REVIEW

Melt blowing (MB) is a one-step process for converting polymer resin into nonwoven web of fine fibers. The constant growth in terms of the number of patents issued for MB technology and its products reflects the strong growth of the technology in an increasing number of fields, such as filtration, absorbency, hygiene and apparel [Zhao, 2000]. McCulloch [1999] gave a brief history of MB technology development and Malkan [1990] presented a detailed discussion on the history of the MB process. However, the development of melt blown technology is seemingly moving towards a mature stage in its history since V. A Wente initiated it 50 years ago [Wente, 1956]

One of the most important components of MB hardware is the die assembly, which consists of a polymer feed distribution system, such as a coat-hanger, a nose tip, and air manifolds. Although several different die designs and geometries are documented in the literature, the single row hole type MB die is currently most commonly used in the industry. This design with an air slot on both sides of die tip has become primarily known as " Exxon MB Die Design". The innovation of the die head with multi-row orifices in air nuzzles [Schwarz, 1983] has been commercialized lately. It may become a strong competitor with the Exxon MB die. The holes in the MB die can be drilled either mechanically or electronically. It can be also made of steel capillaries.

This review will address the available literature of single row, drilled hole type die head MB in three aspects: (1) melt blown process, (2) process-structure-property relationships in melt blowing, and (3) bicomponent melt blown technology.

Melt Blown Process

It is widely accepted that melt blowing is a complicated process involving many factors that contribute to the final fiber and web properties. Polymer type, grade, melt temperature, polymer mass flow rate, air temperature, airflow rate, and the die-to-collector distance (DCD) are among the most important ones.

Malkan [1990] conducted a thorough study on the effects of molecular weight of PP on the melt blown web properties. He found that the overall average fiber diameter increased with the polymer throughput regardless the average molecular weight, if airflow rate was not proportionally increased. Straeffer and Goswami [1990], and Haynes [1991] reported the similar results. This is believed basically due to the facts of enlarged die swell and the increased polymer-to-air ratio. Under the conditions that maintained a constant air-to-polymer ratio, Khan [1993] found that the average fiber diameter decreased as the polymer throughput increased, under the condition of constant mass ratio of polymer and hot air. He reasoned that the overall air velocity and hence the momentum increased and the filament quenching was reduced due to the increased polymer throughput, thus, the hot filaments was attenuated further to produce finer fiber. Haynes's data [1991] showed a correlation between the average fiber diameter

and the momentum of the air jet, i.e. higher air jet exit momentum per unit die span will result in smaller fiber diameter. Wadsworth and Muschelewicz (1987) reported that for a polymer throughput of 0.2 g/hole/min, significantly smaller fiber diameter was observed at a high airflow rate than at a low airflow rate.

Khan [1993] conducted extensive investigations of the effects of die geometry and process variables, including polymer throughput, nose tip setback, die orifice diameter and the orifice L/D ratio, air velocity and momentum on fiber diameter and quality of melt blown PP webs. He concluded that the orifice diameter, orifice L/D ratio, PP resin MFR, air gap and polymer throughput all had a significant effect on the average fiber diameter. Within the measurement range (DCD from 8 to 25 inches), the DCD did not appear to affect the average fiber diameter. Bresee (1999) and Haynes [1991] showed that the filaments were attenuated most quickly at a distance of 2 or 3 inches from the die tip, after which the fiber diameters did not change significantly. Therefore, the data from different authors agreed generally.

The melt blowing process is complex and many efforts had been made to improve the understanding, especially in the development of final fiber diameter. Kayser and Shambaugh [1990] studied the MB process using a single hole, concentric design, in which the air is in parallel flow to the polymer stream. Although their data was not expected to exactly represent the effects attained with a multi-port die (such as the Exxon slot die), it provides valuable information in helping to better understand the Exxon MB process. Based on a PP with a

melt flow rate (MFR) of 54 at 400°C, they found that a smaller air nozzle diameter produces smaller fiber diameter, if a constant mass flow ratio of air and polymer are maintained. At a constant mass flux ratio of air and polymer, higher polymer throughput results in larger fibers. A best-fit power law equation was developed from 117 data points of 17 data sets, which involved over 4000 individual fiber diameter measurements.

$$d_f\left[\frac{d_{1,0}}{d_1}\right]^{1.25}\left[\frac{d_2}{d_{2,0}}\right]^{0.63}\left[\frac{M_{p,0}}{M_p}\right]^{0.47} = 38.1\Psi^{-0.563}$$

where, d_f: average fiber diameter, μm,

d_1, d_2: capillary and annulus inside diameter, mm,

$d_{1,0}$, $d_{2,0}$: capillary and annulus references, mm,

M_p: polymer mass flow rate, g/min,

$M_{p,0}$: reference polymer mass flow rate, g/min, and

Ψ: the mass flux ratio, $(M_a/A_a)/(M_p/A_p)$, A=area.

For a concentric die with each die orifice encircled by an air nozzle, this model equation is of use in exploring the behavior of MB processing, such as the effects of the operation parameters on the fiber diameter and to predict the suitable air mass flow rate for a specified fiber diameter.

Uyttendaele and Shambaugh [1990] have developed a model for steady polymer melt blowing with a single-hole, concentric die by following earlier studies of conventional melt spinning [Kase and Mastsuo, 1965, Ziabicki and Kawai, 1985]. The momentum and mass conservation equations were assumed

over the circular fiber cross-section. Continuity, momentum and energy equations were written for the fiber spinline only and the surrounding air temperature and velocity were taken as the boundary conditions. These equations are summarized as follows,

By assuming the constancy of polymer density, the spin-line continuity equation is

$$A_z V_{fz} = Q = \text{constant}$$

where, A_z: fiber cross-sectional area

V_{fz}: Axial fiber velocity

Q: volumetric polymer flow rate

The momentum equation:

$$\frac{d}{dz}\left[\pi \frac{d_z^{\,2}}{4}\left(\tau^{zz} - \tau^{xx}\right)\right] = j\pi \; d_z C_f \rho_a \frac{\upsilon_{rel}^{\,2}}{2} + \rho_f Q \frac{d\upsilon_{fz}}{dz} - \pi \frac{d_z^{\,2}}{4} \rho_f g$$

where, z: axial position

τ^{zz} , τ^{xx}: component of the extra stress in the spinning and transverse directions, respectively,

C_f: the air drag coefficient

ρ_a: air density

ν_{rel}: difference in velocity between the filament and forwarding air

ρ_f: polymer density

d_z: fiber diameter

g: gravitational acceleration, and

j = -1, when $v_{az} > v_{fz}$; j =1, when $v_{az} < v_{fz}$

The energy equation is

$$\rho_f C_{pf} \upsilon_{fz} \frac{dT_{fz}}{dz} = -\frac{4h_a}{d_z}\left(T_{fz} - T_{az}\right)$$

where, h_a : convective heat transfer coefficient,

T_{fz}: filament temperature,

T_{az}: Air temperature, and

C_{pf} : heat capacity of the fiber.

For a Newtonian fluid, the constitutive equations are (Middleman, 1977),

$$\tau^{zz} = 2\eta \frac{d\upsilon_{fz}}{dz}$$

$$\tau^{xx} = -\eta \frac{d\upsilon_{fz}}{dz}$$

where η: viscosity.

These equations are for Newtonian, nonisothermal melt blowing. Some other equations were also developed from the application of the Phan-Tien and Tanner rheological model to describe the mechanical and thermal history of a viscoelastic fluid in the melt blown process. All these equations were verified experimentally with a "high air velocity" case and a "low air velocity" case. It was found both temperature profiles and velocity profiles of the annular air jet had two regions: in a very short distance (around 1.5 cm) from the die tip, the air jet temperature and velocity decreases linearly with the distance from the die (DFD),

after which it follows the power law relationship. The measured experimental data were compared with the predictions from the above-mentioned models. This comparison showed that the model prediction fit the experimental data well within the region of high fiber attenuation. However, the prediction of final fiber diameters are 10% ~ 20% higher than the actual measurements. The predictions of fiber diameter profiles from the both Newtonian and Phan-Tien-Tanner models did not show significant difference. The temperature dependence of viscosity is more important than the selection of the constitutive equation.

Milligan and Haynes (1995) also conducted modeling research on melt blowing based on a single hole die with the air impinging upon the filament at an angle of 30° from two sides of the spinneret nozzle. The geometry of the nose piece and the air passage were identical to the 20 inch multi-hole die (Accurate Products Co. USA), which had been used extensively at the Textiles and Nonwovens Development Center (TANDEC) of the University of Tennessee, Knoxville. Several dimensionless parameters were defined to better describe the MB process, such as diameter ratio, δ, momentum flux ratio, Ψ, mass flux ratio, Γ, polymer throughput ratio, β, polymer temperature ratio, θ, air temperature ratio, ξ, and die face width ratio, ϕ. Two important modeling equations were developed from a data set of 270 processing conditions, which covers most normal processing conditions.

$$\frac{\delta - 0.047}{0.0149\beta^{-0.65}\phi^{-1.12}\theta^{-3.47}\xi^{-0.92}} = \Gamma^{-1.49}$$

$$\frac{\delta - 0.00646}{3.373\beta^{-0.74}\phi^{-1.14}\theta^{-3.78}\xi^{-0.62}} = \Psi^{-0.81}$$

By keeping the exponents of the dimensionless parameters, but changing the two constants in the equations, this model was used to analyze the data obtained on the 6 inch pilot MB line at TANDEC, which has "Exxon MB Configuration" die with a hole density of 20 holes/inch [Milligan and Haynes, 1995]. The agreement between the actual data and the model predictions has been a continuing goal of research. They recommended the following general equation to describe the common MB process.

$$\frac{\delta - C_1}{C_2\beta^{-0.65}\phi^{-1.12}\theta^{-3.47}\xi^{-0.92}} = \Gamma^{-1.49}$$

where C1and C2 are the constants that could be determined experimentally. This model is closer to the more standard industrial MB equipment. It would be very useful in MB process and product quality control and in the design of MB equipment. However, this model is applicable only for polypropylene with an MFR between 500 and 900 and for the operation that does not generate "shot" or "fly" [Milligan and Haynes, 1995].

Yin, Yan and Bresee [1999] studied the melt blowing process of PP (Exxon polypropylene, 1200 MFR) on the 20-inch wide horizontal MB pilot line at TANDEC by using high-speed digital imaging techniques. Fiber diameter, fiber

orientation in the web, and fiber velocity were measured. It was found the filaments were attenuated most quickly within the first two inches with a maximum fiber velocity around 2-3 inches from the die, after which the fiber velocity and fiber diameter decreased slowly with the increase of DCD. Within the experimental range of DCD's, the fiber velocity exhibited a broad distribution. Images reproduced from high-speed digital cines (frames) showed the filaments were mostly oriented and isolated from each other along the MD direction near the die tip. After 1.5 inches of DCD, fiber entanglement occurred and increased with DCD.

Process-Structure-Property Relationships in Melt Blowing

There is no doubt that the MB processing conditions control the final fiber and web structure; and consequently the web structure governs the performance properties. The relationships among the processing conditions, web structures and application properties have been being broadly investigated by numerous researchers. Therefore, a vast number of studies are available in the literature in the forms of original research papers, reviews, conference presentations and patent.

Choi, Spruiell and coworkers (1988) evaluated the physical properties of the MB webs and that of a single fiber in the web, which included tenacity and Young's modulus, elongation-to-break, flexural rigidity and birefringence. They found both tenacity and Young's modulus generally decreased with an increase

in die temperature, increasing air pressure at the die and greater DCD. Under the processing conditions of higher die temperature and higher air pressure at the die, finer fibers were produced. The fiber orientation in the web was found more random at an increased DCD, which is consistent with the observation that the mechanical properties in MD direction approach those in CD direction. The tenacity, elongation-to-break and Young's modulus of single MB fiber are generally much lower than corresponding properties developed in filaments from high-speed spinning of the same polymer resin. The birefringence values of the MB filaments are generally below those of conventionally melt spun fibers, indicating a low molecular orientation in the filament. This result is well expected due to the absence of a positive drawing device in melt blowing.

Malkan and Wadsworth (Spring, 1991) reported that polymer throughput rate had most significant effects on the physical properties of the final MB web and fibers. Generally, larger fibers were produced at a higher polymer throughput. This agreed with the data reported by other researchers [Haynes, 1991; Khan, 1993]. Consequently, MB webs produced with increased polymer throughputs exhibited higher initial modulus and higher breaking strength. Given the same basis weight of the web, larger average fiber diameters can be equivalently translated to less coverage of the web by the fibers or more open in structure, which results in higher air permeability of the web. The tensile testing results showed that single MB fiber from the web exhibited higher breaking strength and strain than that of the web. The tensile property of the web is a

function of single fiber properties and the web structure. The fiber angular distribution results in less efficiency in force translation, and entanglement and fiber-to-fiber bonding points contribute to the stress concentration during the deformation. By adjusting the operating conditions, melt blown webs may be produced with various structures, and thus, different performance properties. For example, under normal processing conditions, lower DCD, combined with the use of a vacuum suction system beneath the surface of the collector device, is expected to produce a stiffer, denser web with lower air permeability, higher hydrostatic head, and lower elongation. This type of web also tends to show a brittle failure mode during tensile testing.

The effects of processing conditions on the morphological properties of MB web were studied by Malkan and Wadsworth (1991). MB fibers are attenuated by the hot air jet and randomly laid onto the collector screen/belt to form web structures. Under certain processing conditions, defects of the fibers and web occur frequently, such as shot, rope and fly. Shot is a polymer globule in the web with a considerably larger size in diameter than the fiber. Its formation can be attributed to the melt fracture or instability, which depends on the properties of the resin, melt temperature, shear rate, die configuration, air temperature and flow rate, and cleanliness of the die. Fiber bundles or rope is a result of multiple fibers twisting together while traveling toward the collector. Fly is short broken fiber formed under extremely high air velocity conditions, coupled with excessive melt and air temperature and possibly polymer thermal

degradation. The filaments can be broken while being blown to the collector or be broken by the strong air turbulence near the collector surface and blown away from the collector under the conditions of high airflow rates and low DCD's. Roping is normally observed at fly-forming conditions. It is basically accepted that very low melt/air temperature and airflow rate and very high throughput most likely result in shot formation; and that very high melt/air temperature and airflow rate and very low polymer throughput most likely result in rope and fly formation. Therefore, the operating window for producing MB nonwovens with good quality is relatively narrow. Based on the experiments for 35, 300, 600 and 1000 MFR PP resins, Malkan and Wadsworth (Summer, 1991) proposed a chart of perceived MB process conditions.

Lee and Wadsworth (1990) reported that different combinations of processing temperature and airflow rate could produce very similar MB webs in term of fiber diameter and web structure. For example, the fiber diameter produced at an airflow rate of 7.4 standard cubic meter per minute (SCMM) and 246°C showed minimal difference with that produced at an airflow rate of 10.5 SCMM and 230°C.

The MB webs produced at various DCD's were characterized for air permeability and filtration efficiency by Lee and Wadsworth (1990). It was found that higher DCD resulted in a lower degree of fiber-to-fiber bonding and consequently resulted in nearly proportionally increased air permeability and decreased filtration efficiency. The pore size inside the MB web was inversely

proportional to the filtration efficiency. Any variables that lead to reduced pore diameter, such as higher packing density, higher fiber entanglement, and finer fiber, will result in improved filtration efficiency.

Bi-component fiber melt blown technology

Bicomponent melt blowing (BM) refers to the coextrusion process, in which two polymers are processed at the same time and extruded through the same die orifices to form composite fibers with different polymers in the cross-section. Although it is possible to produce various configurations as melt spinning does, side-by-side and concentric geometry are probably the most common two.

Bicomponent MB nonwovens have recently received much interest. Some of the obvious and potential benefits of bico MB nonwovens have been noted by the industry leaders and documented by researchers, which includes, but not limited to: (1) combining the advantages of the two polymers, such as PP/polyethylene (PE), PP/PET, PE/PET, polyamide (PA)/PET, and/or PA/PE, to produce specialty engineered products for heat resistance, chemical resistance, enhanced bonding properties and improved barrier properties; (2) splitting the bicomponent fibers by mechanical, chemical or electrical methods for ultra-fine fibers, which offers significantly high surface area for filtration, separation, absorption and other potential applications in physics, chemistry and life science; (3) producing crimped fibers of circular/non-circular cross-sections with bulkier web structure for softer hand and more comfort when used in apparels; and (4)

many potential applications in functional nonwovens, such as electrical conduction, ion exchange and selective filtration nonwovens, which are used in various hi-tech industries, health-care and environmental protection apparel. It is one of the most simple, economically effective ways to produce and handle ultra-fine fibers.

The market for goods and services to support processing, product R&D, machinery improvements is growing at a rate unprecedented in the history of fiber and polymer science and engineering. Businesses involve institutions and industries in different vectors globally, including machinery designers and suppliers, polymer suppliers, and fabric producers. As the worldwide market share competition is rapidly accelerating, bico MB nonwovens open more opportunities for a broad range of businesses, to name a few, chemical and polymer engineering, textile, filtration and agriculture.

Although the literature on bico MB is very limited, it is widely accepted that the bico MB process is much more complicated. In order to deal with this complexity, a SAS software package with experimental design capability, specifically, the surface response methodology (SRM) was employed by Sun and colleagues [1999, 2000] to systematically investigate the bico MB process. Trials on various polymer pairs, such as PP/PE, PP/PET and PP/PBT were found successful in producing good quality MB webs. Joseph [1997] investigated the extrusion of layered bico MB fiber and the properties of the nonwovens fabric. Berrigan [1999] studied the effect of polymer melt viscosity ratio on the cross-

sectional shapes of the corresponding polymers in the bico fibers. By using a software based on image analysis, he correlated the form factor of the two cross-sectional sides to the viscosity ratio of the employed resins, which illustrated the importance of properly matching the polymer viscosities. However, basic understanding of the bico MB process is far from clear.

Wadsworth and coworkers (1999) reported improved barrier properties from some bico MB fabrics and a potential for improving the productivity of SM and SMS nonwoven laminates with PP/PE bico MB webs.

There is little published data concerning the process/structure/property relationships and the spinline dynamics of bicomponent MB process.

CHAPTER 3

EXPERIMENTAL

Polymer Materials

1. PP_{3546G}, ExxonMobil Chemical Company, white granules, specially designed for melt blowing, nominal MFR = 1200g/10min at 230°C, Tm = 165°C, Tg = -17°C, ρ = 0.91g/cm^3. It will be referred to $PP_{1200MFR}$ hereafter.
2. PP_{3155}, ExxonMobil Chemical Company, white pellets with an average size of 3-5 mm in diameter, specially designed for spunbond, nominal MFR = 35 g/10min at 230°C, Tm = 165°C, Tg = -17°C, ρ = 0.91g/cm^3. It will be referred to PP_{35MFR} hereafter.
3. PET, Wellman Inc., Grade 61418, semi-dull fiber grade, IV=0.645±0.017, crystallized chip, T_m=245-250°C, 0.3% TiO_2, 2.10% (mole %) diethylene glycol; Resins are dried at 120°C for 4 hours in a Conair Dryer prior to extrusion.

Experimental Design and Processing

The melt blown process involves multiple factors contributing to the final product properties. These factors include the type and grade of polymer resins, melt temperature, polymer mass flow rate (throughput), air flow rate, air temperature, die geometry, die-to-collector-distance (DCD) and many others. Investigating the effects of each factor individually will require an extreme amount of time and funding. Surface Response Method (SRM) is one of the powerful

tools to design the experiments, which allows a remarkably reduced number of runs to provide the same amount of information. Importantly, it investigates all selected factors as a whole, and predicts their effects on the properties of interest (responses).

This research was conducted in three different phases utilizing the 24-inch Reicofil® MB pilot line. A schematic of the MB pilot line with bicomponent processing capability is shown in Figure 1-1. The BM die is a single row, hole type drilled into a nose tip with an included angle of 60°, a linear hole density of 25 holes/inch, and an average hole diameter of 0.38 millimeter. For this research, it was configured with an air gap of 0.8 mm and a setback of 1.0 mm. An air gap refers to the distance between the walls of the die tip and the inner walls of the air knives; the setback is the distance from outer edges of die nose tip to the outer edges of the air knives, as shown in the most common "Exxon Design" in Figure 3-1 [Harding, et al, 1974]. Phase 1 concentrated on the preliminary determination of the processing conditions to detect the general trends for 100% PP and 100% PET through the 24-inch Recofil® bico MB pilot line. Some preliminary bico trials were also performed to gain preliminary knowledge on the polymer processability and subsequent MB web quality. Polymer selections from different grades were determined for better processability. Phase 2 focused on the processing of PP/PET bico MB nonwovens. The process-structure-property relationships were studied carefully. Phase 3 focused on spinline dynamics to develop a fundamental understanding of the PP/PET bico MB process.

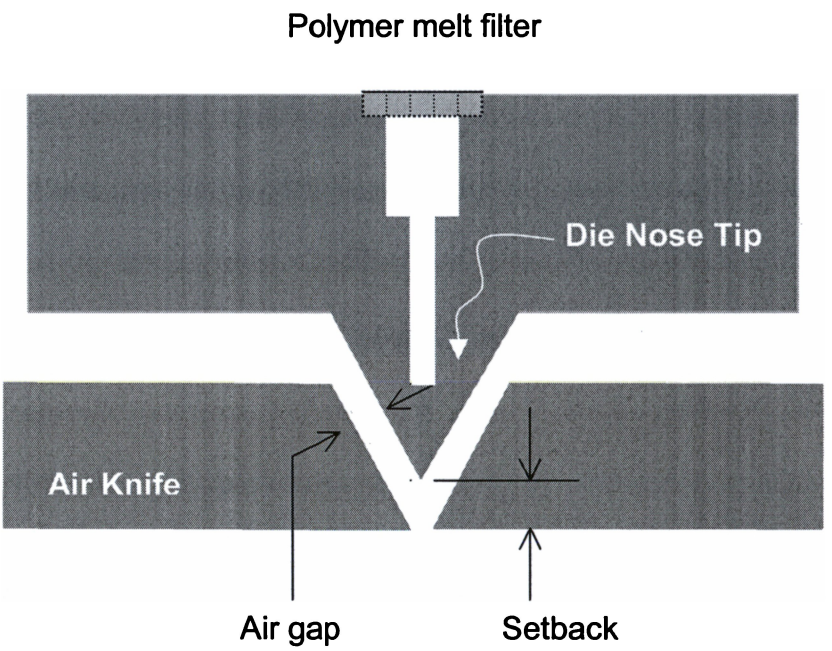

Figure 3-1. The concepts of air gap and setback in an "Exxon Design" MB die

Table 3-1. Factors and levels for experimental design of $PP_{1200MFR}$. (Codes of levels are in the parentheses)

Factor	Label	Low	Center	High
MT	Melt Temp., °C	246.0 (1)	260.0 (0)	274.0 (-1)
TP	Throughput, kg/hr	19.8 (1)	29.3 (0)	38.7 (-1)
AT	Air temp., °C	252.0 (1)	265.5 (0)	279.0 (-1)
AR	Airflow Rate, SCFM	425.0 (1)	550.0 (0)	675.0 (-1)
DCD	DCD, in	6.0 (1)	8.0 (0)	10.0 (-1)

Table 3-2. Factors and levels for experimental design of PET.
(Codes of levels are in the parentheses)

Factor	Label	Low	Center	High
MT	Melt Temp., °C	318.0 (1)	326.5 (0)	335.0 (-1)
TP	Throughput, kg/hr	19.8 (1)	29.3 (0)	38.7 (-1)
AT	Air Temp., °C	324.0 (1)	332.5 (0)	341.0 (-1)
AR	Airflow Rate, SCFM	325.0 (1)	450.0 (0)	575.0 (-1)
DCD	DCD, inch	6.0 (1)	8.0 (0)	10.0 (-1)

Table 3-3. The coded design points for a central composite response surface design (uniform precision)

Run ID	MT	TP	AT	AR	DCD
1	-1	-1	-1	-1	1
2	-1	-1	-1	1	-1
3	-1	-1	1	-1	-1
4	-1	-1	1	1	1
5	-1	1	-1	-1	-1
6	-1	1	-1	1	1
7	-1	1	1	-1	1
8	-1	1	1	1	-1
9	1	-1	-1	-1	-1
10	1	-1	-1	1	1
11	1	-1	1	-1	1
12	1	-1	1	1	-1
13	1	1	-1	-1	1
14	1	1	-1	1	-1
15	1	1	1	-1	-1
16	1	1	1	1	1
17	-2	0	0	0	0
18	2	0	0	0	0
19	0	-2	0	0	0
20	0	2	0	0	0
21	0	0	-2	0	0
22	0	0	2	0	0
23	0	0	0	-2	0
24	0	0	0	2	0
25	0	0	0	0	-2
26	0	0	0	0	2
27	0	0	0	0	0
28	0	0	0	0	0
29	0	0	0	0	0
30	0	0	0	0	0
31	0	0	0	0	0
32	0	0	0	0	0

Phase 1: Preliminary research on PP, PET, and PP/PET bicomponent MB.

Although both $PP_{1200MFR}$ and PET were successfully melt blown else where, it was believed necessary to conduct some trials on the two polymers separately for comparison. Response surface methodology (RSM) was employed to investigate the following five main processing parameters: melt temperature (MT), throughput (TP), air temperature (AT), airflow rate (AR), and die-to-collector distance (DCD). A central composite (uniform precision) design was selected from RSM with 16 factorial points and 6 center points, a total of 32 runs. Fiber diameter was taken as the response. Each factor is quantitative and continuous in exploring the surface of predicted fiber diameter over a range of factor levels, as shown in Table 3-1 (for $PP_{1200MFR}$) and Table 3-2 (for PET). The coded design points are listed in Table 3-3. Corresponding values of coded values may be found by the following equation,

$$\text{Original Value} = (\text{coded value}) \times S + M$$

where M is the average of the highest and lowest values for the factor in the design and S is half their difference. This design allowed the study of the relationship between the response and these factors in more detail.

To determine a polymer pair for bico melt blowing, thermal properties and rheological properties were characterized. The methods were described in Chapter 3, Experimental, Characterizations, of this dissertation.

Phase 2: Research on PP/PET bico MB

The results on $PP_{1200MFR}$ and PET M/C trials provided valuable information for bico MB trials. Based on these results, a similar experimental design was performed for bico MB runs of a selected polymer pair, which concentrated on pre-selected factors by fixing one or two less significant ones at a constant level. The response of the design can be any characteristic of the MB fiber or the web, such as fiber diameter, air permeability, and filtration efficiency. The response surface and the statistical analysis showed the effect level of any factor and the trends for future experimentation. Additional trials were performed to ensure the liability of the predicted results. In order to minimize the problem of die hole plugging, a polymer melt filter screen was employed before the MB die nose tip (Figure 3-1). Except those in phase 1, all trials in this study were run with this filter screen (Filtertechnic GMHB, Willy Spee, Germany). The filter consists of two layers of stainless steel mesh screen. The top layer has a mesh number of 160, which is supported by the second layer, whose mesh number is 80. The wire diameters for the two layers are 0.05 mm and 0.16 mm, respectively.

Phase 3: Study of spinline dynamics of PP/PET bicomponent MB

The spinline dynamics study was motivated by the need for a better understanding of the bico MB processing. It encompassed determinations of temperature and velocity profiles of both air jet and filament streams. Thus, the average elongation viscosity and the air drag force profiles were calculated. A set

of MB trials was conducted for the spinline dynamics study. The processing conditions are listed in Table 3-4 with air temperature and die temperature fixed at 599°F (315°C).

The fibers were collected along the MB spinline at different locations with a specially designed device, as shown in Figure 3-1-1. A mechanism was applied to this instrument to ensure the accurate and reproductive position and fiber sampling speed. A microscope glass slide was attached firmly to the far end of the device arm with a proper angle to the air jet blowing direction. Three fiber-collected slides were produced for each position and special care was taken to protect the samples properly for future off-line characterizations.

A bare thermocouple and a digital thermometer were employed to determine the centerline temperature profile of the air jet. A calibration of the instrument was performed before the on-line measurements. The polymer flow was turned off and the measurements were conducted only when no polymer came out of the die. In order to avoid polymer carbonization, the polymer flow was turned on for a proper period of time to purge out the degraded polymer melt. This procedure was repeated as needed. The experimental design and instrument setup are illustrated in Figure 3-2 and Figure 3-3, respectively. Three readings were recorded for each position along the spinline and the average was reported.

Table 3-4. Trials for MB spinline dynamics study

ID	TP Kg/hr	Air Rate SCFM	DCD in	PP %Wt	Td =Ta °F
Prof-1	15	350	19	100	599
Prof-2	15	450	19	100	599
Prof-3	7.5	450	19	100	599
Prof-4	15	450	19	50	599
Prof-5	15	450	19	25	599
Prof-6	15	450	19	75	599
Prof-7	15	450	15	0	599

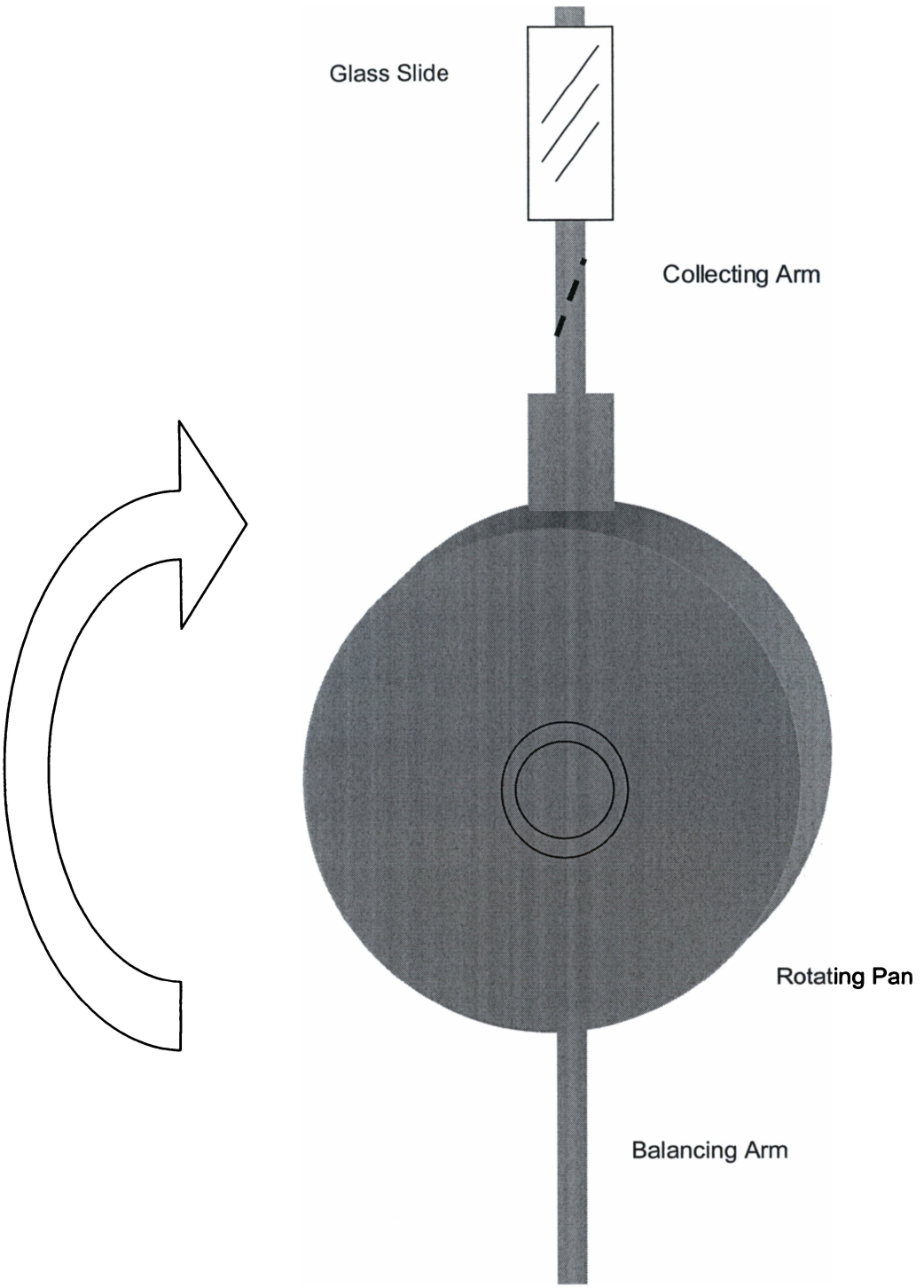

Figure 3-1-1. Top view schematic of the fiber-collecting device (Driving mechanism not shown)

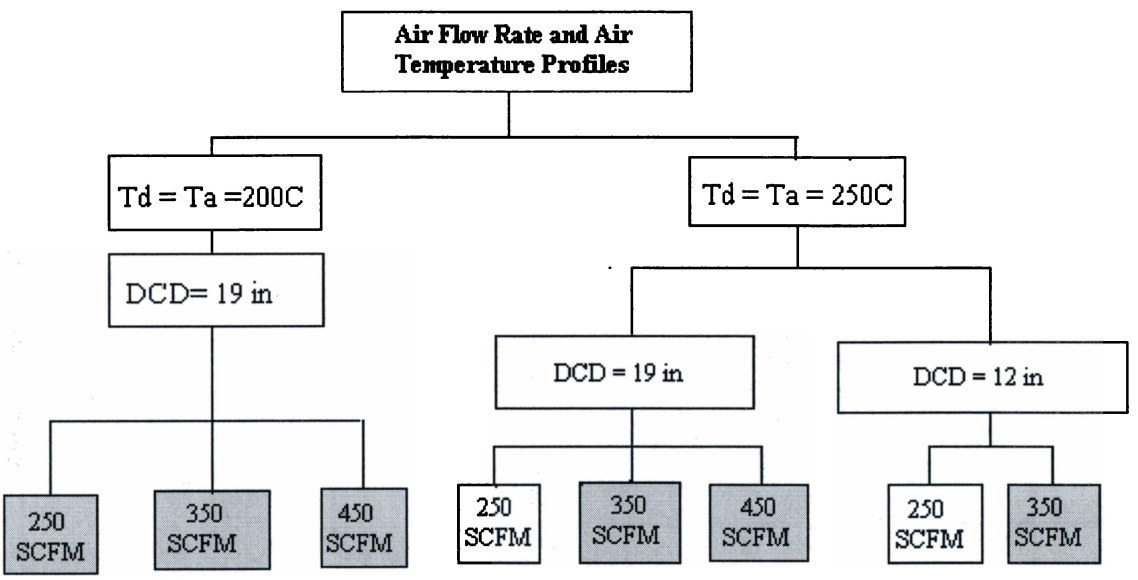

Figure 3-2. Experimental design for determination of air jet temperature profile

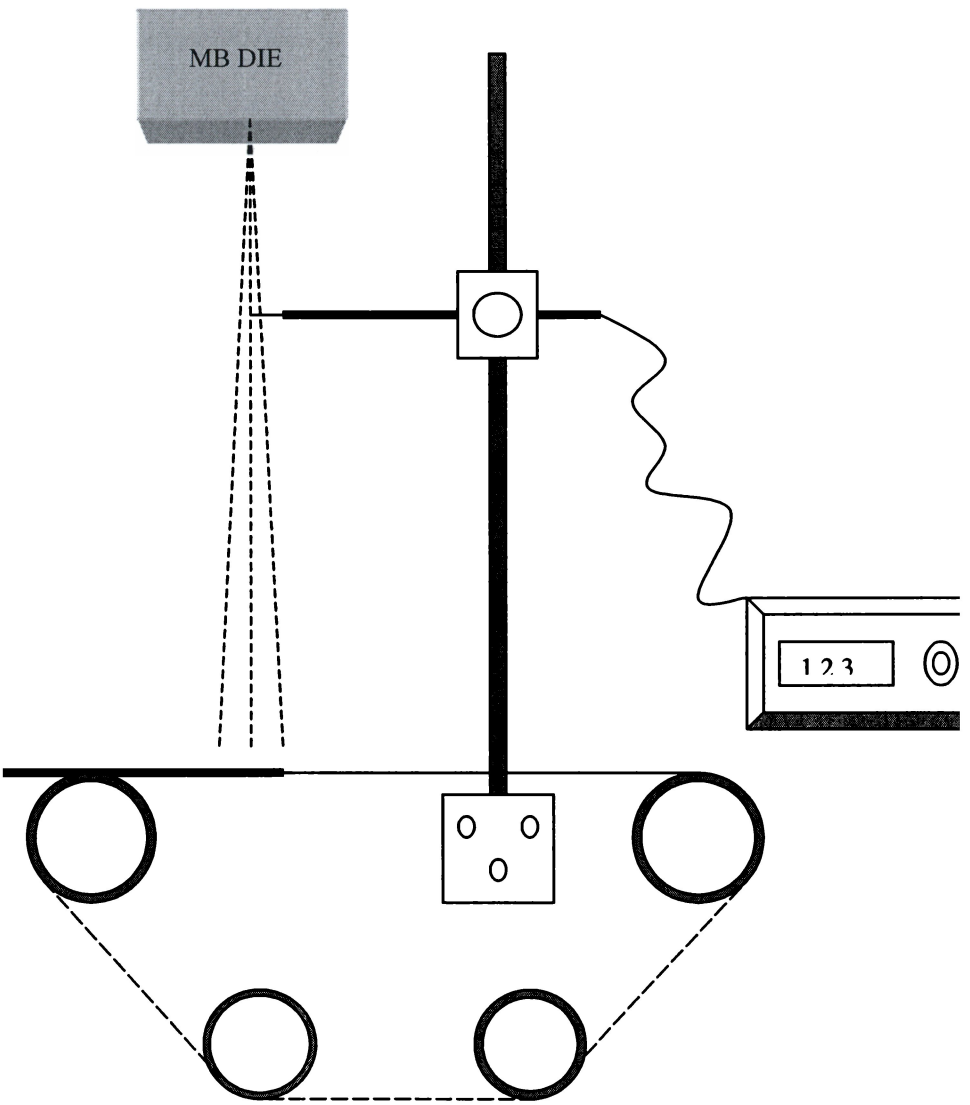

Figure 3-3. Instrument setup for measuring air jet temperature

Characterizations

Characterization of Polymer Resins

Shear Viscosity

The rheological properties of the above three polymers were measured at temperatures between 250°C and 320°C by using an Advanced Capillary Extrusion Rheometer (ACER). As the temperature reached the designated point, a proper amount of polymer granule or pellet was carefully filled into the ACER cylindrical barrow. A smaller ram may be used to compact the softened polymer and minimize air bubbles. Subsequently, after it reached the designated temperature, five to ten minutes were allowed for the melt to reach temperature equilibrium depending on the testing temperature and the nature of the polymer. During the measurement, data were recorded automatically by the computer after the melt pressure became constant at a particular shear rate. All measurements were conducted in the shear rate range of 30 S^{-1} to10,000 S^{-1}.

Thermogravety Analysis (TGA)

A Mettler thermogravity instrument TG25 and a TC11 controller were employed to investigate basic thermal stability of the polymers. The ceramic sample cell was first burnt clean using a butane torch, and then a sample of 5 to 10 milligrams was added into the cell and put into the thermal balance. The scan range was set from 35°C to 600°C with a temperature rate of 10 °C/min. In order

to study the degradation rate, the sample was held at a particular temperature for a specific period of time, such as 30 minutes.

Characterizations of Fiber and Web

Fiber Diameter and Fiber Diameter Distribution

Fiber diameters were determined by two ways: (1) from the microphotographs using a HITACHI S-3500 Scanning Electron Microscope (SEM) and (2) from the microphotographs using an Olympus optical microscope (OP).

For the SEM method, three randomly selected specimens were properly mounted on a circular sample holder for each sample without coating. The images were recorded as TIFF files into floppy disk at a 20 KV accelerating setting, a working distance from 10mm to 15mm and a magnification in the range of 100X to 600X. The image files were opened in the computer and fiber diameters were measured by using an image analyzing software (NIH 1.62, Scion Corporation). For the OP method, a video camera was attached to the trinocular microscope, and the image of the sample was shown on the monitor screen. The fiber diameters were then measured by using the same image analysis software used for SEM analysis. The monitor screen was carefully calibrated with a standard micrometer before measurements. The average of 75-180 fiber diameter measurements was reported for each MB web. The fiber diameter distribution profile was constructed by plotting the frequency of the fiber diameter against the corresponding categorical group of fiber size.

Fiber Cross-section

Fibers were embedded in Spurr's embedding medium [Spurr, 1969] for microtoning. Slides were made in a thickness of 1-2 micrometers. Fiber cross-sections were observed by using the above-mentioned SEM.

Polymer Distribution in the Cross Direction (CD) of Bico Webs

A Mettler thermal analysis system was utilized, which includes a TC11 controller, DSC25 and TMA40 module. A set of DSC scans was performed for single polymer samples and their mixtures of different weight ratios to construct a curve reflecting the relationship between heat of fusion (ΔH_f) and the weight percentage of polymer component. Each scan consisted of four (4) segments, i.e. heating from 70°C to 300°C with a rate of 10°C/min, staying at 300°C for 2 min, cooling from 300°C to 70°C at -15°C/min, and re-heating from 70°C to 300°C with the same rate of 10°C/min. The ΔH_f values of PP and PET in the reheating curves were plotted with polymer weight ratio to achieve a mathematical equation for future calculation.

Bico MB webs were trimmed one inch on each side, which left 20-22 inches in width. Samples were taken from right side to left side in CD direction at uniformly scattered positions, i.e. 2", 4", 6"·····20". These samples were analyzed by DSC with the same conditions as described above.

Basis Weight and Thickness

Ten specimens were cut randomly from a 3-meter-long sample web for both basis weight and thickness measurements. The average values were reported according to the INDA Standard Test Methods: IST 130.1 and IST 120.1 (ASTM 05729-97). An electronic balance (ER-120A, A&D Company, Limited) and a thickness tester (Model 49-70, Testing Machines, Inc.) were utilized.

Air Permeability (AP)

According to ASTM Standard D737-96, air permeability of the MB webs was determined by utilizing an air permeability tester (FX-3300, Textest Instruments) at a pressure drop of 0.5 inches of water. For each sample, five measurements were recorded across the web in CD direction within three meters of length in MD direction. The averages were reported.

Water Resistance (Hydrostatic Pressure Test) (HH)

HH of the MB webs was determined according to IST 80.6 by utilizing hydrostatic head tester (FX-3000, Textest Instruments) with a pressure gradient of 65 inches of water per minute. For each sample, five measurements were recorded across the web in CD direction within three meters of length in MD direction. A polypropylene net was placed down stream of the water to support the web. The averages of the corresponding measurements were reported.

Tensile Strength. Elongation and Tenacity

According to the ASTM Standard D1682, tensile strength and elongation were measured on a united tensile tester (SSTM-I-E-PC, United Calibration Corp.) with a loading cell of 10 lb capacity and a gauge length of 5 inches. Five strips of 8"x1" in MD were randomly taken across the web within 3 meters along the MD direction. The average was used to calculate the tenacity according to the following equation [Choi, et. al., 1988]

$$T = \sigma_b = \frac{F_b \cdot \rho_s}{h \cdot w}$$

T: tenacity, Pa

σ_b: tensile strength at break, Pa

F_b: load at break, (grams x 9.8 m/sec^2)

ρ_s: Polymer density from the density gradient column, Kg/m^3

h: width of the strip being tested, m,

w: Basis weight of web, g/m^2

Flexural Rigidity (FR)

According to ASTM Standard D 5732-95, the bending length was measured on a FRL cantilever bending tester (Testing Machines, Inc.), and the FR was calculated thereafter. Five strips of 6"x1" in MD were randomly taken in the same way as described in tensile testing section.

Filtration Efficiency (FE)

Filtration efficiency of the webs was determined using a latex filtration

efficiency tester developed by Wadsworth and Davis (1985). A solution of mono-dispersed polystyrene particles (Duke Scientific Corporation) with a diameter of 0.806 μm were prepared by adding 3 μl polystyrene micro-sphere latex (10% solids by weight) into 250 ml of distilled water. Dried and micro-filtered compressed air was supplied to a nebulizer at a flow rate of 3.5 L/min, and also to the dilution channel at 61.5 L/min. The airflow rate in the nebulizer generates water droplets of 2-3 μm according to the manufacturer (Wadsworth, 1985). A particle counter (Model 41000, Pacific Scientific) with a Model 1200 Sensor was used under the differential count mode. The No.1 channel threshold was set at 900A for the particle size of 0.806 μm. A 5 sec stabilization delay time and 55 sec of count time were used in the measurement. The pressure drop across the sample was measured by a barometer.

$$FE(\%) = \frac{\text{Count without sample - Count with sample}}{\text{Count without sample}} \times 100$$

Packing Density (c)

The packing density is the ratio of the volume of the fiber and the volume of the nonwoven web or other porous materials. The actual density of the polymer, of which the medium is made, is normally measured by using the density gradient column.

$$c = \frac{Volume\ of\ the\ fiber}{Volume\ of\ the\ medium} = \frac{Basis\ weihjt}{Thickness \times \rho}$$

CHAPTER 4

RESULTS AND DISCUSSION

Phase 1:

Preliminary Research on $PP_{1200MFR}$, PET, and bicomponent MB nonwovens

Preliminary Research on $PP_{1200MFR}$

Extensive research on PP MB has been done in the past decade in both academia and industry. It was generally suggested that the important operational parameters that control final product quality include, polymer grade, melt temperature (MT), polymer mass flow rate (throughput, TP), air temperature (AT), airflow rate (AR), die-to-collector distance (DCD), suction speed, collector surface speed, and ambient temperature. It was also found that increasing the throughput without increasing attenuation airflow rate generally resulted in increased average fiber diameter. However, many of the studies were conducted under a particular condition assuming free of interaction between the interested and the fixed factors. Considering various parameters as a whole is important in revealing their actual effects on final product properties.

In this study, the experimental design for 100% $PP_{1200MFR}$ MB process simultaneously investigated five factors: MT, TP, AT, AR, and DCD in the most frequently used ranges. The data of fiber diameter, HH, AP, tenacity, elongation, FR, and packing density (PD) of these $PP_{1200MFR}$ MB webs are presented in Table 4.1-1. After inputting the actual measurement results of average fiber

Table 4.1-1. General properties of $PP_{1200MFR}$ melt blown nonwoven webs

Run ID	Fiber Dia. μm	HH cm-H_2O	AP ft^3/ft^2 /min	Basis Weight g/m^2	P. Density	F. Rigidity mg-cm	Tenacity MPa	Ext. at Break (MD) %
1	2.00	61.60	63.93	35.48	0.0969	223.68	0.724	20.98
2	1.69	81.70	30.59	34.27	0.1018	707.42	1.439	11.74
3	2.15	81.50	38.54	34.63	0.1140	557.51	1.464	16.62
4	1.67	71.70	49.71	34.27	0.0816	227.66	0.659	15.17
5	1.78	59.70	39.02	34.88	0.1183	510.51	1.294	9.88
6	2.02	53.20	65.26	34.75	0.0955	276.29	0.919	22.06
7	2.52	51.60	73.71	34.88	0.1012	293.09	0.916	22.94
8	2.14	45.20	35.31	34.27	0.0987	476.33	1.419	9.65
9	1.92	90.70	37.38	33.79	0.1042	629.07	1.326	12.55
10	1.44	69.50	47.44	32.57	0.0831	214.76	0.757	17.27
11	1.82	85.80	42.97	31.24	0.0879	166.06	0.689	14.75
12	1.79	56.90	29.46	31.36	0.0940	435.88	1.218	9.40
13	2.51	65.50	57.17	34.03	0.0999	246.76	0.898	26.55
14	1.82	34.30	41.23	32.45	0.0888	274.54	1.102	5.58
15	2.12	58.00	34.41	34.23	0.1065	357.66	1.238	13.42
16	1.81	39.10	51.90	35.24	0.0945	126.64	0.709	12.52
17	2.01	63.00	54.92	35.12	0.1063	333.00	1.127	26.66
18	1.49	66.10	38.70	32.42	0.0957	235.08	0.985	15.77
19	1.71	99.90	34.59	33.79	0.0797	167.03	0.380	6.73
20	2.19	62.74	46.41	34.27	0.1022	446.62	1.135	21.19
21	1.90	62.51	75.07	36.45	0.1170	469.43	0.991	28.57
22	1.82	62.28	42.75	34.39	0.1032	309.22	1.141	19.39
23	2.45	62.06	23.07	31.73	0.0996	548.32	1.379	2.68
24	1.79	61.83	56.18	34.75	0.0895	214.16	0.650	22.02
25	2.25	61.60	43.19	33.66	0.0971	425.82	1.063	17.63
26	1.86	61.38	45.22	34.39	0.1017	404.59	1.080	18.40
27	1.98	61.15	50.36	33.30	0.0921	330.51	1.001	11.65
28	1.89	60.92	48.30	33.20	0.0918	323.16	0.994	12.30
29	1.86	60.70	48.00	33.20	0.0920	325.27	1.004	12.50
30	1.96	60.47	51.30	33.30	0.0918	334.81	0.991	11.65
31	1.93	60.24	59.80	33.30	0.0918	324.13	0.991	12.10
32	1.99	60.02	52.50	33.20	0.0909	335.97	1.015	11.89

diameter from over 3300 readings, the prediction profiles of fiber diameter (FD, μm) were generated by the SAS experimental design software and given in Figure 4.1-1.

The general trends and changing directions of fiber diameter with the processing conditions can be seen in Figure 4.1-1. It is not surprising that these trends agree with previously reported results. It should be kept in mind that these predictive profiles are probably of use only in the experiment range.

Figure 4.1-1 and the statistical analysis (Appendix B) show that the polymer throughput, melt temperature, DCD, and airflow rate are the significant factors affecting fiber diameter. The level of noise left unexplained by the experiment model is still high for accurately estimating the effect of air temperature. The interaction terms of DCD*TP, DCD*AR, DCD*AT and AT*MT were found to be significant at a 0.05 level, indicating the effect extent of each factor depends on the other factors involved.

Figure 4.1-2 shows the effects of MT and TP on the fiber diameter under the following conditions: AT = 270°C, AR = 557.5 SCFM, and DCD = 8.6 in. It is shown that both increased melt temperature and decreased throughput result in a decrease in fiber diameter. The almost flat response surface indicated the minimal interaction of MT and TP. Figure 4.1-3 is similar with Figure 4.1-2, except AT = 300°C. The comparison of Figures 4.1-2 and 4.1-3 leads to the conclusion that fiber diameter is more sensitive to MT and TP at higher air temperatures.

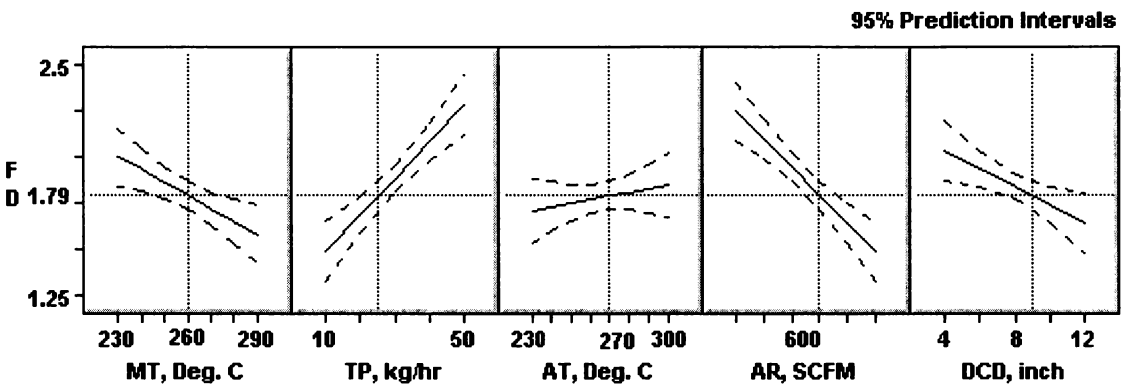

Figure 4.1-1. Prediction profile of PP MB fiber diameter (FD) with operational conditions

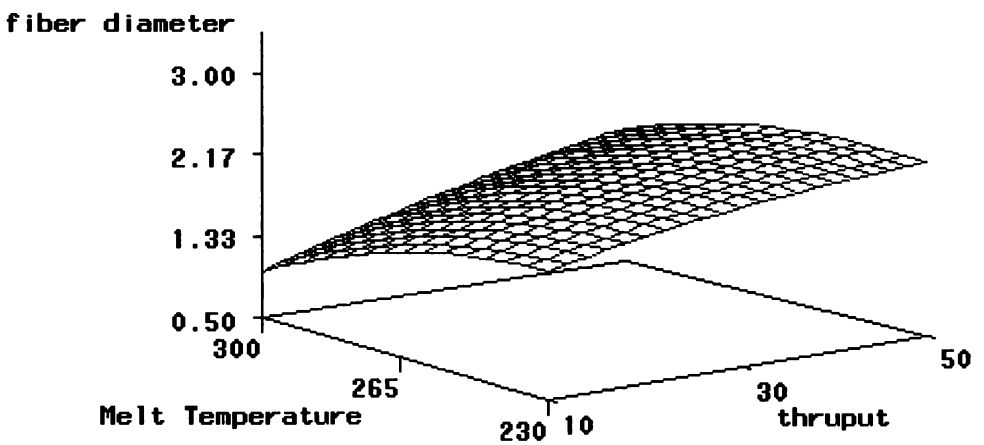

Figure 4.1-2. The effects of melt temperature (MT) and throughput (TP) on the diameter of PP MB fiber
(AT = 270°C, AR = 557.5 SCFM, and DCD = 8.6 inch.)

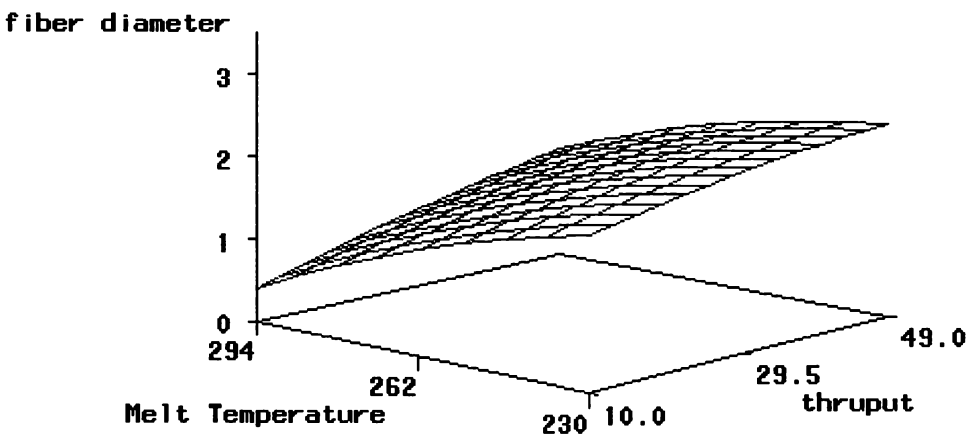

Figure 4.1-3 The effects of melt temperature (MT) and throughput (TP) on the diameter of PP MB fiber
(AT = 300°C, AR = 557.5 SCFM, and DCD = 8.6 inch.)

Statistical ridge analysis (RA) provides information on the direction in which further experimentation should be performed. In this case, the RA (Appendix B) indicated that the smallest fiber might be produced at higher temperature, lower throughput, higher airflow rate and a DCD of 8 inches; the effect of AT is less significant, since A T data are nearly constant.

Figure 4.1-4 shows the effects of AT and MT on the fiber diameter with the following conditions: TP = 15 kg/hr, AR = 580 SCFM, and DCD = 8.6 inch. At low melt temperature, the effect of air temperature on fiber diameter was minimal. As the melt temperature increased to 300°C, the effect of air temperature appeared more significant. Therefore, for the smallest fiber diameter of PP, the air and melt temperatures should be set at higher temperatures.

Figure 4.1-5 shows the effects of DCD and TP on fiber diameter with the following conditions: MT = 270°C, AT= 270°C, and AR = 580 SCFM. It was shown that DCD exhibited notable effects at low throughput conditions. For example, at a throughput of 10 kg/min, increasing DCD led to smaller fiber size, because the filament experienced longer extension. As throughput increases, a proportionally increased air amount is required for the same degree of attenuation. If it is not available, the effect on fiber diameter of DCD will become much less important.

Based on these experimental results, the following operational conditions were suggested for a finer average $PP_{1200MFR}$ MB fiber size by the predictor of the RSM package with a predicted fiber diameter of 1.41 μm.

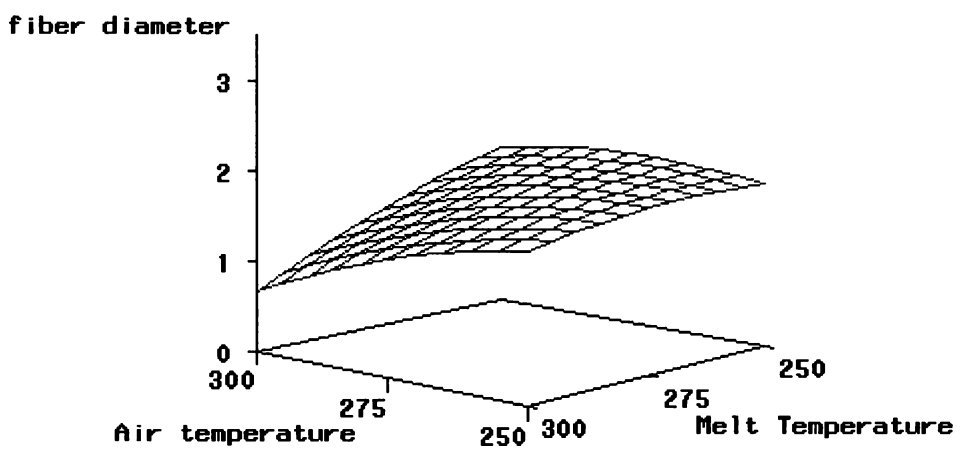

Figure 4.1-4. The effects of air temperature (AT) and melt temperature (MT) on the diameter of pp MB fiber
(TP = 15 kg/hr, AR = 580 SCFM, and DCD = 8.6 inch)

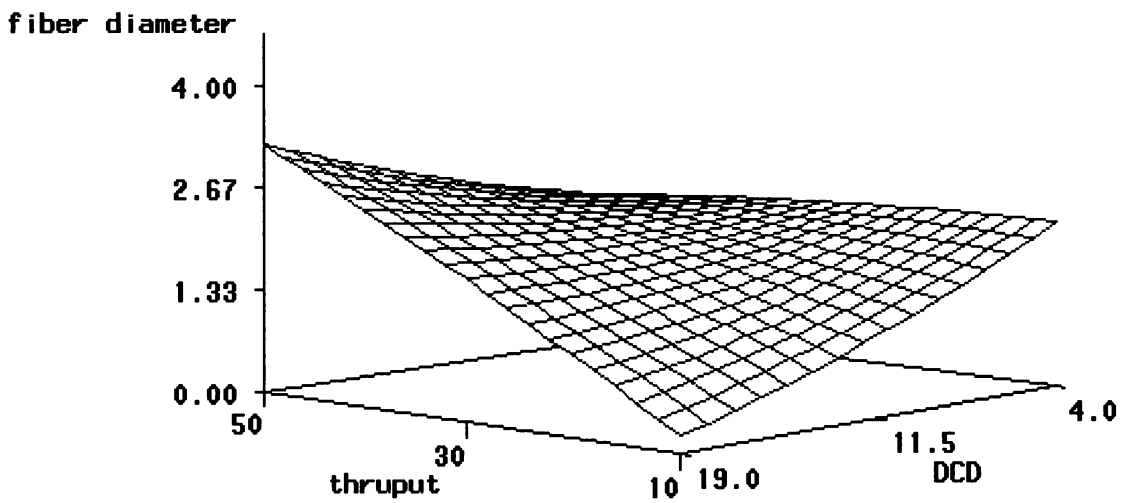

Figure 4.1-5 The effects of DCD and throughput on the diameter of pp MB fiber
(MT = 270°C, AT= 270°C, and AR = 580 SCFM)

MT = 270℃, *TP* = 15.6 *kg/hr*, *AT* = 278.6℃,

AR = 600 *SCFM*, *DCD* = 10 *inch*

For the same fiber size, other processing conditions can also be possible, such as the follows, indicating the operational conditions can be manipulated in different ways for the same purpose.

MT = 298°C, *TP* = 20 *kg/hr*, AT = 279 °C,

AR = 572 *SCFM*, *DCD* = 11 *inch*

Preliminary Research on PET

The experimental design for PET is same as that for $PP_{1200MFR}$ except for factor levels, as shown in Table 3-2. Data of fiber diameter, HH, AP, tenacity, elongation, FR, and packing density (PD) of these PET MB webs are presented in table 4.1-2. Prediction profiles of PET fiber diameter (FD, μm) generated by the experimental design software are given in Figure 4.1-6.

In this case, melt temperature, throughput and airflow rate had significant effects on the fiber diameter, but the DCD and AT showed minimal or no effect. Although the experimental settings were different, it still showed that the inherent properties of PP and PET contributed greatly to the variance of the prediction profiles. Because the air jet immediately after the MB die draws a large amount of secondary air from the ambient surroundings, estimated to be at least 5 times more than the volume of hot air traveling though the die, the air temperature was expected to decrease dramatically within a short distance from the die. Therefore, the AT effect on PET filament (Tg = 75°C) can not be shown.

Table 4.1-2. General properties of PET melt blown nonwoven webs

Run ID	Fiber Dia.	HH	AP	Basis Weight	P. Density	F. Rigidity	Tenacity	Ext. at Break (MD)
	μm	cm-H_2O	ft^3/ft^2 /min	g/m^2		mg-cm	MPa	%
33	8.12	8.53	629.56	37.18	0.083	10.87	0.214	82.20
34	5.74	10.18	243.19	36.33	0.092	39.75	0.392	32.75
35	10.20	8.73	433.50	35.97	0.076	52.90	0.405	69.63
36	6.27	9.55	224.37	36.45	0.107	13.05	0.181	37.51
37	13.37	8.00	660.73	35.97	0.065	107.16	0.454	35.87
38	7.56	8.50	418.68	36.69	0.085	25.57	0.322	47.46
39	12.73	7.18	868.03	36.21	0.065	29.85	0.211	46.72
40	7.84	8.83	280.80	35.72	0.073	79.26	0.496	44.06
41	8.38	9.50	240.22	36.33	0.105	39.75	0.144	19.22
42	4.68	10.85	140.19	36.33	0.112	19.14	0.143	26.55
43	7.74	-----	246.89	36.93	0.104	8.49	----	44.71
44	3.88	12.00	75.83	34.88	0.131	216.60	0.428	12.12
45	7.52	8.08	517.07	29.79	0.079	8.71	0.140	79.39
46	4.18	10.33	141.59	35.36	0.108	150.31	0.766	34.94
47	8.68	8.53	362.71	25.91	0.069	43.98	0.375	67.52
48	5.48	8.85	174.11	35.84	0.105	29.10	0.339	40.54
49	18.90	7.12	989.35	34.56	0.053	37.96	0.178	48.35
50	4.87	9.58	167.49	30.27	0.110	15.95	0.138	41.53
51	5.22	10.38	117.73	37.66	0.121	24.23	0.120	50.27
52	7.20	8.65	273.53	36.09	0.102	24.37	0.289	65.93
53	17.20	7.58	960.41	34.51	0.056	36.75	0.181	49.62
54	4.57	9.90	164.84	25.72	0.069	31.70	0.594	34.43
55	8.12	10.03	157.20	35.60	0.083	348.78	1.111	49.23
56	7.97	8.70	354.35	36.09	0.089	13.44	0.202	58.57
57	7.49	9.00	289.09	36.57	0.102	17.65	0.570	84.97
58	6.86	9.93	270.42	36.09	0.103	16.21	0.231	66.39
59	9.60	9.13	376.81	35.97	0.083	46.68	0.396	45.00
60	6.54	9.10	377.21	35.90	0.083	44.83	0.397	46.00
61	8.12	8.97	378.90	35.78	0.083	47.03	0.408	43.00
62	7.50	9.21	374.21	35.96	0.083	50.34	0.396	47.00
63	7.83	9.11	376.52	35.98	0.083	43.21	0.415	45.00
64	6.93	9.15	378.91	35.94	0.083	46.64	0.397	45.29

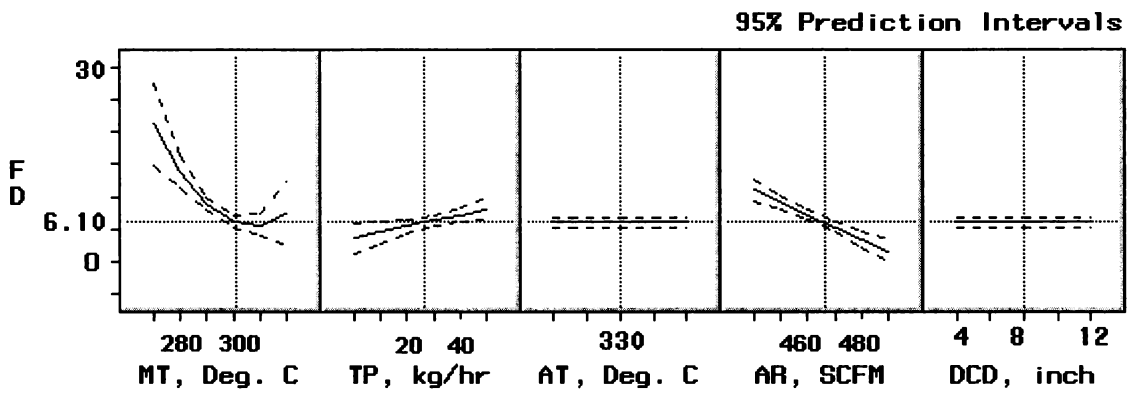

Figure 4.1-6. The prediction profiles of diameter for PET MB fiber

Consequently, greatly increasing AT has little benefit for this case, considering the already high energy consumption. Based on the same reasoning, PET filament may be quenched by the air stream within 3 or 4 inches from the die, resulting in the minimal effect of the DCD, when the collecting distance is larger than 6 inches. In comparison, AT and DCD have some effects on PP fiber diameter due to a much lower glass transition temperature (Tg, pp = -17°C), although they are not as significant as TP.

Figure 4.1-7 shows the effects of TP and MT on PET fiber diameter with the following conditions: AT = 310°C, AR = 557.5 SCFM, and DCD = 8.63 in. It can be seen that the effect of melt temperature on the fiber diameter is predominant. Comparatively, that of throughput is much less significant. This behavior of PET remarkably differs with that of PP due to their different physical and chemical properties. When the melt temperature is low, such as 300°C, fiber diameter decreases with polymer throughput. This effect is minimized when the MT increases to 330°C or higher.

Figure 4.1-8 shows the effects of TP and MT on PET fiber diameter at an increased air temperature and airflow rate. It appears that their effects on the fiber diameter are minimal.

Figure 4.1-9 shows the effects of AR and MT on PET fiber diameter with the following conditions: TP = 25 kg/hr, AT = 310°C, and DCD = 8.63 in. Fiber diameter is much more sensitive to melt temperature compared to the airflow rate. The effects of airflow rate remain constant in the experimental range

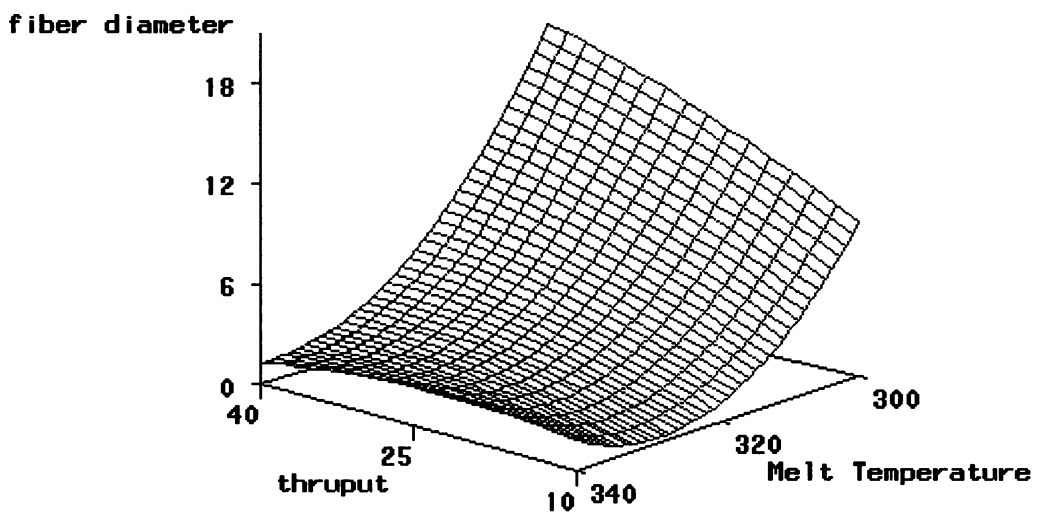

Figure 4.1-7. The effects of TP and MT on the fiber diameter of PET (AT = 310°C, AR = 557.5 SCFM, and DCD = 8.63 inch)

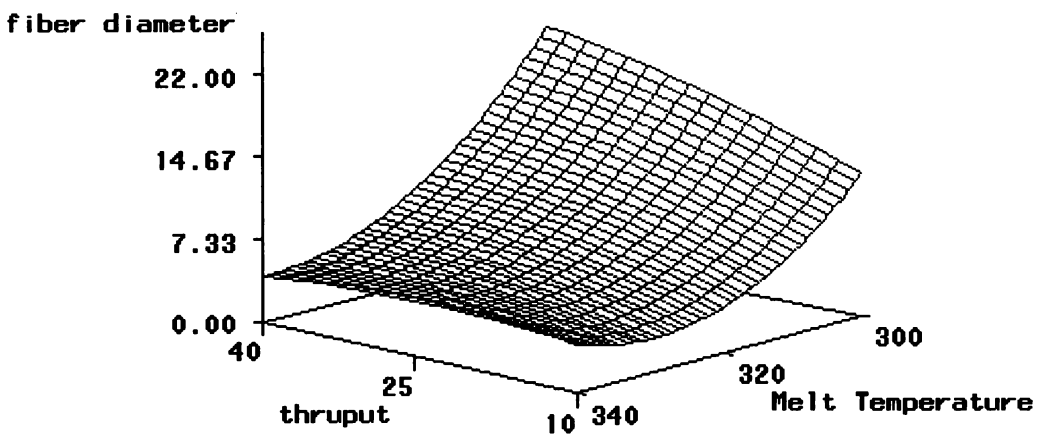

Figure 4.1-8. The effects of TP and MT on the fiber diameter of PET at higher air temperature.
(AT = 340°C, AR = 590.5 SCFM, and DCD = 8.63 inch)

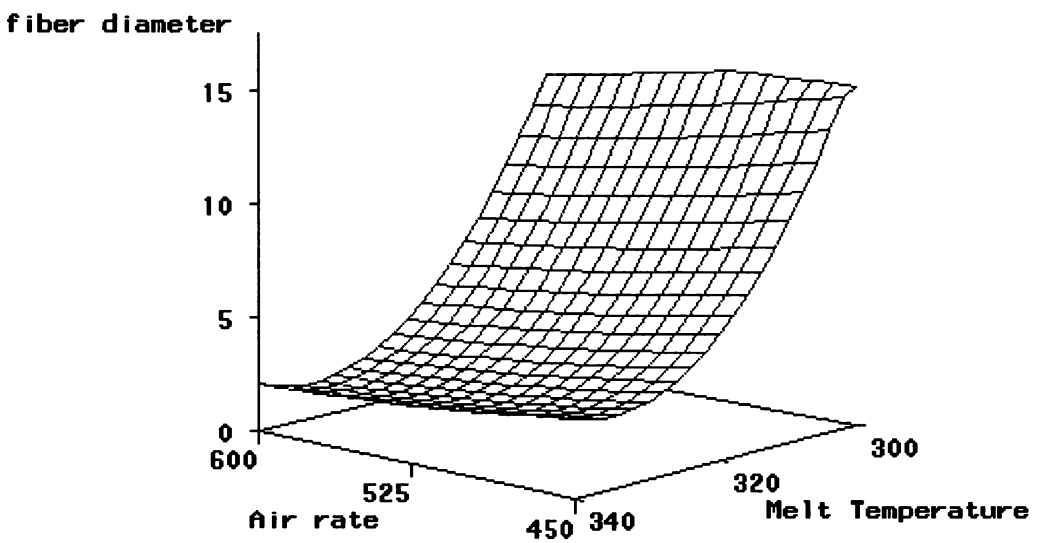

Figure 4.1-9. The effects of AR and MT on the fiber diameter of PET (TP = 25 kg/hr, AT = 310°C, and DCD = 8.63 inch)

of melt temperature, indicating there is no interaction between these two factors.

Based on these experimental results, the following operational conditions are suggested for an average PET MB fiber size of 3.54 μm by the predictor of the RSM package. Again, this is not the only choice for this fiber size.

MT = 339°C, TP = 19.8 kg/hr, A T = 330°C,

AR = 548 SCFM, DCD = 8 inch

In summary, PP and PET present notable differences in regards to processing conditions and final fiber diameter. The distinguishable properties and characteristics should be considered and utilized during bico processing of these two polymers

Preliminary Research on $PP_{1200MFR}$/PET Bico MB

According to the results obtained above, a few trials of bico $PP_{1200MFR}$ /PET were conducted to obtain basic information on processability and web properties. The operational conditions were arbitrarily selected within the range of above experiments and presented in Table 4.1-3. The nonwoven webs were characterized for several basic physical properties and compared with those of pure PP and PET webs, as shown in Table 4.1-4. Within the experimental range, the average fiber diameters of bico PET/PP MB webs fell between of 100% PP and 100% PET as illustrated in Figure 4.1-10. This was expected due to the much higher glass transition temperature of PET compared with that of PP. The hydrostatic head, air permeability, tenacity, flexural rigidity, and packing density are all apparently significantly different from those of both pure PET and pure PP.

Table 4.1-3. Preliminary Melt Blowing Trials on Bicomponent $PP_{1200MFR}$/PET

ID	Components	Melt T. °C	Throughput (kg/hr)		DCD inch	Air R SCFM	Air T. °C	Belt ft/min
			PET	PP				
Bico-1	28%PET:72%PP	315	5.76	14.8	9.9	450	310	90
Bico-2	48%PET:52%PP	315	10.79	11.69	7.9	500	310	95
Bico-3	74%PET:26%PP	315	19.14	6.58	7.1	400	310	108

Table 4.1-4. An overview of the properties of PP, PET and $PP_{1200MFR}$ /PET bico fiber MB nonwovens

ID	Components	Fiber Dia. μm	HH [1] cm	AP [1] ft^3ft^2/min	Tenacity MPa	Ext. %	FR[1] mg-cm	c %
Bico-1	28%PET:72%PP	3.649	24.9	192.8	7.173	39.49	55.35	4.48
Bico-2	48%PET:52%PP	3.697	21.1	173.0	9.570	45.84	82.74	4.56
Bico-3	74%PET:26%PP	3.516	17.4	260.8	9.890	76.59	52.10	4.73
PP	100% PP-Min [2]	1.445	69.5	47.44	0.757	17.27	214.67	8.31
PP	100% PP-Max [2]	2.52	51.6	73.71	0.916	22.94	293.09	10.01
PET	100% PET-Min [2]	4.184	10.33	141.59	0.766	34.94	150.31	10.8

Note: [1] Data were normalized to basis weight of 35 g/m^2.
[2] For comparison, runs with smallest (Min) and largest (Max) fiber diameter were selected from those in Table 4.1-1, and Table 4.1-2

By direct observation, the process ran smoothly and the bico webs were better bonded compared to pure PET, which agrees with the tensile testing results in Table 4.1-4. For similar basis weight, pure $PP_{1200MFR}$ web exhibited the highest coverage and pure PET the lowest coverage; the bico webs had the coverage in the middle, which is partially reflected in the fiber diameter data. The effect of the percentage of each component on the fiber diameter does not appear significant as long as the fibers are bicomponent. However, their fiber sizes fell in the between of single $PP_{1200MFR}$ and PET fibers. The web uniformities in terms of fiber diameter and basis weight across the web were also determined; the selected data of a 28%PET/72%$PP_{1200MFR}$ were presented in Figure 4.1-11 (Note: although the targeted polymer ratio was 25%PET/75%PP, the actual ratio was determined to be 28%PET/72%PP). The data for the other polymer ratios exhibit similar trends. Keeping in mind that the processing conditions for these runs are different, one needs additional data to draw any firm conclusions. A thorough experimental investigation on TP, MT AT, AR, and polymer mass flow ratio (MR) was performed, and the results are presented and discussed in Chapter 4, Phase 2.

Bico fiber cross-section is one of the major concerns at this stage. Figure 4.1-12a is a top view microphotograph of a 50%$PP_{1200MFR}$/50%PET bico MB web by a scanning electron microscope with variable pressure capability in a back-scattered mode. It shows good contrast of different regions, indicating the difference in their chemical natures. The white side represents the polymer PET,

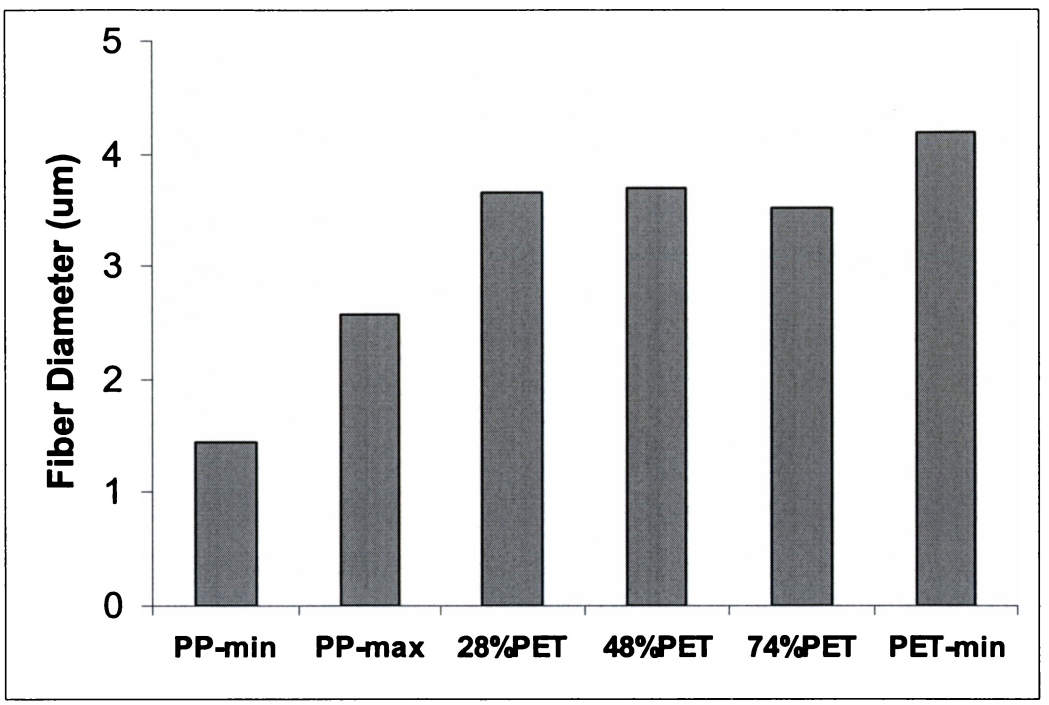

Figure 4.1-10. A comparison of fiber diameters of PP, PET and bico PP/PET MB webs

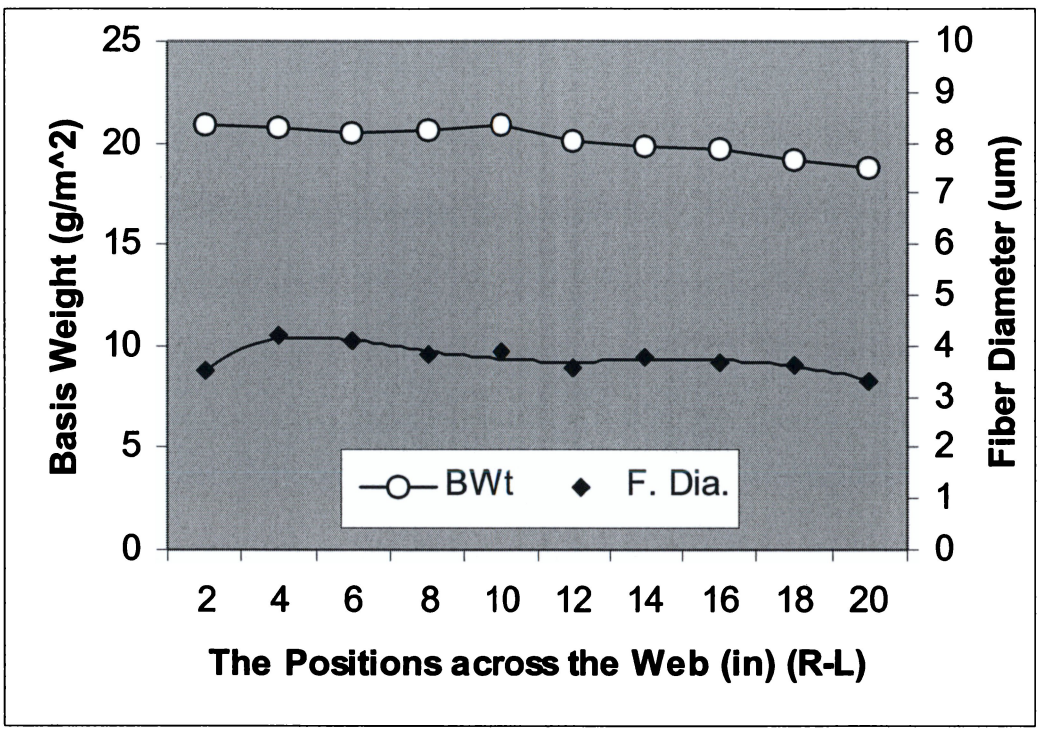

Figure 4.1-11. The web uniformity in terms of fiber diameter and basis weight

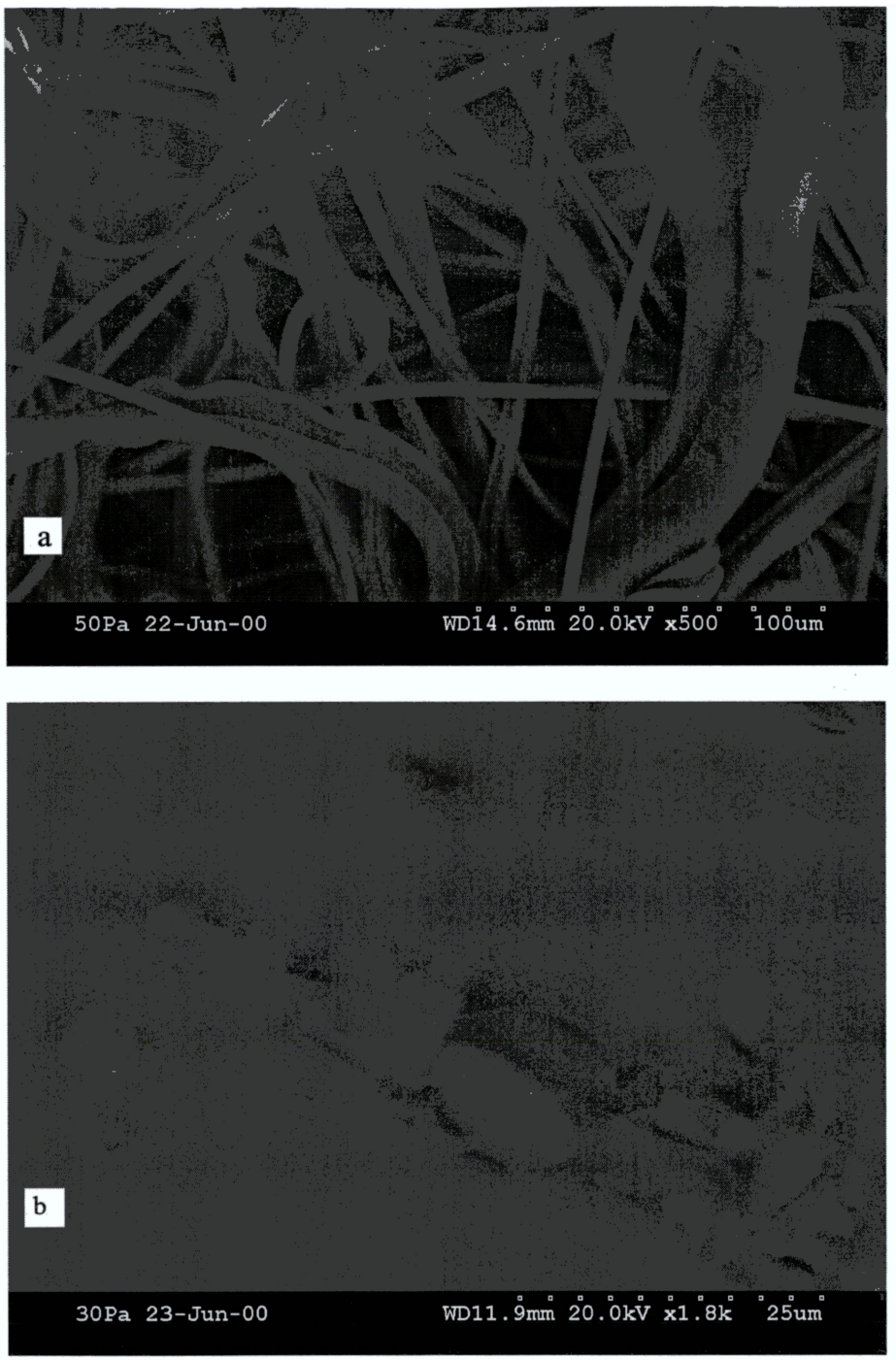

Figure 4.1-12. SEM microphotograph showing the side-by-side configuration of the bico 50%PP/50%PET MB fibers, (a) top-view of the web, (b) cross-section

and the black side represents the polymer PP. The originally expected high crimp of the PP/PET bico MB fiber was rarely observed. Figure 4.1-12b is the cross-sections of the 50%PP/50%PET bico MB fiber by the same SEM technique except the fibers were mounted in a Spurr embedding media [Spurr,1969]. Based on these two typical images, one may conclude that the bico fibers are nearly circular in cross-section with a side-by-side geometry. In addition, the fiber size seemingly has a relatively broad distribution. The cross-sections of 50%PP/50%PET bico MB fibers produced under the same processing conditions with a screen filter at the entrance of die tip are shown Figure 4.1-12-1. It suggests that the side-by-side configuration was most likely undisturbed by the filter.

Although the bico web exhibited excellent uniformity in terms of basis weight and fairly good fiber diameter constancy across the web, as shown in Figure 4.1-11, it was noticed that there was a significant variance in tensile properties at different positions across the web. The results of the Phase 1 were plotted in Figure 4.1-13. The tenacity distribution of the bico webs strongly depended on the polymer ratio. As PET is the main component in the polymer combination, the web tenacity is non-uniform across the web. This result indicated the polymer distribution across the web was possibly not uniform.

Polymer distribution (DSC analysis)

To quantitatively determine the distribution of individual components across the web, a standard curve was developed between the weight percentage

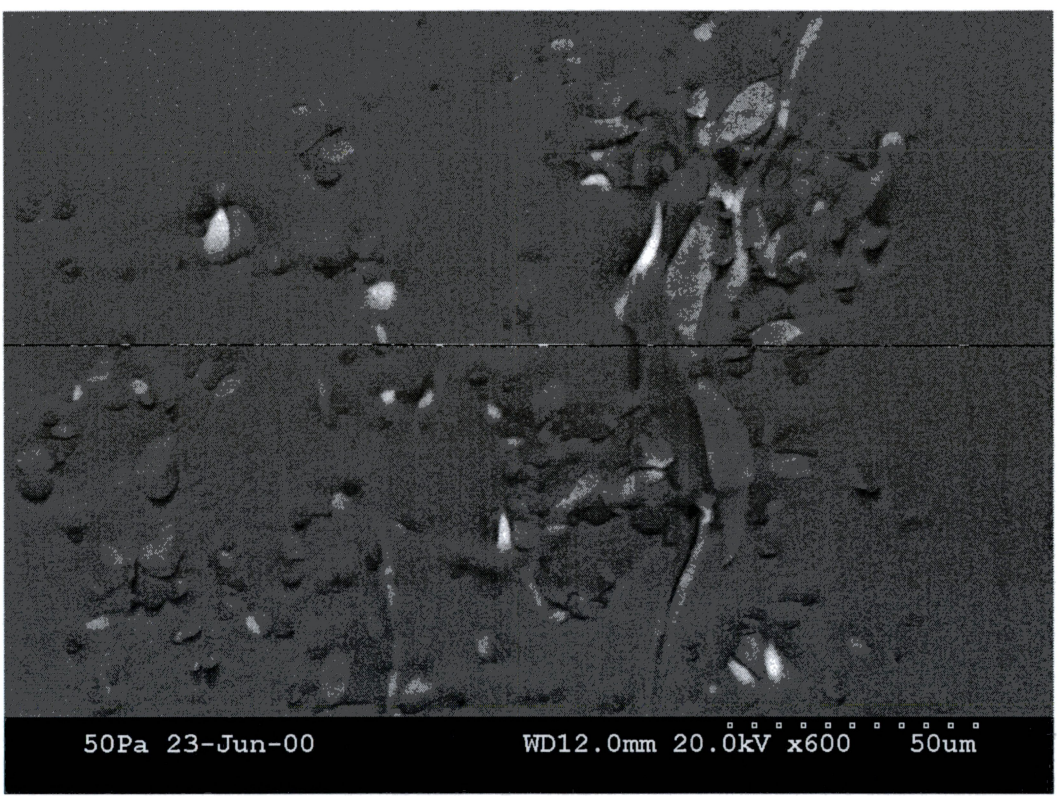

Figure 4.1-12-1. The side-by-side configuration of the 50%PP/50%PET bico MB fibers produced with a polymer melt filter at the entrance of MB die tip

and heat of fusion (ΔH_f) for each component. The following two assumptions were made: (a) The area of the melting peak in a DSC curve is proportional to polymer crystallinity; (b) given the same conditions, a given semicrystalline polymer develops to the same degree of crystallinity. A typical DSC curve of bico PET/PP MB fiber is shown in Figure 4.1-14. The PP endothermic peak is around 165°C and PET is about 256°C. The linear relationship between heat of fusion and component weight percentage is illustrated in Figure 4.1-15. Each sample was heat treated to eliminate the effects of thermal history.

For each bico web, samples were taken at designated positions across the web to measure ΔH_f of each component, as described in Chapter 3, EXPERIMENTAL. The heats of fusion of PP and PET components were measured from corresponding melting peaks in re-heating curves. By utilizing the fitted equation of the standard line, the weight percentage of PP and PET in the bico MB web at each position was obtained. The calculated data were plotted against their positions across the web from the right to left in CD direction, as shown in Figure 4.1-16 and 4.1-17. For all three cases, the edge areas present higher weight percentage of PP than the center area. However, the PP component in the 25%PET/75%PP web distributed more evenly than in the other two cases.

Factors that affect polymer distribution uniformity in the web include the coat-hanger die geometry, rheological properties of components under the processing conditions, compatibility of the components, the total throughput, and

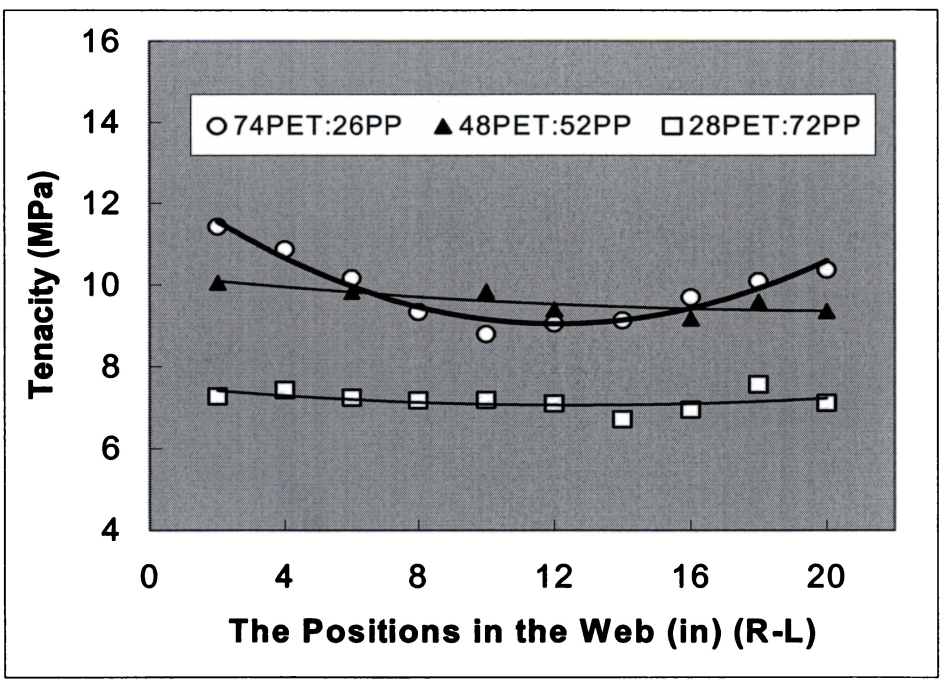

Figure 4.1-13. The tenacity distribution of bico PET/$PP_{1200MFR}$ MB webs

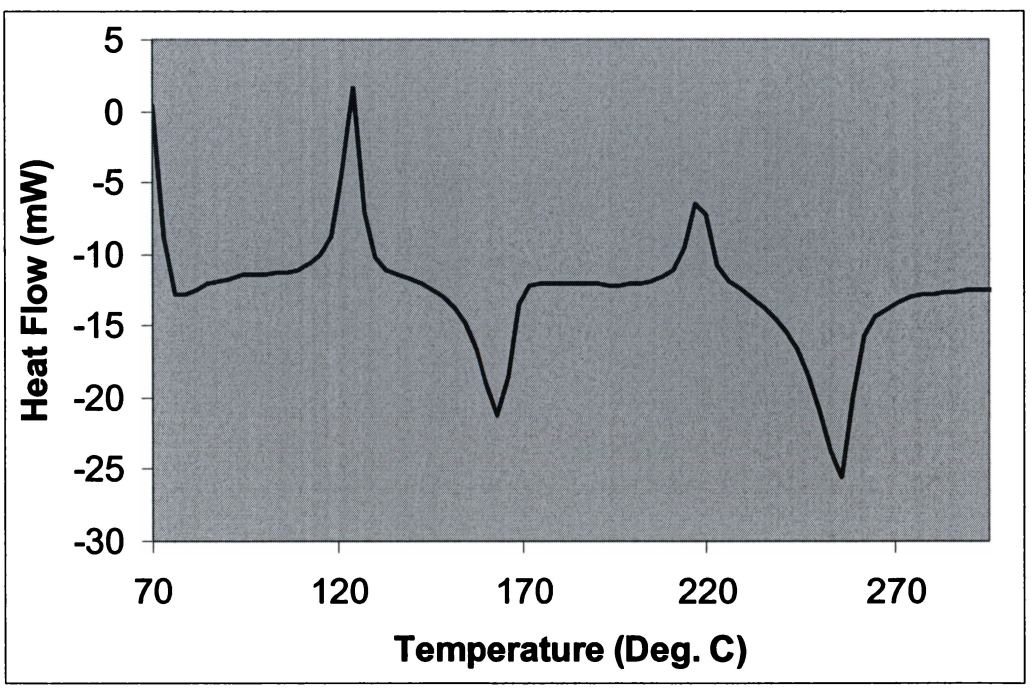

Figure 4.1-14. A typical DCS curve for PET/$PP_{1200MFR}$ bicomponent MB fibers

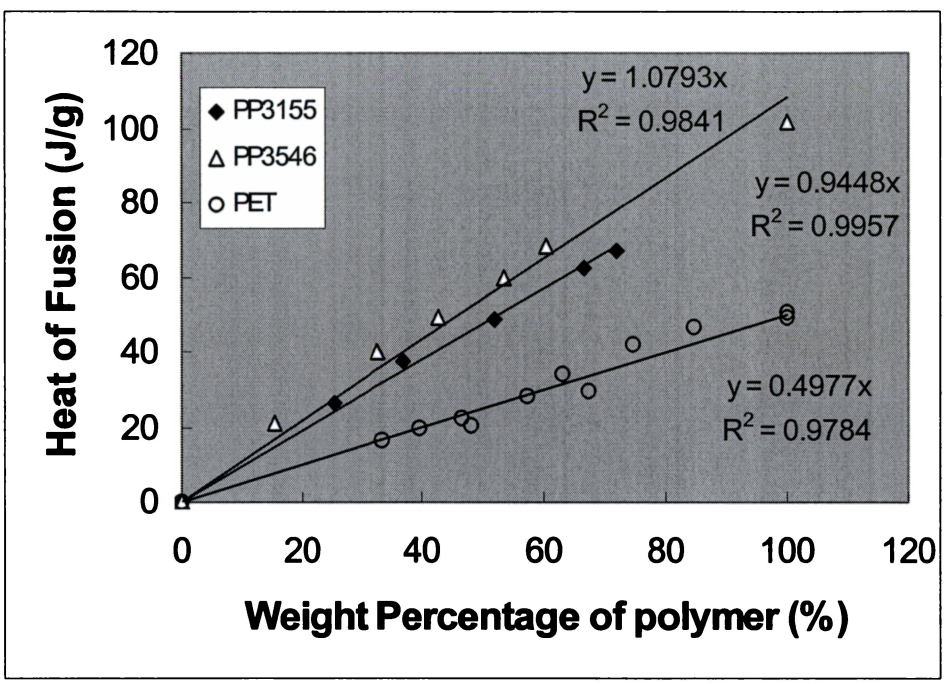

Figure 4.1-15. The relationship between heat of fusion and weight percentage of PET and $PP_{1200MFR}$ measured by DSC

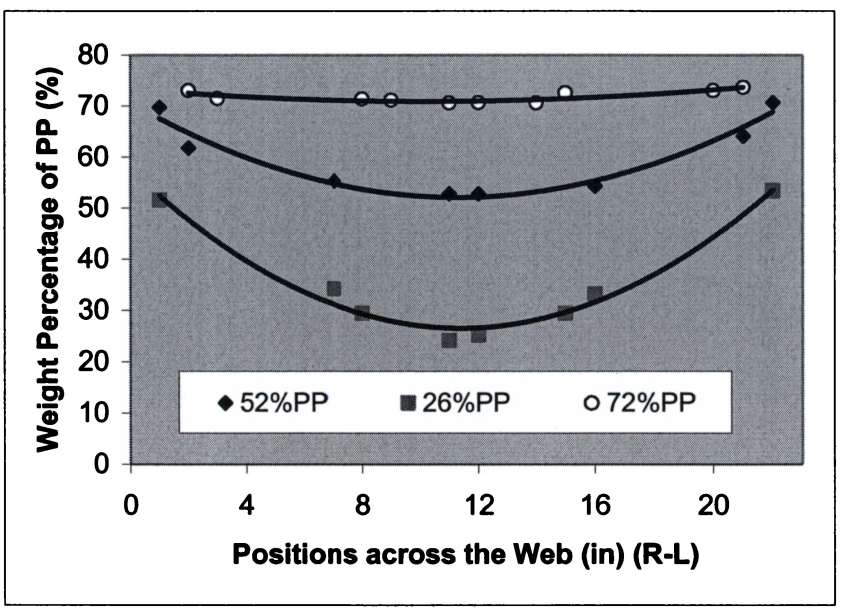

Figure 4.1-16. The distribution of $PPP_{1200MFR}$ in the B/C PET/$PPP_{1200MFR}$ MB webs by DSC analysis

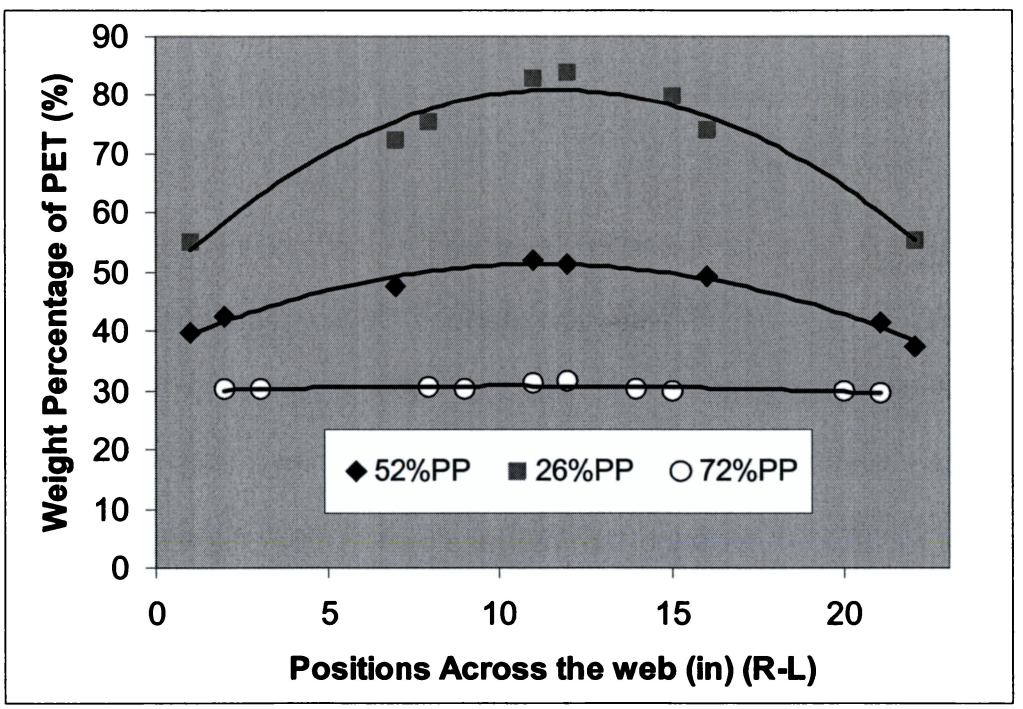

Figure 4.1-17. The distribution of PET in the B/C PET/$PP_{1200MFR}$ MB webs by DSC analysis

their ratios. The viscosity of the polymer melt is one of the most influential factors. Because PP and PET are non-compatible, one may assume their melt in the coat-hanger die is a stratified two-phase system. According to Yu and Han (1973), the pressure gradients in both phases are the same. The velocity profiles of the two phases are very much dominated by their viscosities. The results of the weight percentage distribution across the web suggest that the PP component is less viscous with a higher velocity than PET under the processing conditions. It is also suggested that the cross-sectional phase interface of the polymer melt before entering the die tip changes with the in-put polymer ratio, as shown in Figure 4.1-18.

The less viscous upper PP layer has a concave interface and the more viscous PET layer presents a convex interface. These results are in agreement with the experimental studies of Han and co-workers (1973) who studied the coextrusion system of low-density polyethylene (LDPE) and polystyrene (PS) through a slit die, They found the interface moved from the less viscous LDPE side to the more viscous PS side.

In the melt blowing process with a coat-hanger die, the interface distortion at the die tip entrance controls the polymer distribution across the die; thus, it controls the component uniformity across the MB web. This further affects the web qualities and the end-use properties. However, polymer distribution in bico MB web may be improved if the component viscosities are well matched by adjusting molecular weight, polydispersity, temperature, and concentrations of

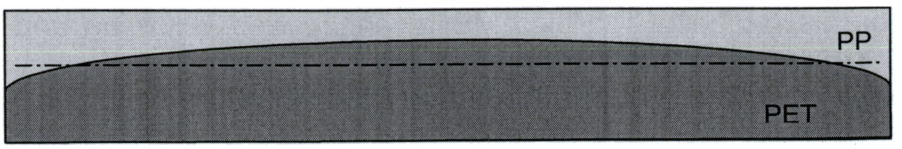

25%PP/75%PET

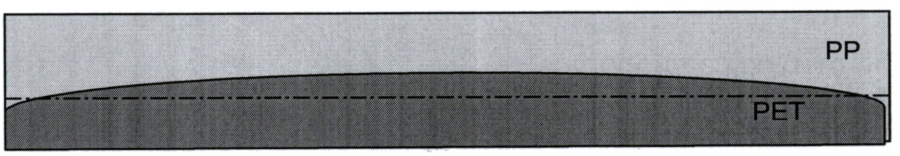

50%PP/50%PET

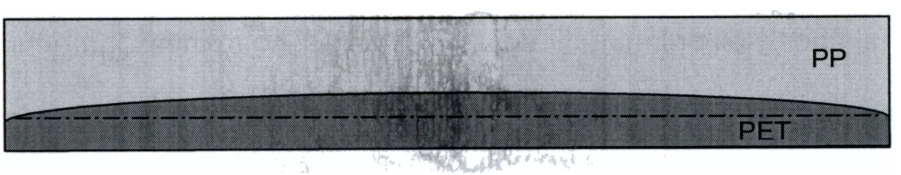

75%PP/25%PET

Figure 4.1-18. Cross-sectional phase Interface profiles of the polymer melts before entering the die tip

solid additives and processing conditions. In the scope of this research, the selection of different grades of PP and the temperature control in order to match the viscosity of the polymer pair (PP/PET) were investigated in detail.

In the first stage of the bico MB research, web yellowing and die hole plugging were observed, while the operational temperature was high. This may be due to the thermal degradation of the one or both of the polymers. In order to prevent future problems in both operation and product quality, it is necessary to collect sufficient basic data about the polymer system of interest, such as thermal stability and rheological properties.

Selection of polymer resins

Since PET with an intrinsic viscosity of 0.645 dl/g is popular in the conventional fiber melt spinning, it would be interesting to investigate its potential in the MB process. PET is sensitive to absorbed moisture in the presence of heat, which accelerates hydrolysis. However, this problem can be minimized by the adequate drying of the polymer resins immediately prior to processing. At our melt blown conditions, well-dried PET exhibits minimal thermal degradation or carbonization. Figure 4.1-19 shows the TGA curve of PET with a period of 30 min at 320°C in air, indicating the thermal stability of PET.

There are several grades of PP in the market for nonwoven production, which have a melt flow rate (MFR) ranging from 30 to 1200 MFR or higher. In this research, Exxon PP_{3546G} (1200 MFR, designed for melt blowing process) and

PP_{3155} (35 MFR, designed for spunbond process) were employed to investigate the bico MB norwovens with Wellman PET (grade 61418, IV=0.645±0.017).

The first concern in selecting the PP resin was the thermal degradation property, and the second was its viscosity match with PET.

Thermal Degradation

In Phase 1, several uniform PET MB webs were produced at melt temperatures of 310°C and higher. If bico PET/PP are melt blown at the same temperature, thermal degradation would occur and cause problems such as die hole plugging. As shown in Figure 4.1-20, weight loss (which is indicative of thermal degradation) of PP starts at 280°C in air and the $PP_{1200MFR}$ lost more weight than PP_{35MFR} while being held at 320°C for 30 min. The weight loss rates of the two polymers were determined by the TGA method, which is briefly described as follows.

During the test, the sample was kept at a constant temperature for a period of 30 minutes, and the actual weight of the sample was recorded automatically. It is found that the percentage of weight loss exhibited an almost linear relationship with heating time at this constant temperature. The slope of the line is defined as weight loss rate (% Wt-loss/min). As shown in Figure 4.1-21, at relatively low temperature (~ 280°C), PP_{35MFR} and $PP_{1200MFR}$ showed similar weight loss rate. At a higher temperature (>280°C), PP_{35MFR} apparently degraded slower than $PP_{1200MFR}$, i.e., PP_{35MFR} is more thermally stable.

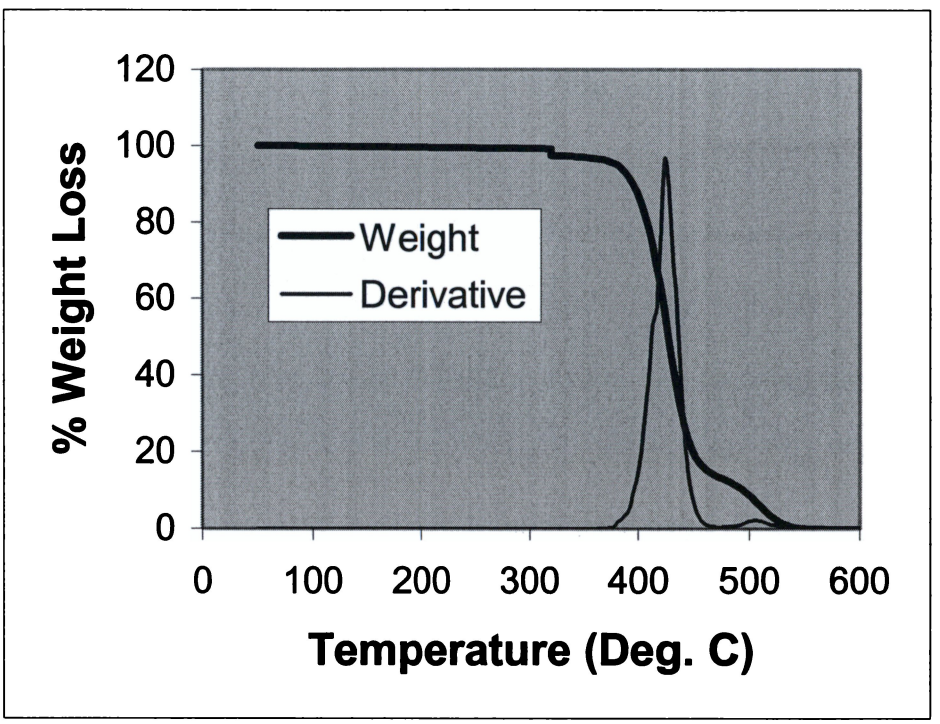

Figure 4.1-19. TGA curve of PET showing its weight loss in air. The sample was kept at 320°C for 30 min

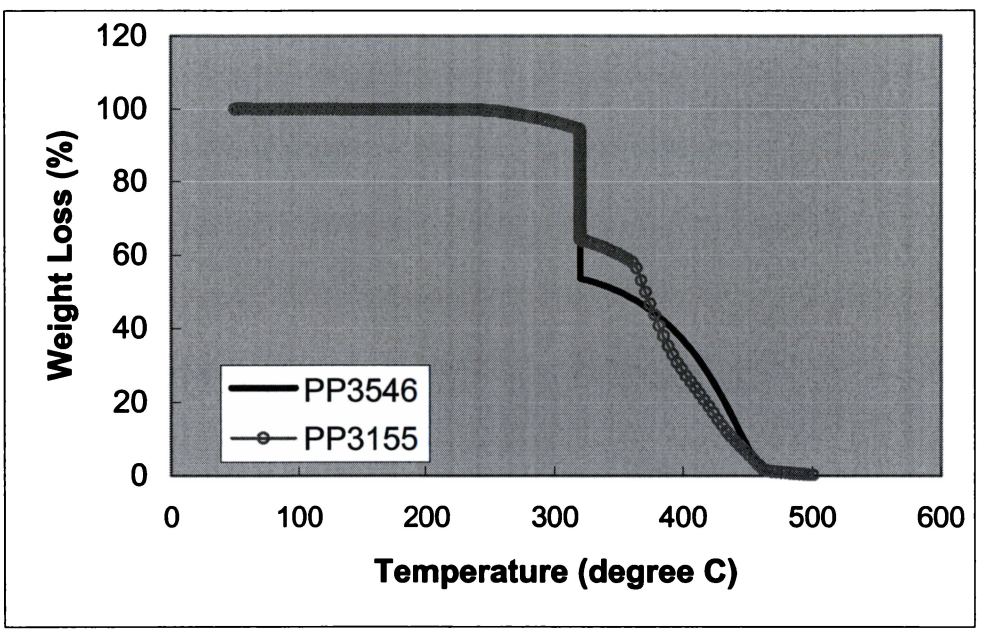

Figure 4.1-20, Comparison of weight loss of selected PP (PP_{3155}, 35MFR; PP_{3546G}, 1200MFR). The samples were held at 320°C for 30 min. The percentage of weight loss has a linear relationship with heating time at constant temperature of 320°C

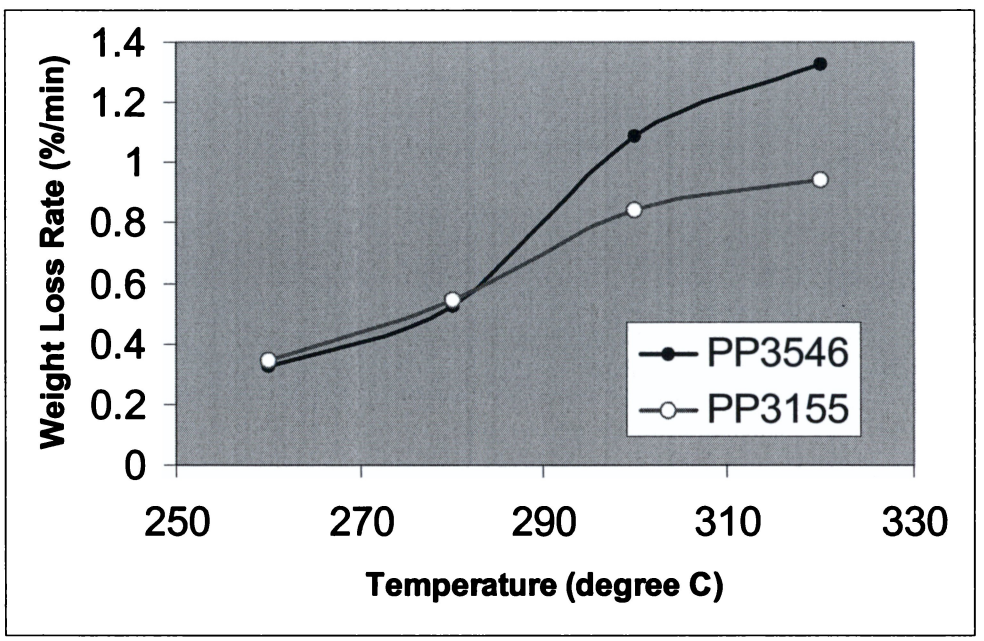

Figure 4.1-21. Thermal Weight Loss Rate of PP's determined by TGA (PP_{35MFR} = PP_{3155}; PP_{3546G} = $PP_{1200MFR}$)

Although the amount of air encapsulated in the polymer melt is significantly reduced compared to that during the TGA testing, it is nearly inevitable in this study. Therefore, at a temperature of 310°C or higher, thermal degradation occurs, which is at least partially responsible for the observed MB die hole plugging.

By properly sealing the die bottom and carefully filling in 95% industrial ethanol, the total volume of the polymer flow in co-connector, coat-hanger and die tip of the 24-inch Reicofil® MB pilot line was roughly estimated 514.9 cm^3 in this research. Normally, high temperatures are employed in these areas during bico MB process. Thus, the polymer residence time in the high temperature region can also be estimated. For example, at 300°C, density of PP is 0.77 g/cm^3 [Kikutani, 1996]; if throughput is 20 kg/hour, PP will be exposed to this high temperature for about 1.19 minutes. With this in mind, a higher throughput of PP is desirable to reduce the polymer residence time, and to minimize the possibility of carbonization-induced die hole plugging. In the viewpoint of thermal stability, PP_{35MFR} is superior to $PP_{1200MFR}$.

Viscosity Matching

The rheological properties of the above-mentioned polymers were determined by using an Advanced Capillary Extrusion Rheometer (ACER 2000, Rheometric Scientific). At a temperature around 270°C or higher, the viscosity of $PP_{1200MFR}$ is well below that of PP_{35MFR}, as shown in Figure 4.1-22. Both of them

are significantly different from PET, as shown in Figure 4.1-23. In the same temperature environment, it would be difficult to match the viscosity of $PP_{1200MFR}$/PET by adjusting temperature and throughput, if it is not impossible.

By combining the data of thermal analysis and viscosity, PP_{35MFR} was selected for further research in producing bico PP/PET MB microfiber nonwovens. It is observed that at a temperature between 280°C and 300°C, and a shear rate lower than 1000 1/sec, the PET exhibits Newtonian flow property. In this same region, PP shows more non-Newtonian behaviors (more like power-law flow). These results indicate that the viscosities of the two polymers respond differently depending on the temperature and shear rate.

In our melt blown process, the uniformity of polymer distribution across the web is mainly controlled by the polymer melt distribution in the coat-hanger, where the pressure drop is significantly low compared to that in die orifices [Sun, 1998]. Therefore, it is more important to match the viscosity of the polymer pair in the coat-hanger. In the die orifice region, the polymer viscosity match mainly affects the cross sectional geometries of the bico micro-fibers, but has little effect on the overall polymer distribution across the web. The typical polymer throughput for melt blowing falls in the range of 0.1 to 2 g/h/min with the die orifice diameter around 0.5 mm. For PP and a die temperature of 300°C the corresponding shear rate in the die orifices, computed by using the following equation, is in the range of 176.8 S^{-1} to 3536.6 S^{-1}.

$$Shear\ rate = \frac{4Q_p}{\pi \cdot r^3}\ (s^{-1}) \qquad (4.1\text{-}1)$$

where Q_p is polymer volumetric flow rate, m^3/s, and *r* the radius of the die orifice, m. The shear rate in the coat-hanger is expected to be much lower than that in the orifice, possibly falling in the region of 1 to 1000 s^{-1} in the viscosity - shear rate curve. Thus, it may be possible to find a close match in viscosity *for* the two polymers by adjusting throughput (shear rate) and the temperature across the die, although the tolerance may be very narrow.

Phase 2: Effects of selected variables on the fiber and web properties

For the polymer system of PET/PP_{35MFR}, the processing temperature of melt blowing has to be determined by considering at least the following two factors:

1. A temperature is high enough for easily melt blowing the high melting temperature component, i.e. PET, whose melting temperature is nearly 90°C higher than that of PP_{35MFR}.
2. A temperature is suitable for the lower melting temperature component, i.e. PP_{35MFR}, to minimize possible thermal degradation.

The temperature window for PET/PP is thus limited to the experimental range of 300°C to 330°C. The fiber diameter testing results shown in Figure 4.2-1 indicate that the effect of die temperature is minimal within the specified conditions. In addition, both die and air temperatures are slow to change and require a relatively long time to stabilize. For the 24-inch Reicofil® MB pilot line, it normally

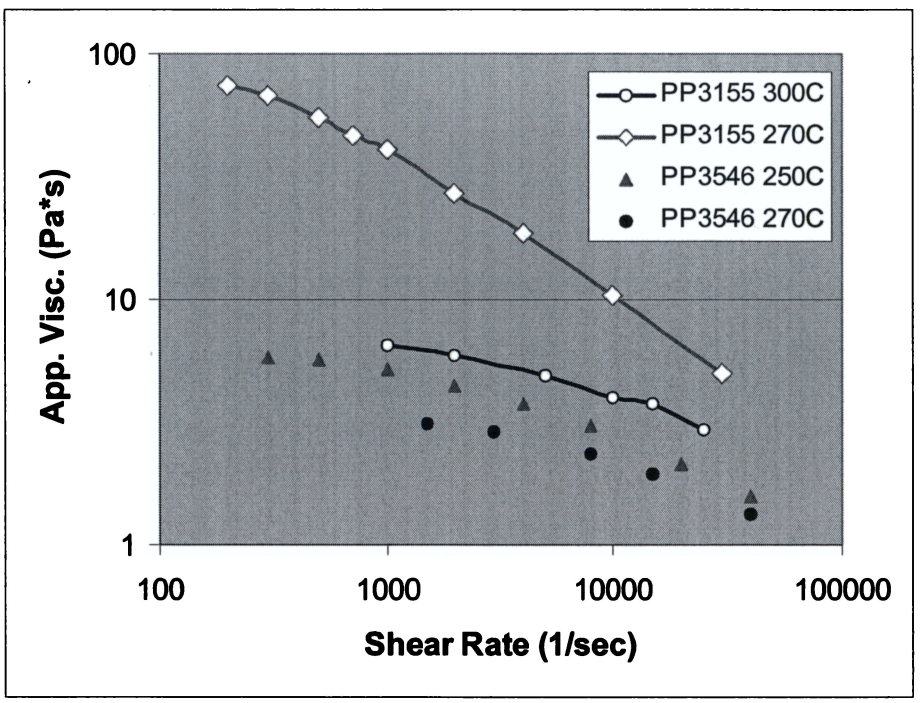

Figure 4.1-22. Comparison of Shear Viscosity of PP's
(PP_{3155} = PP_{35MFR}; PP_{3546G} = $PP_{1200MFR}$)

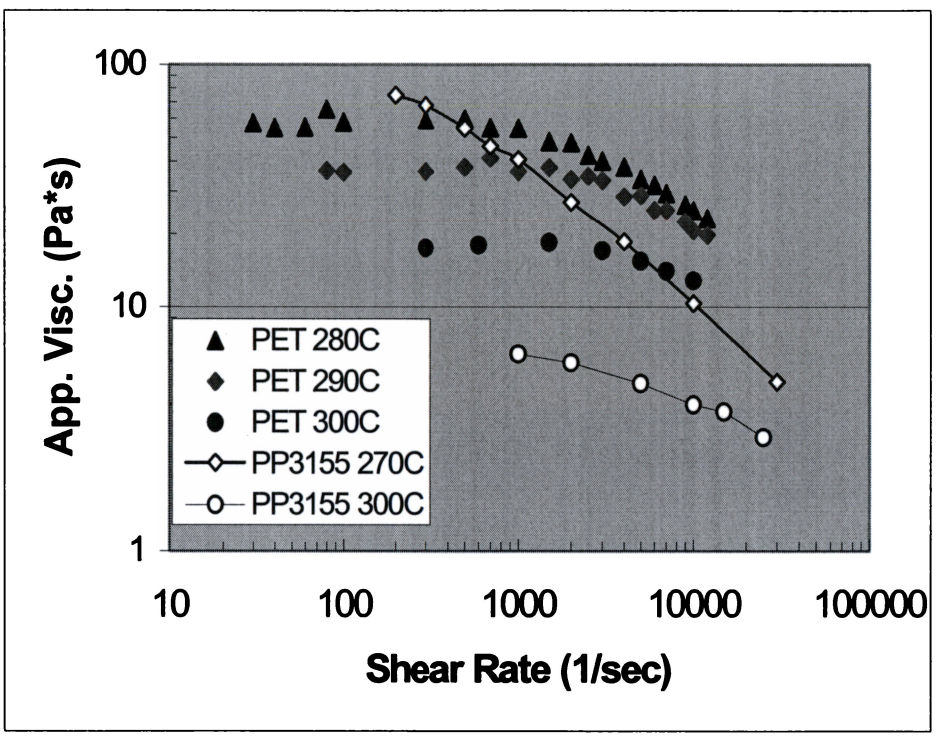

Figure 4.1-23. Rheological properties of Wellman PET and PP_{35MFR} (PP_{35MFR} = PP_{3155})

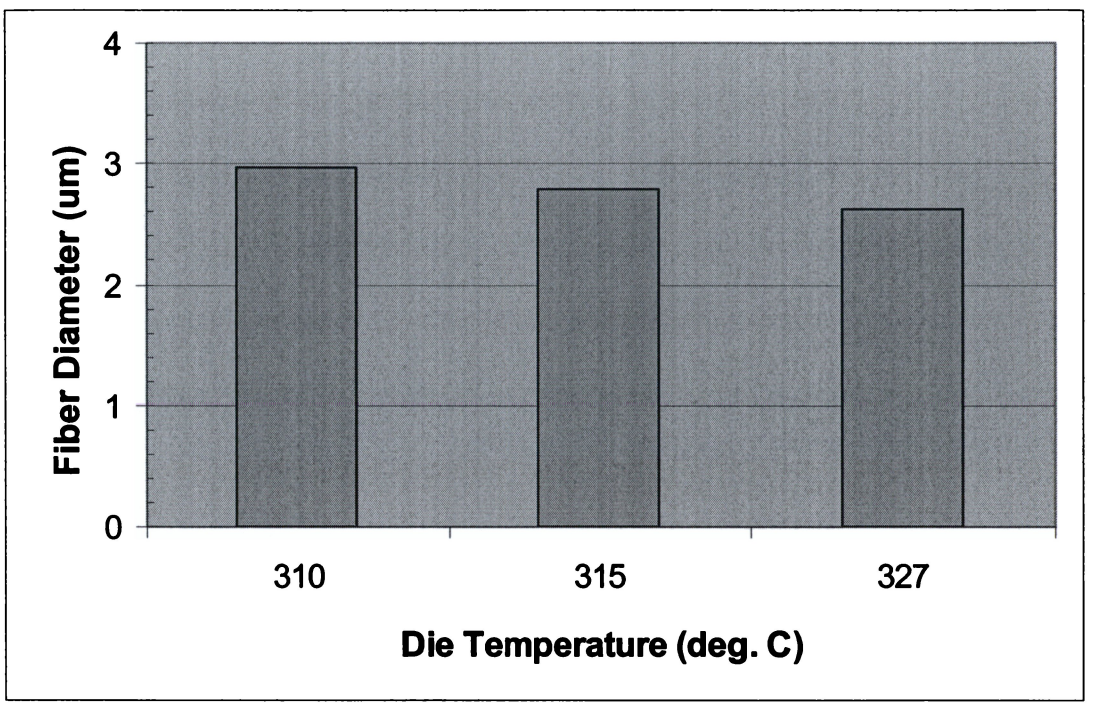

Figure 4.2-1. The effect of Die Temperature on the PET/PP_{35MFR} Fiber Diameter (TP = 19.8 kg/hr, AR = 500 SCFM, DCD = 10.5 inch, PP% = 25.1%, $T_a = T_d$)

takes 30 to 45 minutes to change melt or air temperature depending on the amplitude of adjustment and the combinations with other operation parameters. In order to optimize the effectiveness of the experiment design, both melt and air temperatures were set at 310°C, based on the results in Phase 1. The RSM experimental design method (Hybrid design: Roquemore R416C) was applied to investigate the effects of TP, AR, DCD and the weight percentage of PP_{35MFR} in the polymer system (PP%). The designed levels of the four factors are listed in the Table 4.2-1 and the design points in Table 4.2-2.

Effect of Operational Conditions on Fiber Diameter

General Results

The properties of the webs were characterized extensively according to the corresponding testing standards or procedures, which include average fiber diameter, basis weight, thickness, air permeability, hydrostatic head, tensile strength, latex filtration efficiency and flexural rigidity. The data are presented in Table 4.2-3. The process/structure/property relationships were explored based on these and additional data later in this chapter. Since the fiber size is one of the most important properties and is most directly related to the processing conditions, it was selected as the response to investigate the multi-factor effects.

The predicted effect trends of operational parameters on the diameter are presented in Figure 4.2-2. A 95% confidence interval was applied to these predictions. At a condition with fixed melt and air temperature of 315°C, the airflow rate exhibited the most significant effect on the fiber diameter for the bico PET/PP_{35MFR} MB filaments. As the airflow rate increases, fiber size decreases

Table 4.2-1, Factors and levels for experimental design of PP_{35MFR}/PET with the code in parentheses

Factor	Label	Low	Center	High
TP	Throughput, kg/hr	10 (1)	15 (0)	20 (-1)
AR	Airflow Rate, SCFM	250 (1)	350 (0)	450 (-1)
DCD	DCD, in	7 (1)	11 (0)	15 (-1)
PP%	Wt % of PP	26 (1)	43 (0)	60 (-1)

Table 4.2-2. The uncoded (coded) design points for a central composite response surface design (Roquemore R416C)

Run ID	TP Kg/hr	AR SCFM	DCD inch	PP%
Bico 4	15 (0)	350 (0)	11 (0)	73.01 (1.77)
Bico 5	10 (-1)	250 (-1)	7 (-1)	52.55 (0.57)
Bico 6	20 (1)	250 (-1)	7 (-1)	52.55 (0.57)
Bico 7	10 (-1)	450 (1)	7 (-1)	52.55 (0.57)
Bico 8	20 (1)	450 (1)	7 (-1)	52.55 (0.57)
Bico 9	10 (-1)	250 (-1)	15 (1)	52.55 (0.57)
Bico 10	20 (1)	250 (-1)	15 (1)	52.55 (0.57)
Bico 11	10 (-1)	450 (1)	15 (1)	52.55 (0.57)
Bico 12	20 (1)	450 (1)	15 (1)	52.55 (0.57)
Bico 13	22.35 (1.47)	350 (0)	11 (0)	25.13 (-1.05)
Bico 14	7.65 (-1.47)	350 (0)	11 (0)	25.13 (-1.05)
Bico 15	15 (0)	497 (1.47)	11 (0)	25.13 (-1.05)
Bico 16	15 (0)	203 (-1.47)	11 (0)	25.13 (-1.05)
Bico 17	15 (0)	350 (0)	16.88 (1.47)	25.13 (-1.05)
Bico 18	15 (0)	350 (0)	5.12 (-1.47)	25.13 (-1.05)
Bico 19	15 (0)	350 (0)	11 (0)	43 (0)

Table 4.2-3. The properties of PP_{35MFR} /PET bicomponent MB webs

Run ID	F. Dia μm	B. Wt g/m^2	Thickness mm	P. Density	HH[1] cm	AP ft^3ft^2/min	Tenacity MPa	FR mg-cm	LFE %	ΔP^2 inch-water	Pore size μm
Bico 4	2.81	23.14	0.324	0.07003	27.28	236.4	8.332	49.18	50.45	0.013	4.81
Bico 5	3.81	21.85	0.375	0.05248	22.43	375.20	11.371	44.46	47.12	0.010	11.65
Bico 6	4.20	32.16	0.595	0.04868	8.78	493.80	10.123	80.89	26.76	0.007	14.97
Bico 7	2.4	24.86	0.279	0.08026	42.17	131.60	11.200	126.95	72.35	0.017	3.13
Bico 8	2.41	24.97	0.362	0.06213	25.16	213.00	5.318	72.96	51.61	0.012	5.25
Bico 9	3.61	23.78	0.378	0.05666	17.40	450.20	4.503	38.06	32.62	0.008	9.46
Bico 10	5.88	24.5	0.487	0.04531	8.14	896.40	6.294	8.77	16.79	0.002	24.26
Bico 11	2.47	25.1	0.376	0.06013	28.12	211.40	5.461	38.75	70.54	0.012	5.74
Bico 12	3.74	25.01	0.391	0.05761	16.87	382.80	0.856	31.23	35.56	0.008	9.48
Bico 13	3.55	27.5	0.421	0.05302	9.05	653.40	2.765	16.85	30.22	0.002	10.64
Bico 14	2.81	27.21	0.284	0.07777	30.16	188.20	2.795	10.33	64.38	0.011	3.9
Bico 15	2.78	26.08	0.326	0.06494	21.14	293.80	3.645	22.47	49.37	0.007	5.54
Bico 16	7.66	27.23	0.562	0.03933	7.71	1287.40	2.269	12.46	9.96	0.001	42.39
Bico 17	4.70	28.03	0.351	0.06483	14.25	468.00	1.696	6.16	36.56	0.004	9.4
Bico 18	3.69	27.18	0.411	0.05368	20.45	249.40	11.891	119.56	49.01	0.008	10.78
Bico 19	2.73	25.11	0.342	0.06367	18.82	367.80	6.024	33.43	34.88	0.008	5.66

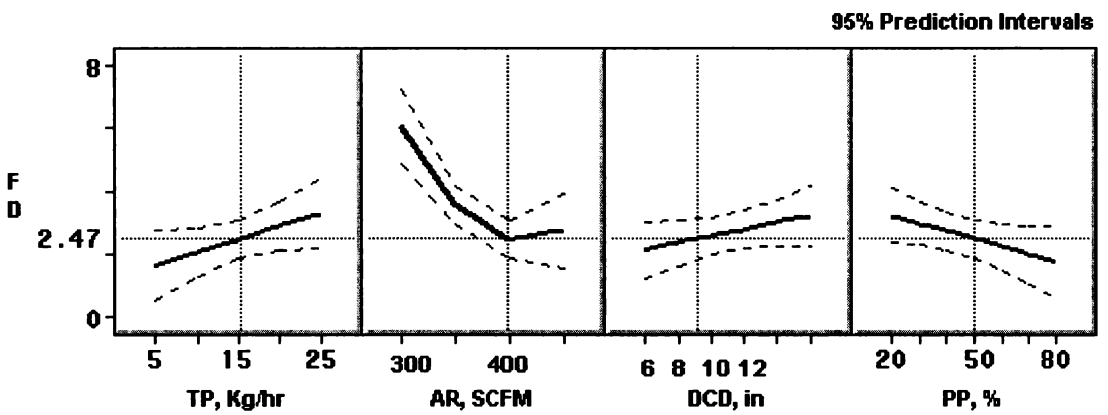

Figure 4.2-2. The predicted effect trends of processing variables on the PP_{35MFR} /PET fiber diameter

notably. This result agrees with the observations reported in the literature [Khan, 1993, and Haynes, 1991], although those observations are mainly for mono-component MB. It seems that this decreasing trend levels off as the airflow rate reaches about 400 SCFM. The reason for this is not clear at this time. The effects of throughput, DCD, and weight percentage of PP were apparently less significant.

The Figure 4.2-2 and the statistical analysis indicated that airflow was the only factor that had a significant over-all effect and the noise level unexplained by the model was too high to estimate the effects of other factors accurately. Further experimentation should be performed before a firm statement is made concerning the underlying process.

Thus, additional trials on both mono- and bi-component systems were added to the above-described central composite response surface design. The operational conditions and the web properties are listed in Table 4.2-4 and Table 4.2-5, respectively. An RSREG procedure from the SAS® statistical package was performed to build a quadratic response-surface regression model. This model was used to search for factor values that optimize the response. The additional experiments provided information to ensure the exploration of the effects of all the factors. As shown in (Appendix F), the model should include linear, quadratic and cross-product terms, although the cross-product terms are comparatively less significant.

The statistical tests on the contribution of each variable, i.e. TP, AR, DCD and PP, indicate that omitting anyone of them will result in a poorer fit of the

model, because they are all statistically significant factors with a P-value level of 0.001. Their effects on the fiber diameter (response) decrease in the order of AR, PP%, DCD and TP.

Because the primary goal of this phase of research was to investigate each factor, all the terms are kept in the model, as shown in the model equation 4.2-1. This model gave an R^2-value of 0.9406, which was made up of 0.6769 of linear terms, 0.1725 of quadratic terms and 0.0912 of cross-product terms. R^2-value is a measure for the fit of a model to the actual data. The ideal model has an R^2-value of 1. This model will be used to predict the effects of the four operation parameters.

$$\begin{aligned} FD = {} & 16.338 + 2.063\times10^{-1}\cdot TP - 5.784\times10^{-2}\cdot AR - 2.353\times10^{-1}\cdot DCD - 7.883\times10^{-2}\cdot PP \\ & - 5.62\times10^{-3}\cdot TP^2 + 6.514\times10^{-5}\cdot AR^2 + 1.163\times10^{-2}\cdot DCD^2 + 3.875\times10^{-5}\cdot PP^2 \\ & - 3.53\times10^{-4}\cdot AR*TP + 1.484\times10^{-2}\cdot DCD*TP - 2.020\times10^{-5}\cdot PP*TP \\ & - 2.06\times10^{-4}\cdot DCD*AR + 1.96\times10^{-4}\cdot PP*AR - 2.058\times10^{-3}\cdot PP*DCD \end{aligned}$$

.....(4.2-1)

The statistical analysis (Appendix F) shows that the response surface has a saddle point, indicating the surface is not a simple hill or valley shape. Therefore, neither a maximum nor a minimum exists within the range of experimentation. However, the ridge analysis provided the direction for smaller fiber diameter, i.e., a lower throughput, a higher air rate, a smaller DCD and a higher PP weight percentage. It should be noted that this result is from a set of experiments at a fixed die and air temperature and fixed die geometry.

Table 4.2-4. The additional experiments to the response surface design with Ta =Td =599°F (315°)

Run ID	TP Kg/hr	AR SCFM	DCD Inch	PP Wt %
Prof-1	15.0	350.0	19.0	100.0
Prof-2	15.0	450.0	19.0	100.0
Prof-3	7.5	450.0	19.0	100.0
Prof-4	15.0	450.0	19.0	50.0
Prof-5	15.0	450.0	19.0	25.0
Prof-6	15.0	450.0	19.0	75.0
Prof-4.1	15.0	350.0	19.0	50.0
Prof-7	15.0	450.0	15.0	0.0
Bico-20	19.3	500.0	10.0	47.6
Bico-21	19.8	500.0	10.0	23.4
Bico-22	18.8	550.0	14.0	73.1
Bico-23	19.8	500.0	10.6	23.4
Bico-24	15.0	497.0	11.0	25.1
Bico-25	20.7	500.0	10.0	26.0
Bico-26	14.5	349.0	11.0	73.0
Bico-27	10.0	250.0	7.1	52.7
Bico-28	15.0	350.0	5.1	25.1
Bico-29	22.4	350.0	10.1	25.5
Bico-30	16.0	345.0	16.8	25.4

Table 4.2-5. The selected web properties of the additional experiments in Table 4.2-4

Run ID	F. Dia μm	B. Wt g/m^2	Thickness mm	P. Density	HH[1] cm	AP ft^3ft^2/min	Tenacity MPa	FR mg-cm	LFE %	ΔP^2 inch-water	Pore Size μm
Prof-1	2.34	26.16	0.409	0.07107	30.63	191.40	6.371	15.77	52.16	0.006	3.89
Prof-2	1.66	25.95	0.419	0.06881	33.09	164.00	7.092	16.43	55.19	0.010	2.95
Prof-3	1.41	18.39	0.337	0.06063	62.74	170.80	4.532	3.42	51.78	0.011	3.22
Prof-4	3.77	24.58	0.514	0.04262	16.63	456.40	3.522	20.56	32.98	0.004	17.65
Prof-5	4.63	28.37	0.581	0.0396	11.72	552.20	1.341	23.73	36.27	0.003	25.26
Prof-6	3.0	23.82	0.453	0.05201	19.57	361.78	4.749	26.42	38.17	0.007	9.35
Prof-4.1	4.51	25.32	0.538	0.04195	10.27	581.60	3.248	37.24	31.23	0.003	21.83
Prof-7	5.18	24.07	0.397	0.04511	9.74	415.16	2.063	4.16	48.38	0.004	21.57
Bico-20	3.08	--	--	--	--	--	--	--	--	--	--
Bico-21	2.96	--	--	--	--	--	--	--	--	--	--
Bico-22	3.76	--	--	--	--	--	--	--	--	--	--
Bico-23	3.12	--	--	--	--	--	--	--	--	--	--
Bico-24	2.75	--	--	--	--	--	--	--	--	--	--
Bico-25	2.63	--	--	--	--	--	--	--	--	--	--
Bico-26	2.85	--	--	--	--	--	--	--	--	--	--
Bico-27	3.80	--	--	--	--	--	--	--	--	--	--
Bico-28	3.69	--	--	--	--	--	--	--	--	--	--
Bico-29	3.55	--	--	--	--	--	--	--	--	--	--
Bico-30	4.5	--	--	--	--	--	--	--	--	--	--

The effects of individual variables and their interactions are discussed in the following sections.

Effects of Throughput and Air Rate on the Fiber Diameter

It is reported in the literature that fiber diameter increases with polymer throughput in many cases (e.g., when airflow rate is not also increased), while other operational parameters remain constant. Increased die swell and decreased air-to-polymer flow ratio are the two possible reasons [Khan, 1993]. For bico PP_{35MFR}/PET MB nonwovens, similar trends were found under different conditions, as shown in Figure 4.2-3. However, the extent of throughput effect on fiber diameter was seldom quantified. In the scope of this research, the effect of throughput on fiber diameter is less important than the others. Comparatively, the effect of airflow rate is much more significant. As shown in Figure 4.2-4, fiber diameter decreases notably faster with the increasing airflow rate for the given experimental conditions. However, due to the complexity of the bico MB process and the possible interactions among the processing parameters, a simultaneous investigation of these factors would be more meaningful.

Figure 4.2-5 shows the 3-D plot of fiber diameter with throughput and air rate. The air and die temperatures were set at 315°C, weight percentage of PP_{35MFR} at 50% and DCD at 12 inches. As airflow rate increases, the fiber diameter decreases at all throughput levels in the range of 10 to 25 kg/hr (or from 0.2773 to 0.6933 g/hole/min). Comparatively, fiber diameter changed little with throughput. The interaction of throughput and airflow rate is minimal, as shown in

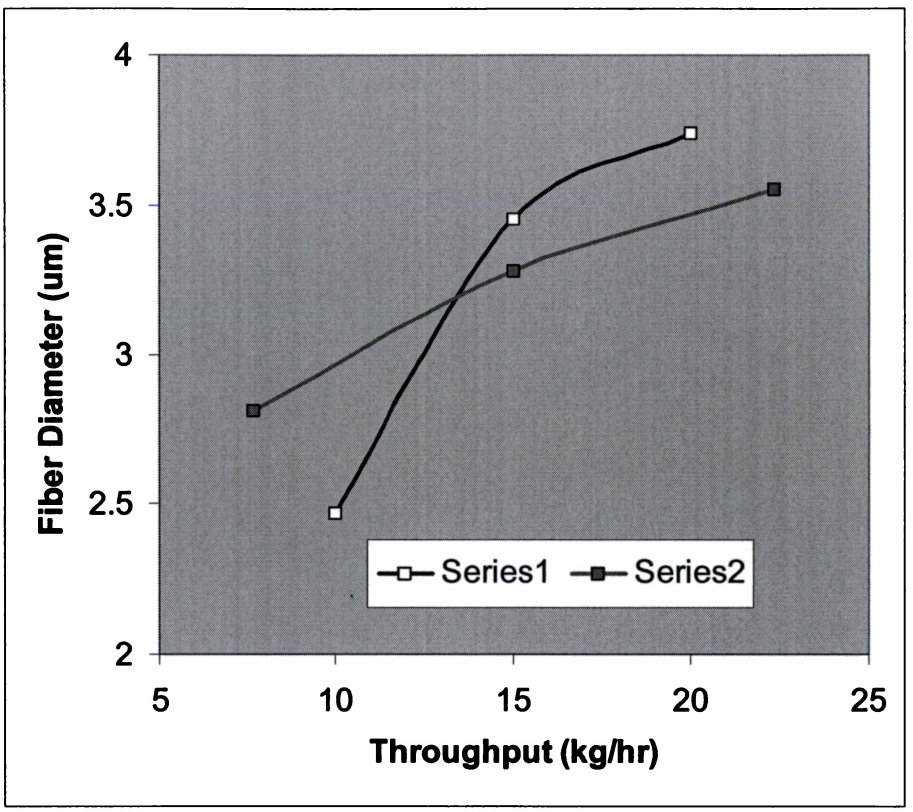

Figure 4.2-3. Effect of throughput on PP_{35MFR} /PET bico MB fiber diameter (Series 1: $T_a = T_d = 315°C$, AR = 450 SCFM, DCD =15 inch. PP% = 52.55% Series 2: $T_a = T_d = 315°C$, AR = 350 SCFM, DCD = 11 inch. PP% = 25.13%)

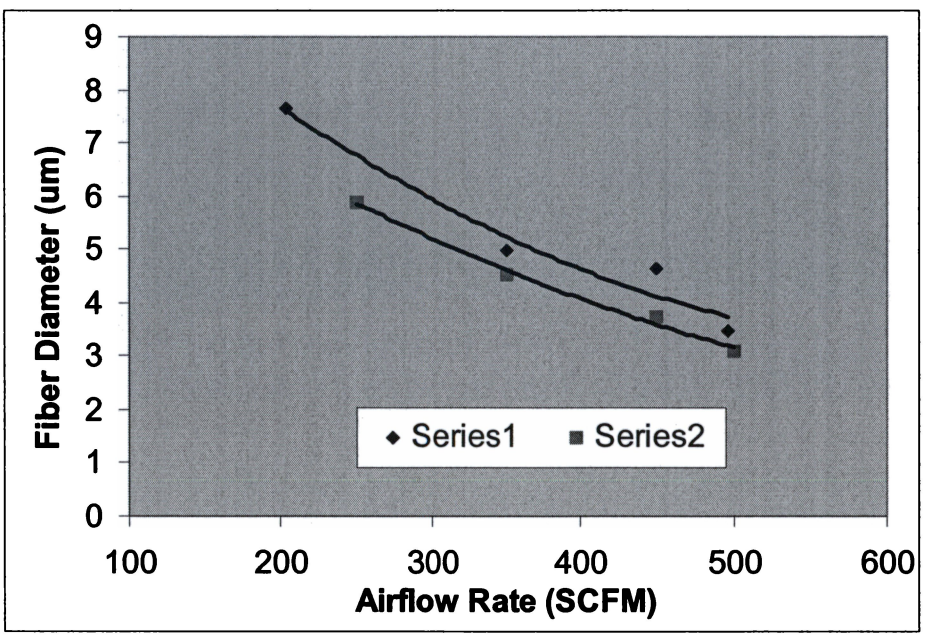

Figure 4.2-4. Effect of airflow rate on PP_{35MFR} /PET bico MB fiber diameter (Series 1: $T_a = T_d = 315°C$, TP = 15 kg/hr, DCD = 11 inch. PP% = 25.13% Series 2: $T_a = T_d = 315°C$, TP = 20 kg/hr, DCD = 15 inch. PP% = 52.55%)

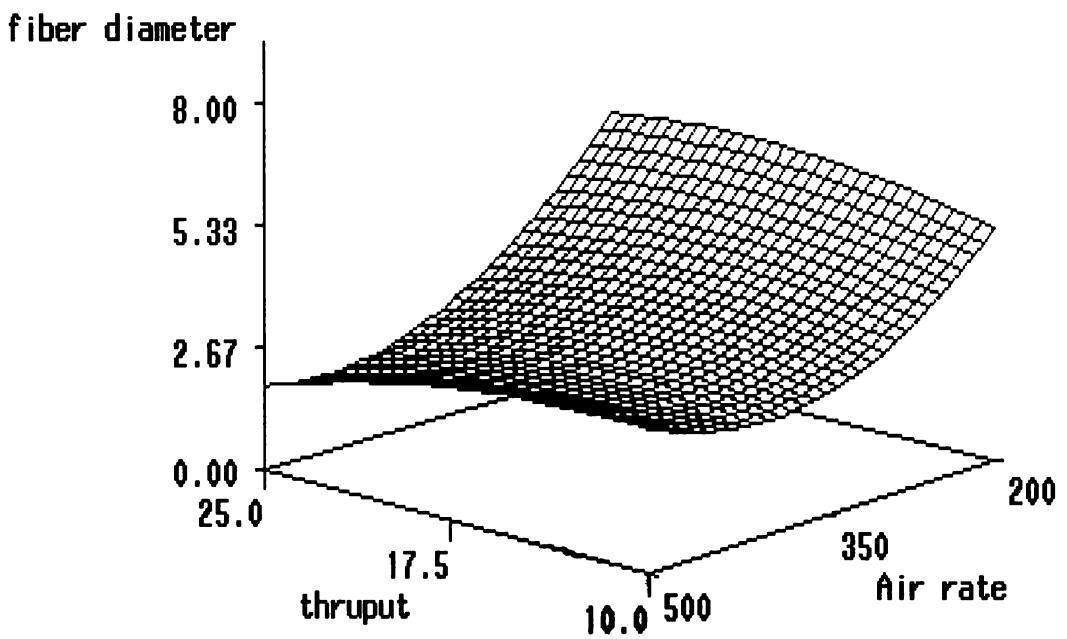

Figure 4.2-5. The effects of throughput and airflow rate on the diameter of PP_{35MFR} /PET fiber
(T_a = T_d = 315°C, DCD = 12.0 inches, PP% = 50.0%)

the statistical analysis (Appendix F). While keeping all conditions the same except for a lower PP percentage of 25%, the basic trends remained. However, fiber diameter was more sensitive to airflow rate at a higher weight percentage level of PET, as shown in Figure 4.2-6.

Effects of PP_{35MFR} Weight Percentage and Air Rate on Fiber Diameter

As noted earlier, the weight percentage of PP_{35MFR} in the polymer system is the second most significant variable after airflow rate. In Figure 4.2-4, higher PP_{35MFR} percentage, at least partially, resulted in smaller fiber size, although the throughput and DCD are different for the two series. This result agrees with the general observations that with PP_{35MFR}, it is easier to produce smaller fiber than with PET. Among several other possible reasons, the differences in thermal and rheological properties of the two polymers are the major contributors.

Figure 4.2-7 showed effects of PP weight percentage and airflow rate on the fiber diameter with a throughput of 20 kg/hr and a DCD of 10 inches. At a lower airflow rate, the fiber diameter was inversely related to the PP_{35MFR} weight percentage. As the airflow rate increases, the effect of PP% decreased and it became minimal at about 500 SCFM. In general, a higher airflow rate will result in a lower average fiber size. However, the degree of effect varies with the PP_{35MFR} weight percentage. In other words, the effect of airflow rate on the fiber diameter depends on the PP_{35MFR} weight percentage. Therefore, the interaction between percentage of PP and AR is notable, as also indicated in the statistical analysis (Appendix F). Similarly, polymer ratio and DCD exhibit an interaction as shown in Figure 4.2-8

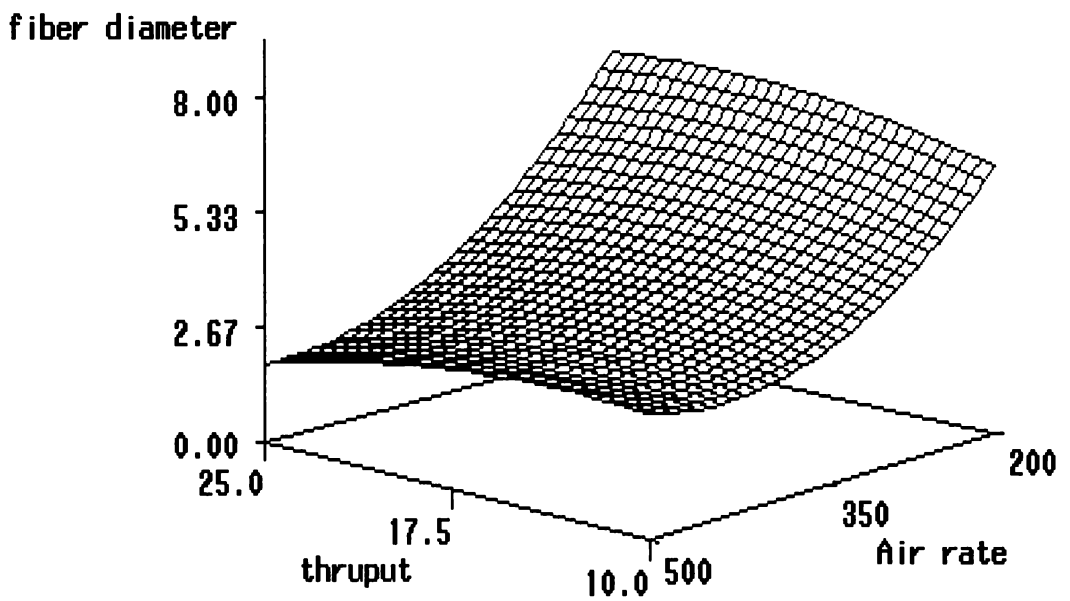

Figure 4.2-6. The effects on fiber diameter of throughput and air rate at a lower weight percentage of PP_{35MFR}
(T_a = T_d = 315°C, PP% = 25.1%, and DCD = 12 inches)

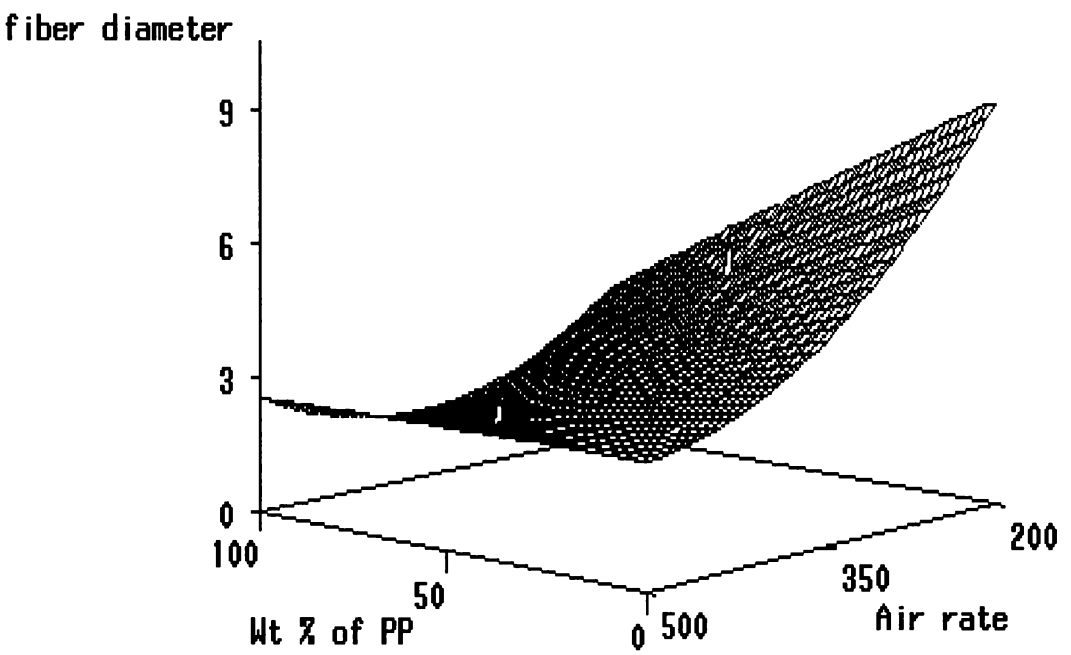

Figure 4.2-7 The effects of airflow rate and weight percentage of PP_{35MFR} on the fiber diameter
($T_a = T_d = 315°C$, TP = 20 kg/hr, and DCD = 10 inches)

Effects of DCD and Throughput on the Fiber Diameter

In this study, the results showed that the DCD affects the average fiber diameter to a different extent depending on the other operational conditions. This observation appears different with the results obtained on 35 MFR PP by Khan (1993), where the DCD effect on fiber diameter was negligible in the range of 8 to 25 inches from the die. Figure 4.2-9 illustrates the effect of DCD on the fiber diameter. Obviously, the fiber diameter is more responsive to higher throughput, where a lower DCD results in smaller fibers. Although the DCD basically defines the filament flying distance, it does not necessarily control the total drag force placed on the filaments by the air jet. Therefore, other reasons need to be explored to understand this observation.

Figure 4.2-10 shows the predicted effects of DCD and throughput on the fiber size for a 50%PP_{35MFR} /50%PET system and an airflow rate of 450 SCFM. It can be seen that the effect of one variable depends on the other. At very low DCD, such as 4 inches, the fiber diameter decreases as the throughput increases. At a medium DCD, such as 12 inches, the fiber diameter profile with throughput apparently shows a maximum. When the DCD is as high as 19 inches, fiber diameter decreases with polymer throughput. Since DCD is related to the traveling distance of both filaments and air jet, it may have an effect on both filament and air jet temperature decay profiles. As DCD influences the air drag force, its effect on the temperature profile may be more significant, which consequently affects the total average elongational viscosity of the filaments.

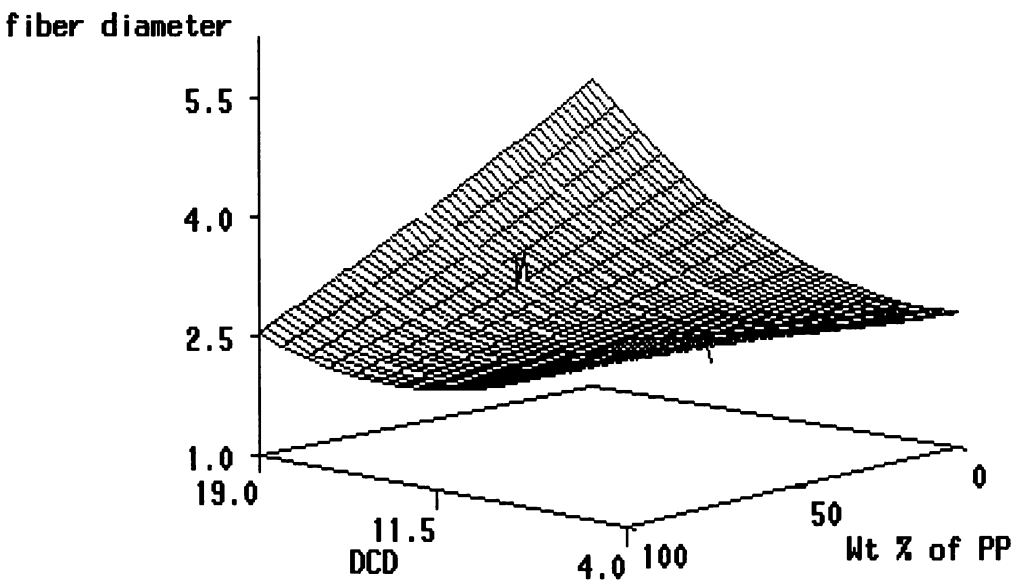

Figure 4.2-8. The effects of DCD and weight percentage of PP_{35MFR} on the fiber diameter
($T_a = T_d = 315°C$, TP = 15 kg/hr, and AR = 450 SCFM)

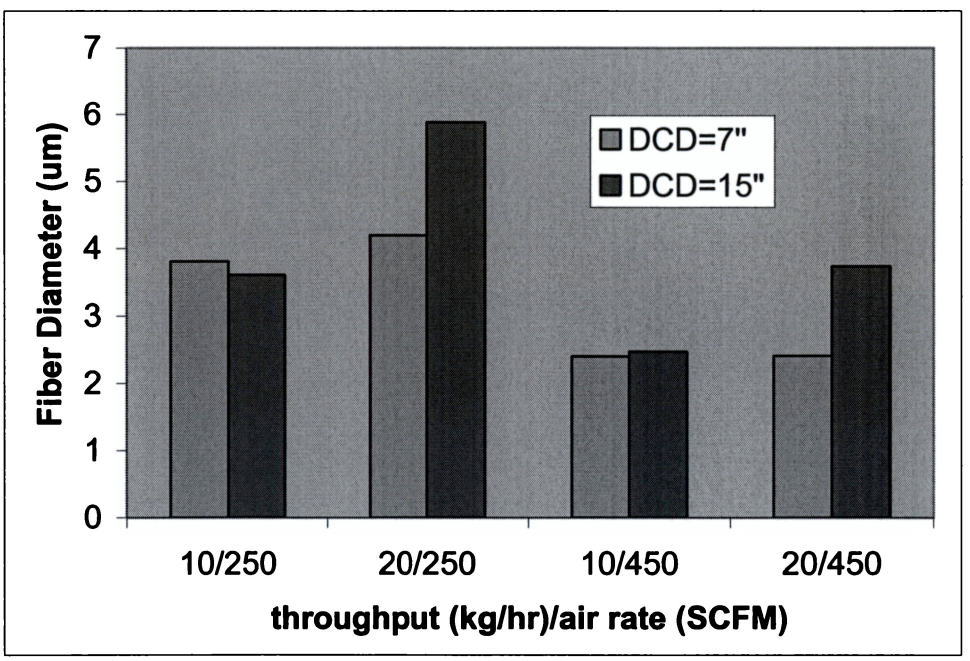

Figure 4.2-9. Effects of DCD and throughput on the fiber diameter (T_a = T_d = 315°C, PP%=52.6%)

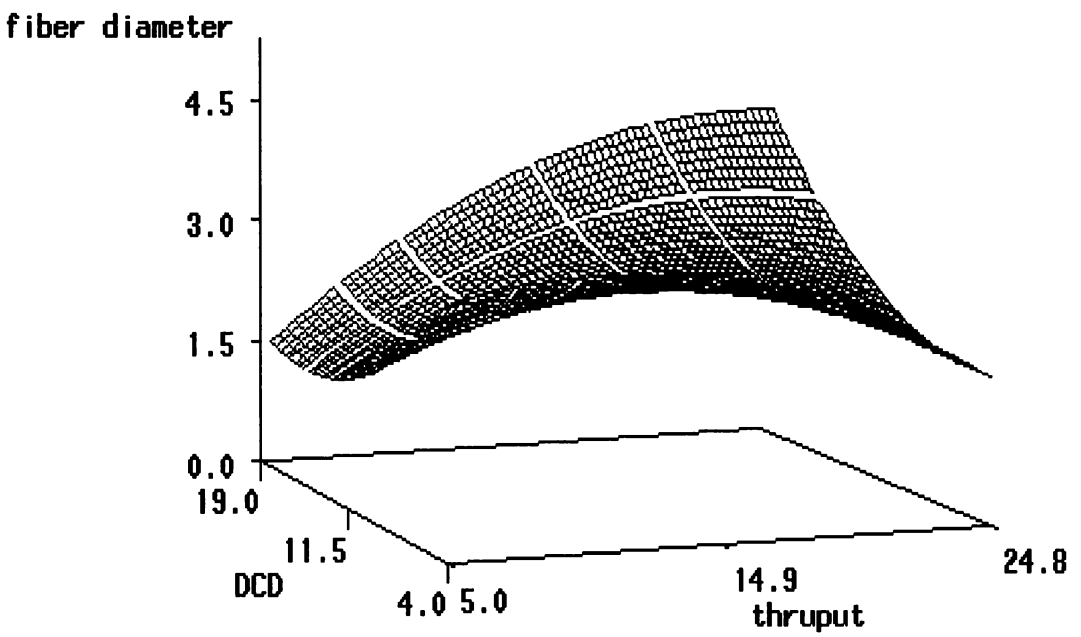

Figure 4.2-10. The effects of DCD and throughput on the fiber diameter (T_a = T_d = 315°C, PP% = 50 %, and AR = 450 SCFM)

Figure 4.2-11 shows the predicted effects of DCD and throughput on the fiber size under the same conditions as in Figure 4.2-10 except for the airflow rate of 250 SCFM instead of 450 SCFM. One can see the similar response surface profile with overall higher fiber diameter.

These results indicate that a general conclusion on either DCD or polymer mass flow rate (throughput) can be suspicious until other operational conditions are specified. Although the reasons for this seemingly complex observation are not currently clear, it may be closely related to the thermodynamic properties of the polymer system and the whole process. An attempt has been made to gain a better understanding of this phenomenon and the fundamentals of the bico MB process. The results will be discussed in Chapter 4, Phase 3 of this dissertation.

Effect of Airflow Rate on the Fiber Diameter Distribution

Although the final average fiber diameter is normally reported, the fiber size distribution during the process of attenuation is more or less ignored by many researchers. Monitoring the fiber distribution along the spinline may reveal important information on the fundamentals of fiber attenuation, structure development and the effects of processing conditions.

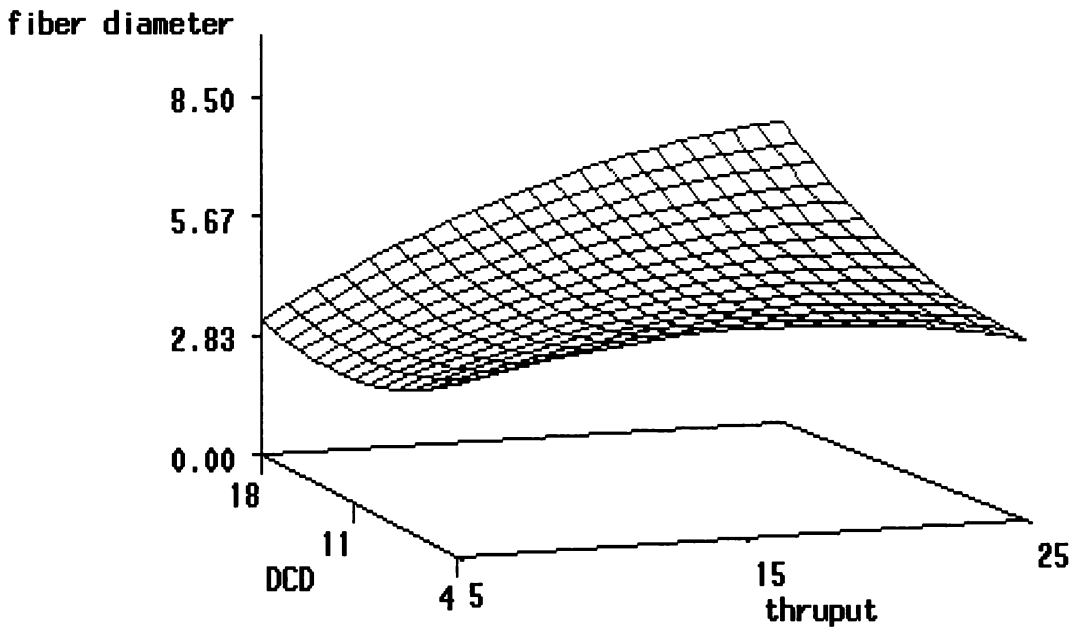

Figure 4.2-11 The effects of DCD and throughput on the fiber diameter (T_a = T_d = 315°C, PP% = 50 %, and AR = 250 SCFM)

Figure 4.2-12 shows PP_{35MFR} fiber diameter distributions at different positions along the spinline. It can be seen that at one inch from the die, the fiber diameter distribution is very broad, covering fiber size from 1 μm to 20 μm with no significant predominance. As the distance-from-the-die (DFD) increases, the predominant population appears at the smaller fiber diameter range and the distribution becomes narrower. At a DFD of 6.5 inches, 92 percent of the fiber population is in the range from 0.5 μm to 4 μm; at 11.5 inches, this number increases to 98%. Therefore, the attenuation of the filament happens all the way in its journey toward the collector and becomes increasingly uniform in fiber size.

Figure 4.2-13 shows PP fiber diameter distributions at different positions along the spinline at a higher airflow rate. The same trends of fiber attenuation development and the changes in fiber diameter distribution can be seen as shown in Figure 4.2-12. The difference between Figure 4.2-12 and Figure 4.2-13 is primarily at the locations near the die. At higher airflow rate, the filament is attenuated to a higher extent with a relatively narrower fiber distribution. It is reasonable by considering the filament temperature and increased air drag force applied onto the filaments at a short distance from the die. The difference between the low and high airflow rate cases appears to have disappeared as the DFD increases up to 4.5 inches. This observation indicates that the effect of airflow rate on fiber attenuation is mainly manifested in a narrow range close to the die. Figure 4.2-14 shows the fiber diameter distributions of 50%PP/50%PET bico filaments at different positions along the spinline. The experiment was conducted under the following conditions: throughput was 15 kg/hr, die

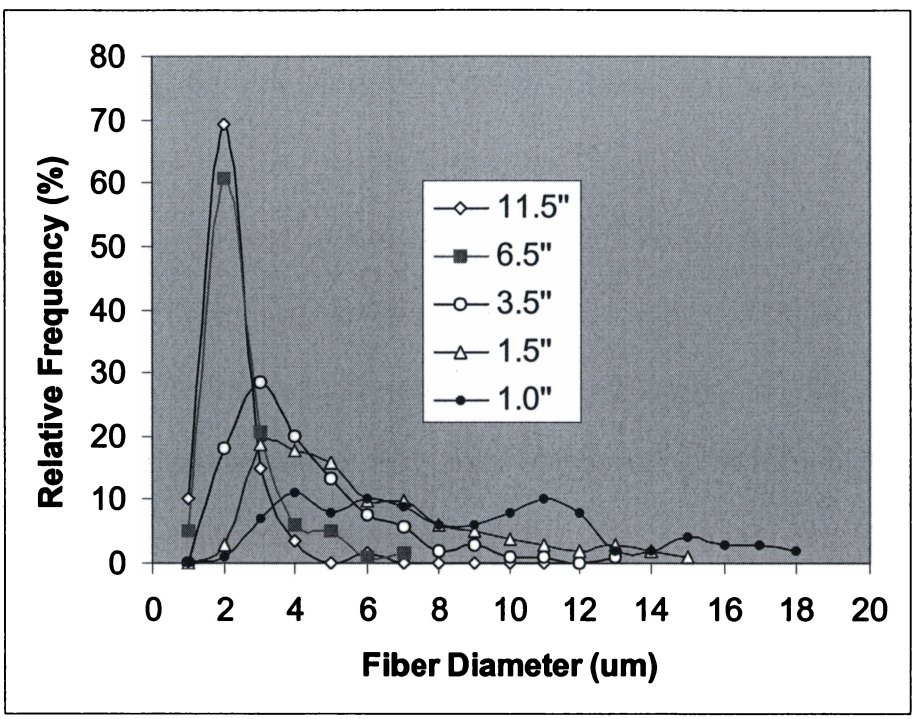

Figure 4.2-12. PP_{35MFR} fiber diameter distributions at different positions along the spinline at an airflow rate of 350 SCFM
(TP =30 kg/hr, T_a = 590°F, T_m = 599°F, AR = 350 SCFM, DCD=19 inches)

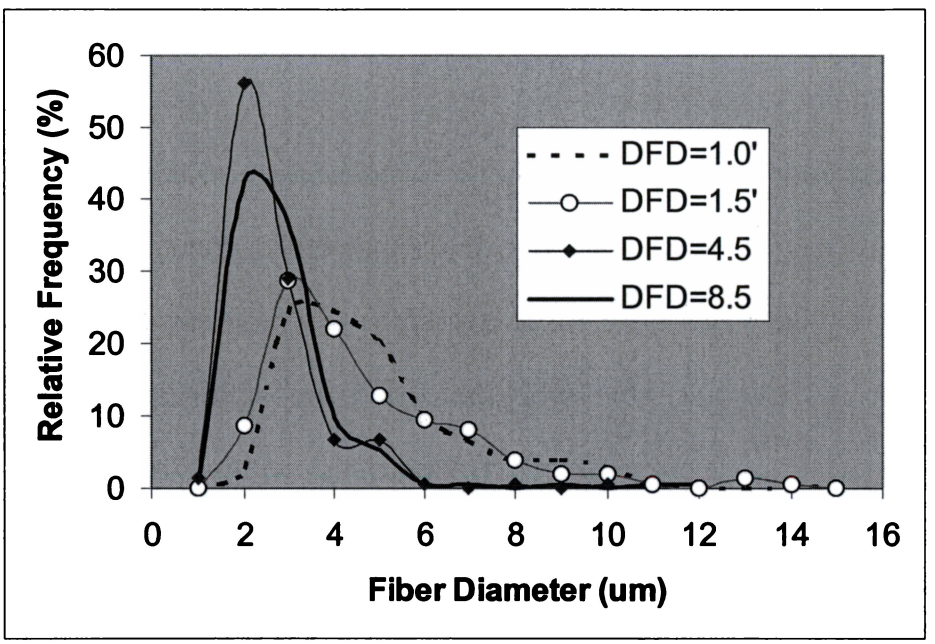

Figure 4.2-13. PP_{35MFR} fiber diameter distributions at different positions along the spinline at an airflow rate of 550 SCFM
(TP =30 kg/hr, T_a = 590°F, T_m = 599°F, AR = 550 SCFM, DCD=19 inches)

temperature and air temperature were set at 599°F, airflow rate at 350 SCFM, and DCD was 19 inches. Again, as the DFD increases, the fiber diameter distribution becomes narrower with the major population in the smaller fiber size region. It seemingly becomes narrower at a higher airflow rate, as shown in Figure 4.2-15. This difference appears at a greater distance from the die, such as 8 inches. In the range close to the MB die, the fiber diameter distribution exhibits similar broadness.

By comparing the fiber diameter distribution profiles of bicomponent filament with those of single PP, one finds that the distribution profile of bico filaments is relatively broader. As discussed in the previous session, the PET component has distinguishable properties, such as high glass transition and melting temperatures. It presents a hindering effect on the filament attenuation, which is responsible for the apparently broad fiber diameter distribution. The other important observation is that the fiber distribution profiles of bico filaments exhibit a double-peak, although one of the two peaks becomes stronger than the other as the DFD approaches 8 inches. It may relate to the property differences of the two components, but the exact reasons for this phenomenon are not clear at this point.

In summary, airflow rate affects the fiber diameter profiles differently for 100% PP and PP/PET bicomponent filaments. A higher airflow rate leads to a relatively narrower fiber diameter distribution for the bico MB filaments.

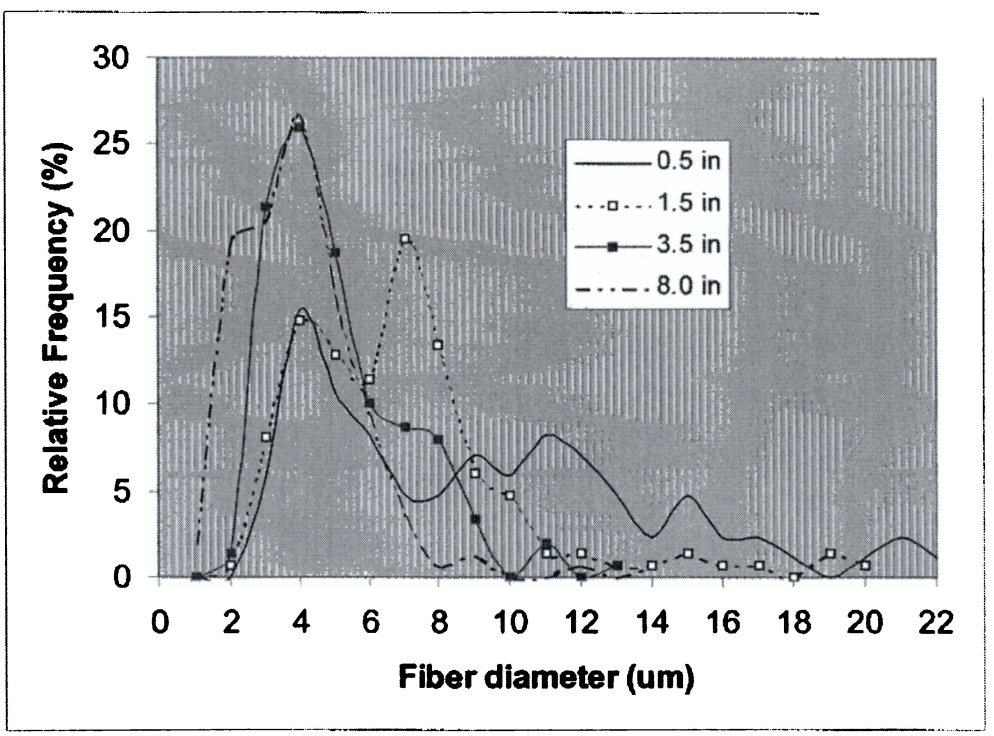

Figure 4.2-14. Fiber diameter distributions of 50%PP_{35MFR} /50%PET bico filaments at different positions along the spin-line at an airflow rate of 350 SCFM (TP = 15 kg/hr, Ta = Tm = 599°F, AR = 350 SCFM, DCD = 19 inches)

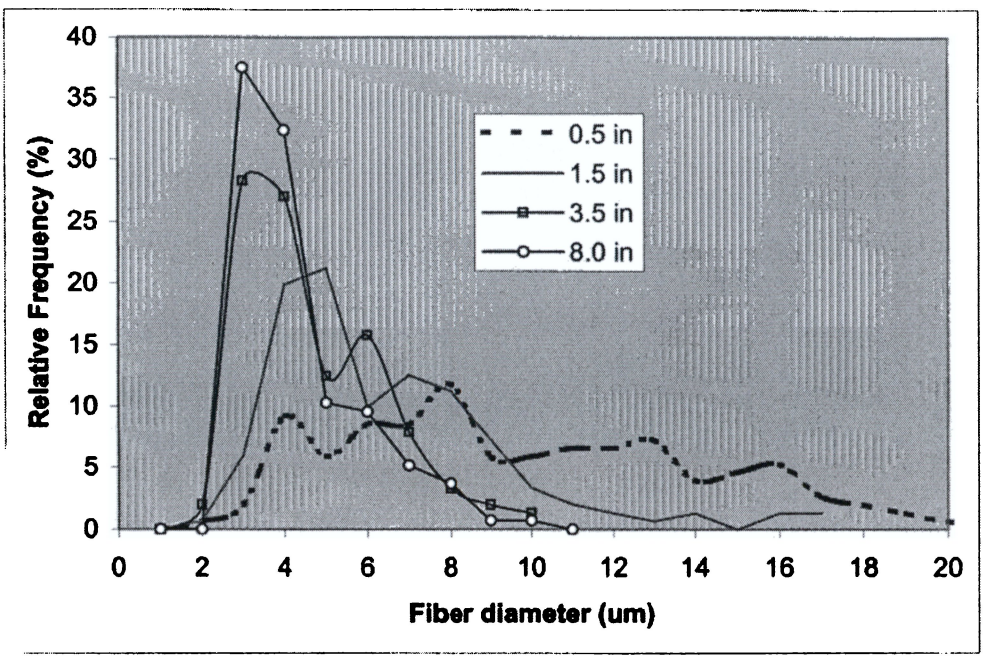

Figure 4.2-15. Fiber diameter distributions of 50%PP_{35MFR} /50%PET bicomponent filaments at different positions along the spinline at an airflow rate of 450 SCFM
(TP = 15 kg/hr, Ta = Tm = 599°F, AR = 450 SCFM, DCD = 19 inches)

Effects of Operational Conditions on Web Properties

Effect of Die Temperature Profile on The Polymer Distribution

As discussed in Chapter 4, Phase 1, polymer distribution across the web in PP/PET bico MB nonwovens should be better controlled, especially for the cases in which PET is the predominant component. In this research, the two polymer melts flow and distribute within the same coat-hanger, and their temperatures can not be controlled separately. However, an attempt had been made to investigate the possibility of improving the polymer distribution by adjusting the die temperature profile. The die temperature control system and the experimental temperature profiles are shown in Figure 4.2-16 and Table 4.2-6, respectively. In Case 1, the die temperature was decreased from 315°C (599°F) at the center to 299°C (568°F) at the edge with a polymer ratio of 15%PP_{35MFR} /85%PET. In Case 2, the die temperature was decreased from 315°C (599°F) at the center to 304°C (579°F) at the edge with a polymer ratio of 18%PP_{35MFR} /82%PET. In Case 3, the die temperature was set constant at 315°C across the die width with a polymer ratio of 18%PP_{35MFR} /82%PET. All the other processing conditions of these three cases were kept the same, for example, the total throughputs were all 40 kg/hr. The polymer distribution across the web was determined by DSC method as described in Chapter 3, Experimental, and the data is presented in Figure 4.2-17.

Compared with Case 3, the polymer distribution is more uniform with a controlled multi-temperature profile at the die. It is obvious that the profile of die

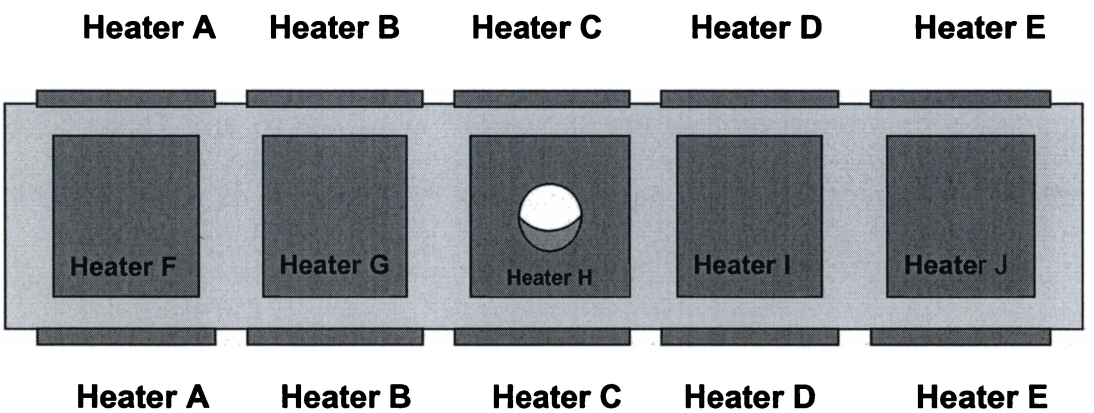

Figure 4.2-16 A schematic of the top view of the vertical MB die heating system

Table 4.2-6. The die temperature profile for PP/PET Bicomponent MB Trials

Heaters at The Die	Temperature (°C)		
	Case 1 15%PP/85%PET	**Case 2** 18%PP/82%PET	**Case 3** 18%PP/82%PET
Heater A	299	304	315
Heater B	304	310	315
Heater C	315	315	315
Heater D	304	310	315
Heater E	299	304	315
Heater F	299	304	315
Heater G	304	310	315
Heater H	315	315	315
Heater I	304	310	315
Heater J	299	304	315

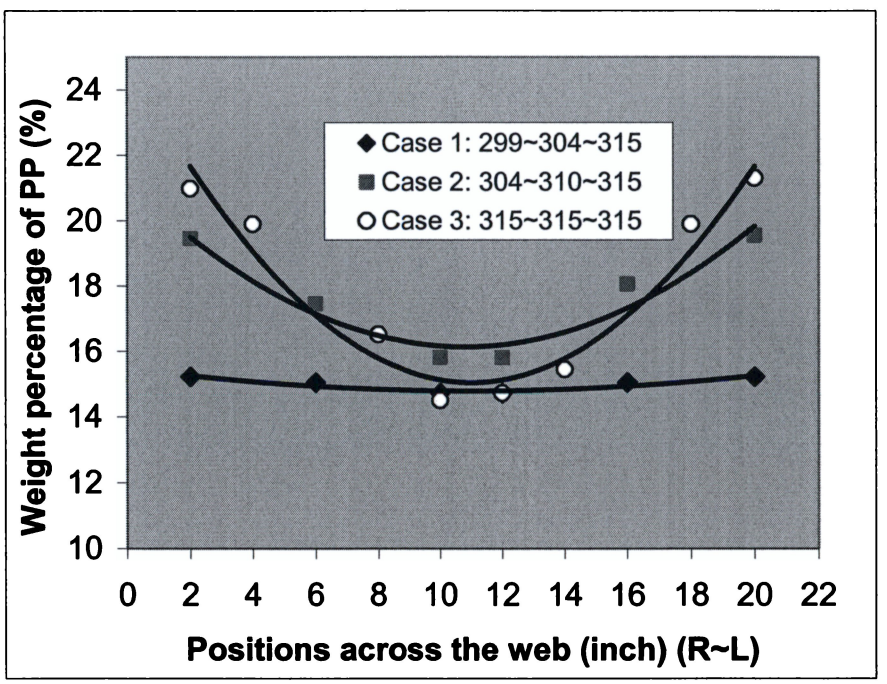

Figure 4.2-17. Improving polymer distribution across the MB web by adjusting the die temperature profile.
(Case 1: 15%PP_{35MFR} /85%PET, Cases 2, 3: 18%PP_{35MFR}/82%PET.
The die temperature profiles are listed from edges to enter with the unit of °C)

temperature has an effect on the polymer distribution. Therefore, it is practical to improve the polymer distribution across the web by adjusting the MB die temperature profile. When PET is the major component in the bicomponent MB fibers, the die temperature profile, such as in Case 1, is necessary for better polymer distribution across the MB web. This observation may result from the differences in heat transfer effectiveness of the two components. Because the PET phase takes the major volume of the coat-hanger, it apparently flows quicker but is relatively slow in changing temperature, which results in minor viscosity variation. On the other hand, PP melt is a much thinner layer in the coat-hanger, it may respond faster to the die temperature profile, resulting in increased viscosity while flowing towards the edges of the die. This effect probably led to the viscosity match of the two polymer melts and improved polymer distribution across the coat-hanger width. It is expected that a suitable die profile should be explored for a particular situation. Since the polymer melt viscosity is a function of temperature and shear rate (among other), as polymer ratio and throughput varies, the viscosity match will change correspondingly. Therefore, the die temperature profile should be adjusted to minimize the viscosity mismatch, accordingly.

Effect of Operational Conditions on Web Structure

The nonwoven web structure may be described by many parameters depending on the final application, which include, but are not limited to fiber diameter, fiber size distribution, fiber orientation, fiber distribution, packing

density, basis weight, thickness, pore size, pore orientation, and web uniformity. In melt blowing, fiber diameter, fiber distribution, packing density, and basis weight are directly controlled by the operational conditions. Many other web structure properties are functions of one or more of these inherent characteristics. The effects of the selected processing conditions on the fiber diameter and their distributions have been discussed previously. This part will explore the effects of selected processing conditions on the packing density and average pore size.

The packing density c, is defined and calculated by the following equation,

$$c = \frac{volume\ of\ fiber}{volumeofmedium} = \frac{basis\ weight\ (g/cm^2)}{Thichness\,(cm) \times \rho\,(g/cm^3)} \qquad (4.2\text{-}2)$$

where ρ is the polymer density normally measured by a density gradient column. In this study, the density of PP is 0.91 g/cm^3, and the density of PET is 1.34 g/cm^3. The density of the PP/PET bicomponent filament is determined by the following relation, assuming the simple rule of mixtures applies,

$$\rho_{bico} = PP_{Wt}\% \cdot \rho_{PP} + PET_{Wt}\% \cdot \rho_{PET} \qquad (4.2\text{-}3)$$

$$PP_{Wt}\% + PET_{Wt}\% = 1 \qquad (4.2\text{-}4)$$

The average pore size is calculated from the following relationships, adapted from Tsai (1999) and Langmuir (1942)

$$\overline{D}^2 = \frac{32 d_f{}^2}{(1-c)^2 \cdot f(c)} \qquad (4.2\text{-}5)$$

$$f(c) = \frac{1.4 \times 4c}{-\ln c + 2c - 0.5c^2 - 1.5} \qquad (4.2\text{-}$$

where d_f is fiber diameter, c web packing density, and $\overline{D}$ is average circular-capillary-equivalent pore size (average pore size, hereafter).

For a given polymer system, the packing density of a nonwoven web is a dependent variable on the fiber diameter, fiber distribution, bonding properties, and some others, which are governed by the processing conditions. Therefore, packing density is indirectly controlled by the processing parameters. Similarly, the average pore size, which is strongly related to fiber diameter and packing density, should also be influenced by the processing conditions.

The relationships among measured fiber diameter (OP method), packing density, and the calculated average pore size are presented in Figure 4.2-18. As fiber diameter increases, for the almost randomly oriented MB web, there will be more room left among the fibers, leading to a larger average pore size. If the web is more densely packed, the fibers will be squeezed closer together, which results in a smaller average pore size. Since the average pore size is a function of both fiber diameter and packing density, they are closely related to each other. There is a strong correlation between the average circular-capillary-equivalent pore size and the ratio of fiber diameter and packing density, alternatively reflecting the relationship presented in Tsai's equation 4.2-5.

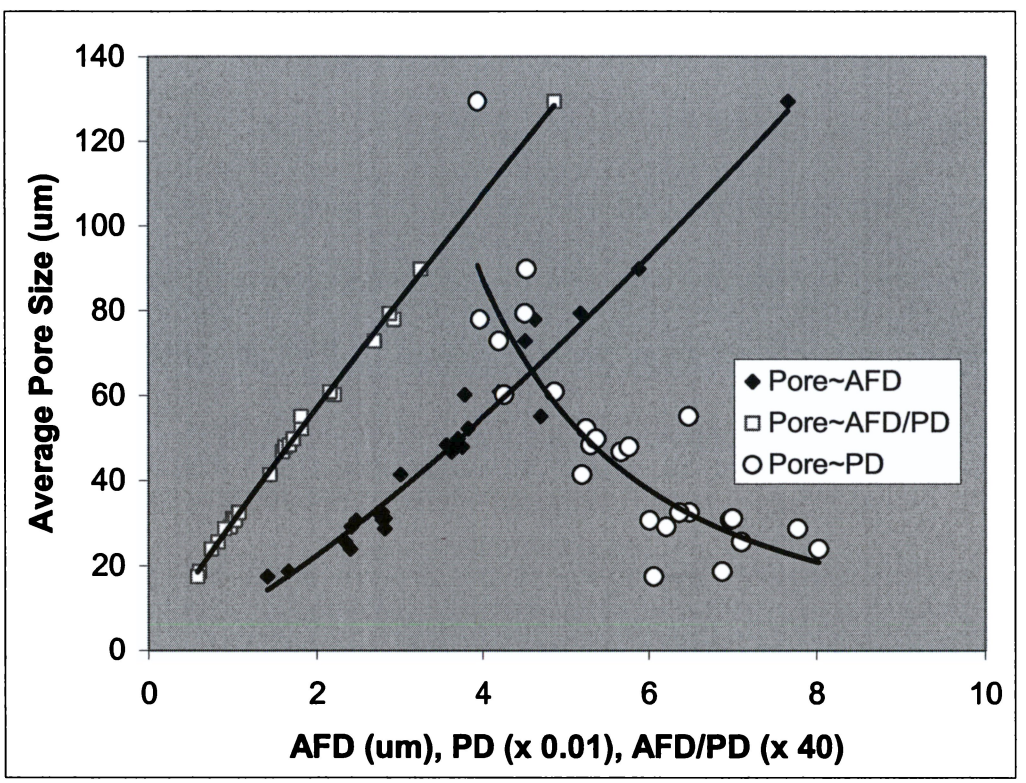

Figure 4.2.18. The relationships among average fiber diameter (AFD), packing density (PD), and the calculated average pore size

Since the ratio of average fiber diameter (AFD) and the packing density (PD) encompasses important web structural information, it also correlates very well with their performance properties, such as latex filtration efficiency (LFE), hydrostatic head (HH), and air permeability (AP), as shown in Figure 4.2-19. Under normal MB processing conditions, average fiber diameter inversely relates to the packing density. Therefore, the web with finer fiber is usually packed denser with smaller pore size, which leads to higher LFE, higher HH, and lower AP.

In melt blowing, all the processing conditions that contribute to the ratio of AFD/PD will affect web structure, and consequently affect performance properties, such as air permeability, hydrostatic head and filtration efficiency. There is no doubt of the importance of exploring the effects of the processing conditions on this ratio.

Figure 4.2-20 shows the effects of throughput and the airflow rate on the AFD/PD ratio with a die temperature 315°C, a weight percentage of PP 25%, and a DCD 8 inches. It is clear that the web structure changes dramatically with the airflow rate. Within a throughput range from 10 kg/hr to 25 kg/hr, the AFD/PD ratio increases monotonically, as the airflow rate decreases. At a high airflow rate, the filaments are attenuated further and accelerated to a higher velocity, which results in greater packing density. Under these processing conditions, the effect of throughput seems to be minimal.

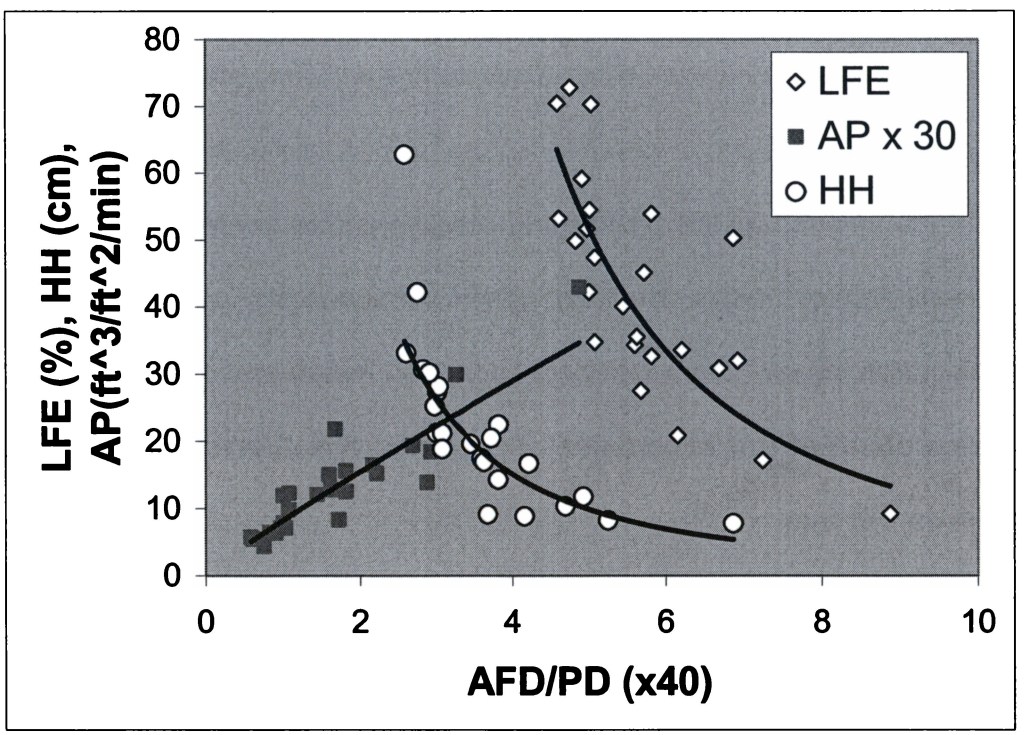

Figure 4.2-19 The relationships among AFD/PD, Latex filtration efficiency (LFE), hydrostatic head (HH), and air permeability (AP)

(For better presentation, the LFE curve is shifted right 4 units; the HH curve is shifted right 2 units. AFD = average fiber diameter, PD = packing density)

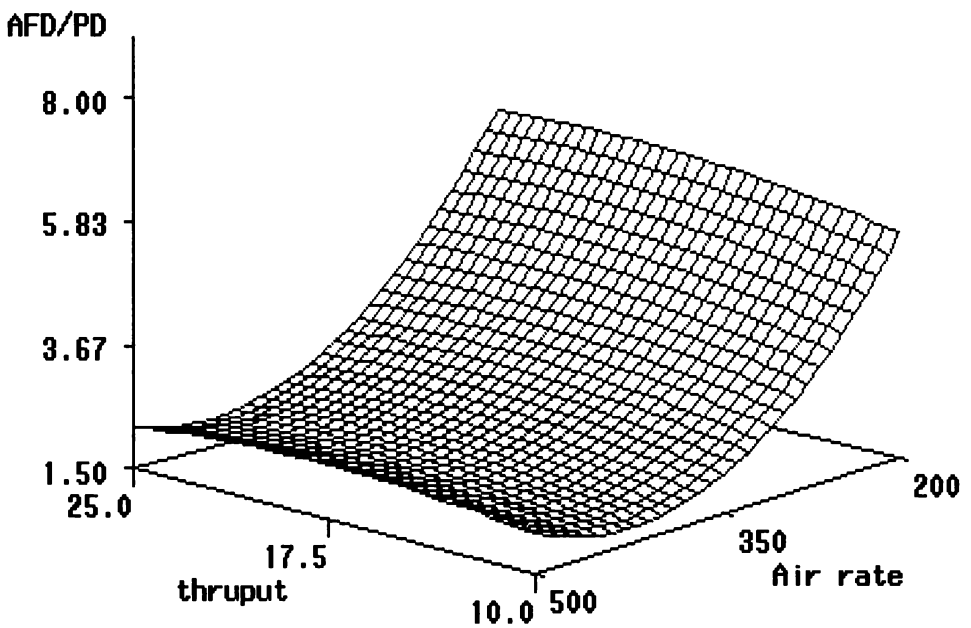

Figure 4.2-20 The effect of throughput and airflow rate on the ratio of AFD/PD

(T_a = T_d = 315°C, PP% = 25%, and DCD = 8 inches, AFD = average fiber diameter, μm; PD = packing density)

Figure 4.2-21 shows the effects of throughput and DCD on the AFD/PD ratio with a die temperature 315°C, a weight percentage of PP 50%, and an airflow rate 450 SCFM. The response surface appears twisted, showing that the effect of DCD on AFD/PD dependents on throughput. At a high throughput, such as 25 kg/hr, the ratio of AFD/PD increases proportionally with the DCD. At a low throughput, such as 5 kg/hr, AFD/PD was inversely related to DCD. By comparing with the results shown in Figure 4.2-10, one finds that the fiber diameter plays the predominant role in the ratio of AFD/PD.

Figure 4.2-22 shows the effects of weight percentage of PP and DCD on the AFD/PD ratio with a die temperature 315°C, a throughput 15 kg/hr, and an airflow rate 450 SCFM. It is reasonable that the AFD/PD increases with the weight percentage of PET in the bicomponent filaments. Under the same conditions, an increased weight percentage of PET leads to relatively high fiber diameter and low packing density; therefore, the ratio of APD/PD is high. This result suggests that the lowest possible percentage of PET in the bicomponent MB filaments should be selected, when higher filtration efficiency and high water repellency are desired.

The effect of DCD on the web structure is not significant when PP is the predominant component in the filaments. It appears more important in the case of the higher percentage of PET. This prediction is acceptable because PET is more sensitive to the temperature variation resulting from the change of DCD.

In summary, at a higher airflow rate and a higher PP_{35MFRd} weight percentage in the component filaments, the resulting webs tend to be denser. At a constant polymer ratio and airflow rate, the packing density can be adjusted by changing the polymer throughput. Thus, the ratio of AFD/PD is also closely related to the processing conditions, as shown in Figure 4.2-23.

Phase 3:

A Study of Spinline Dynamics of PP_{35MFR}/PET Bicomponent MB Process

Background and Assumptions

The spinline dynamics of high-speed melt spinning of several bicomponent polymer systems has been studied by different researchers. Recently, Kikutani and colleagues (1996) studied high-speed melt spinning of PET/PP system to investigate the mechanism of fiber structure formation. Radhakrishhan and coworkers (1997) studied high-speed melt spinning of low and high molecular weight PET system. Radhakrishnan and coworkers (1999) also studied ultra-high speed spinning of liquid crystalline copolyester with PET, the fiber structure development, spinnability, and their mechanical properties. The filament take-up speed in these researches ranged from 1000 m/min to 8000 m/min. Although there are significant differences between high-speed melt spinning and melt blowing in detail, they are similar, at least conceptually, in many important components such as the extruder, heater, gear pump and spinneret. According to Yin, Yan and Bresee (1999), the maximum velocity of MB filament is in the range of 40-70 m/s (2400 -4200 m/min) under their experimental

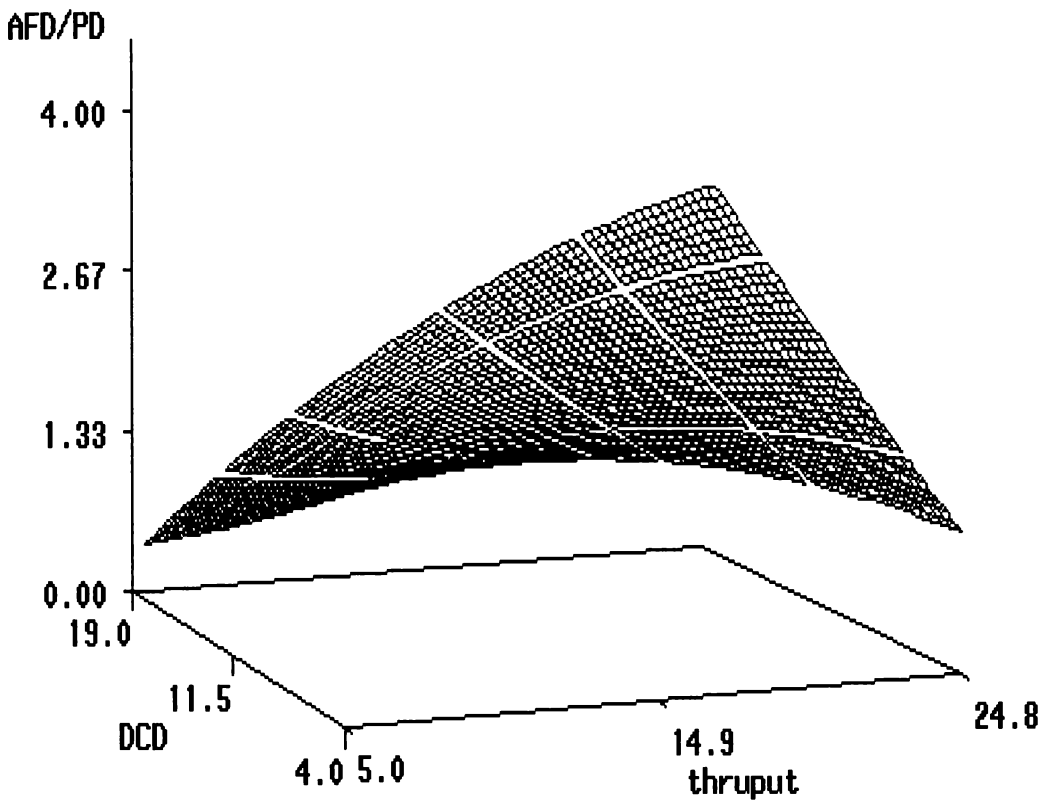

Figure 4.2-21. The effects of throughput and DCD on the ratio of AFD/PD (T_a = T_d = 315°C, PP% = 50 %, and AR = 450 SCFM, AFD = average fiber diameter, μm; PD = packing density)

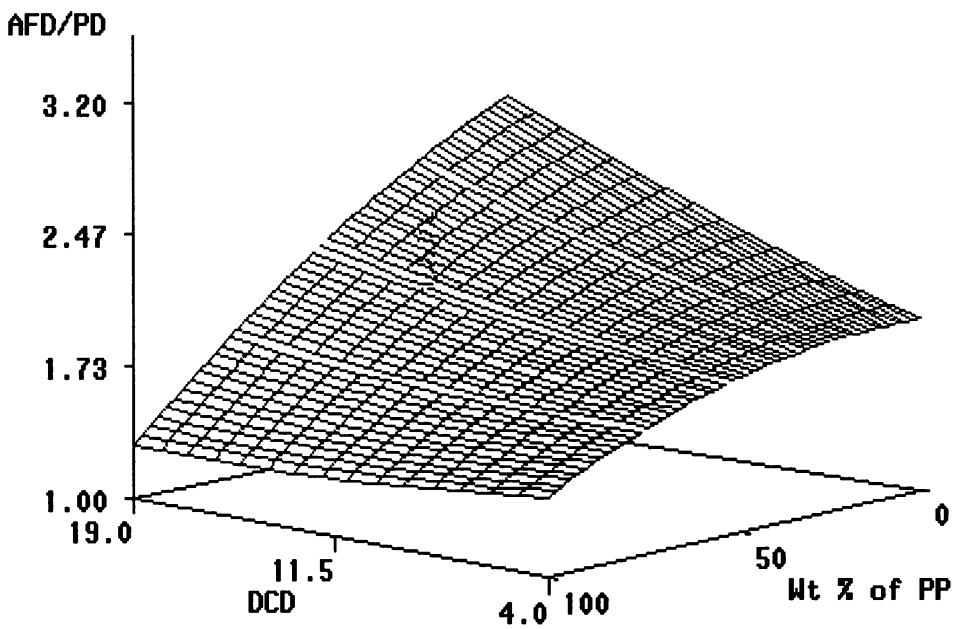

Figure 4.2-22 The effects of DCD and weight percentage of PP on AFD/PD (T_a = T_d = 315°C, TP = 15 kg/hr, and AR = 450 SCFM, AFD = average fiber diameter, μm; PD = packing density)

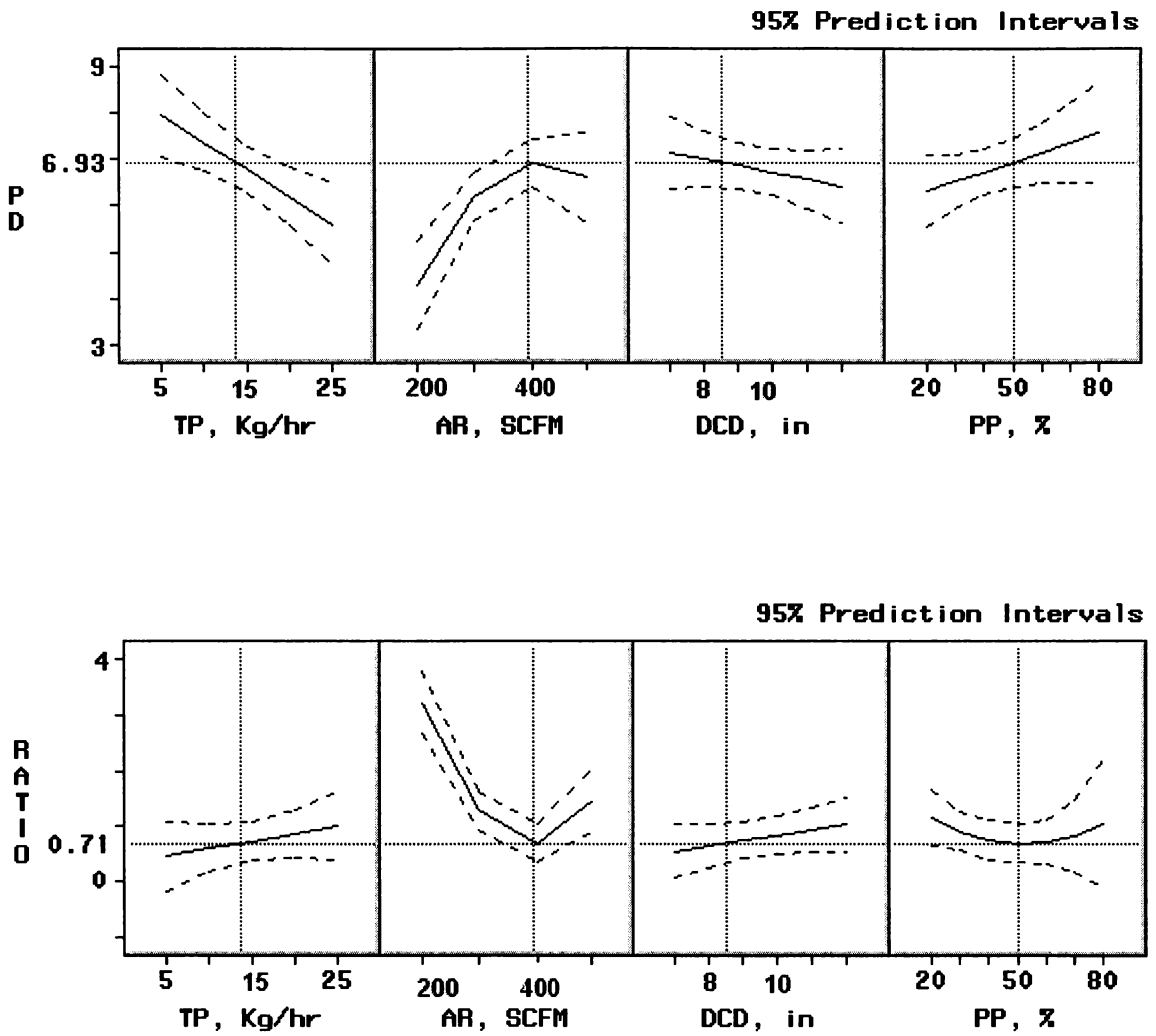

Figure 4.2-23. The predicted relationships among web structure properties and the selected processing conditions
(AFD = average fiber diameter, μm; PD = packing density; ratio = AFD/PD)

conditions. There is no doubt that this number will change with the primary air jet velocity and it can be much higher depending on the MB die setup and the processing conditions employed, such as airflow rate and air temperature. Therefore, the MB filament velocity can be in the range of regular melt spinning and high-speed melt spinning. This section attempts to utilize the basic theories of high-speed melt spinning to explore the spinline dynamics of the melt blown process. In order to do this, the profiles of air jet velocity, air jet temperature, fiber diameter, fiber velocity and fiber temperature need to be determined.

A steady-state Newtonian model is assumed for the bicomponent melt blowing process. The other assumptions include: (1) there is no velocity gradient in a cross section of the bicomponent filament; (2) the temperatures of the two polymers are identical at a cross-section; (3) all extruded polymer is collected on the web-forming collector; (4) the fiber diameter is frozen quickly after collected at an position in the spinline; (5) the melt temperature at the die is uniform across the die width and equal to the die temperature, and (6) there is no fiber splitting during the MB process.

For this study, the principal equations adapted from melt spinning are given as follows:

Mass balance equation:

$$W = W_{PP,1} + W_{PET,1} = W_{PP,2} + W_{PET\,2} \qquad (4.3\text{-}1)$$

Energy balance equation:

$$\frac{dT}{dz} = -\frac{\pi d_f h}{C_{p,PP} \cdot W_{PP} + C_{p,PET} \cdot W_{PET}} (T - T_a) \qquad (4.3\text{-}2)$$

where W, T, z, and C_p are the mass flow rate, filament temperature, distance from the die, and polymer specific heat, respectively. T_a, h, and d_f are air jet temperature, heat transfer coefficient, and average filament diameter, respectively. The subscripts 1 and 2 represent the different locations in the spin-line. Equation 4.3-2 neglects the effects of crystallization during MB processing.

Air Jet Velocity

Haynes (1991) applied the air jet velocity equation from Applied Fluid Dynamics Handbook [1984] to a single-hole MB die to study the air jet velocity decay, The following equation was found to provide the best correlation with the experimental results for the centerline velocity decay of the air jet,

$$\frac{v_a}{v_{j,0}} = 2.92\left(\frac{W}{Z}\right)^{\frac{1}{2}} \quad for\ Z \geq 8.6W \qquad (4.3-3a)$$

$$v_a = v_{j,0} \quad for\ Z \leq 8.6W \qquad (4.3-3b)$$

Since the geometry of the die tip and the final air passage are very similar as that of the 24-inch Reicofil® bicomponent MB pilot line, the above equations will be utilized to determine the air jet centerline velocity profile. The airflow rate

in SCFM used in operation must be converted to the actual airflow rate in order to calculate the air jet velocity at the air knife exit. By assuming the ideal gas law is valid, the air jet velocity at the exit was determined by the following equation [Khan 1993]:

$$Q_a = Q \cdot \left(\frac{T_{a,0}}{530} \right) \cdot \left(\frac{14.5}{P_{a,0}} \right) \qquad (4.3-4)$$

where, Q: the airflow rate in SCFM under standard conditions, (14.5 psi and 70°C)

Q_a: the actual air flow rate, ACFM,

$T_{a,0}$: the actual air jet temperature at the exit, °R, (°R = °F + 459.67), and

$P_{a,0}$: = (14.5+stagnation pressure, psi),

The dimension of the face gap of the 0.8 mm air gap and 1.0 mm setback (0.8/1.0) die geometry was determined as 0.0462 inch x 27.1 inch, i.e. the measured face gap as 0.0462 inch and the span of the face gap as 27.1 inches, under the experimental conditions. Then, the actual air jet velocity at the exit can be calculated by,

$$v_{a,0} = \frac{Q_a}{A_{Air\ \ exit\ \ slot}} \qquad (4.3\text{-}5)$$

Figure 4.3-1 shows the air jet velocity decay profile at different airflow rates. It can be seen that air velocity drops most significantly in the first 2 inches from the die. In this region, the air velocities at various airflow rates generally differ from each another. As the distance from the die (DFD) increases, the air jet velocity decays at a much slower rate and levels off towards zero. The differences among various profiles decrease as the DFD increases, indicating the effects of airflow upon the filaments becomes minimal at a high DFD.

Air Jet Temperature

The centerline temperature of air jet is determined by a bare thermocouple that is mounted to a specially designed stand with a digital thermometer, as show in Figure 3-2. The measurements were conducted for various conditions based on the experimental design and data are presented in Figure 4.3-2. It shows that the air jet temperature decreases dramatically near the die and then drops slowly. At a DCD of 8 inches, the air jet temperature becomes slightly higher than the ambient temperature of 67.1°F at the time of this study. Since the primary air jet proportionally draws in a certain amount of ambient air, it is not surprising to find that the air jet temperature profiles are nearly identical for various operational conditions of this study. These experimental data correlated very well with the following empirical formulation [Haynes, 1991].

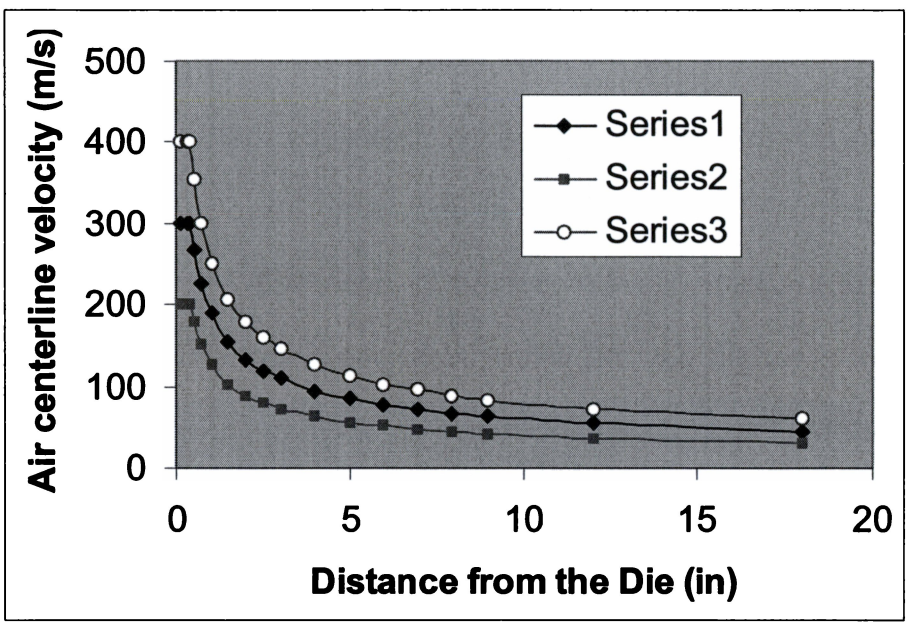

Figure 4.3-1. The air jet velocity decay profile of different airflow rates (Die geometry: 0.8 mm air gap/1.0 mm setback; Series 1: $v_{a,0}$ = 300 m/s; Series 2: $v_{a,0}$ = 200 m/s; Series 3: $v_{a,0}$ = 400 m/s)

$$\frac{T_a - T_\infty}{T_{j,\,0} - T_\infty} = 1.79\left(\frac{w}{z}\right)^{0.465}, \; if \; z \geq 3.5w \qquad (4.3-6)$$

$$T_a = T_{j,\,0}, \; if \quad z \leq 3.5w \qquad (4.3-7)$$

where, T_∞ : the ambient temperature,

$T_{j,0}$; air jet temperature at the exit, and

T_a: the local air jet temperature.

However, by a careful examination, one finds that the airflow rate and DCD may have an effect on the air jet temperature profile. Figure 4.3-3 is a close-up plot of the same data presented in Figure 4.3-2. It shows that the jet temperature of a certain position in the centerline is higher for a higher airflow rate case when the DCD is constant. It also shows that a lower DCD results in a higher jet temperature of a certain position in the centerline when the airflow rate is constant. This observation suggests the space between the MB die and the collector surface somehow affects the heat transfer from the air stream to the surrounding environment. One of the possibilities is the amount of secondary air involved, whereby the turbulent pattern might change with the DCD. Figure 4.3-2 also show that the most significant variation in temperature among the designed experiments occurred near the die and within the first 2 or 3 inches.

The Fiber Diameter Profile

The fiber diameter profiles are determined by measuring the fibers collected at different positions in the spinline, as described in the Chapter 3,

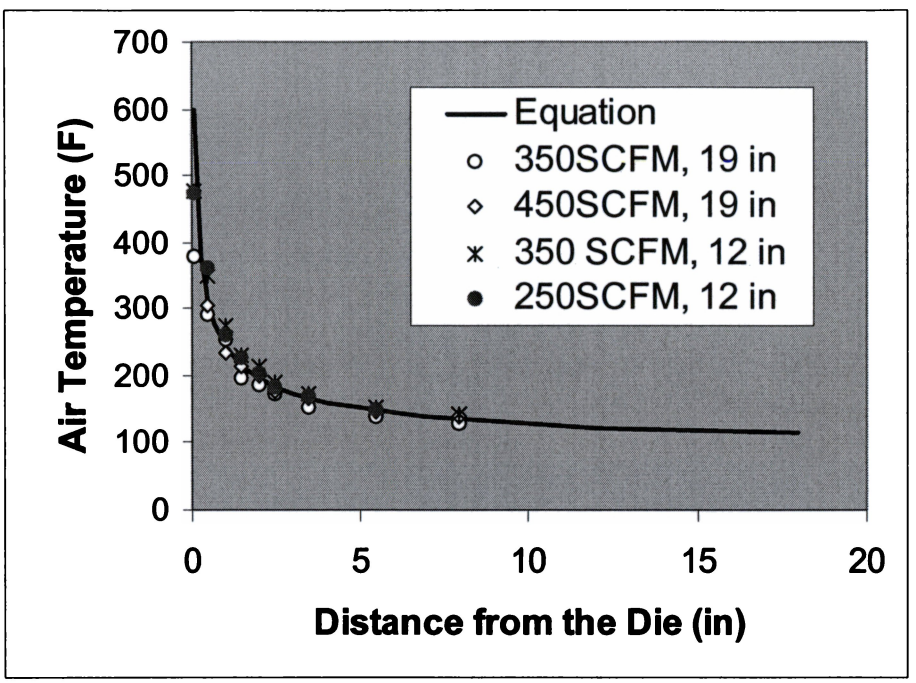

Figure 4.3-2. The measured centerline temperature profile of MB air jets and its comparison with the reference equations 4.3-6 and 4.3-7 from Haynes

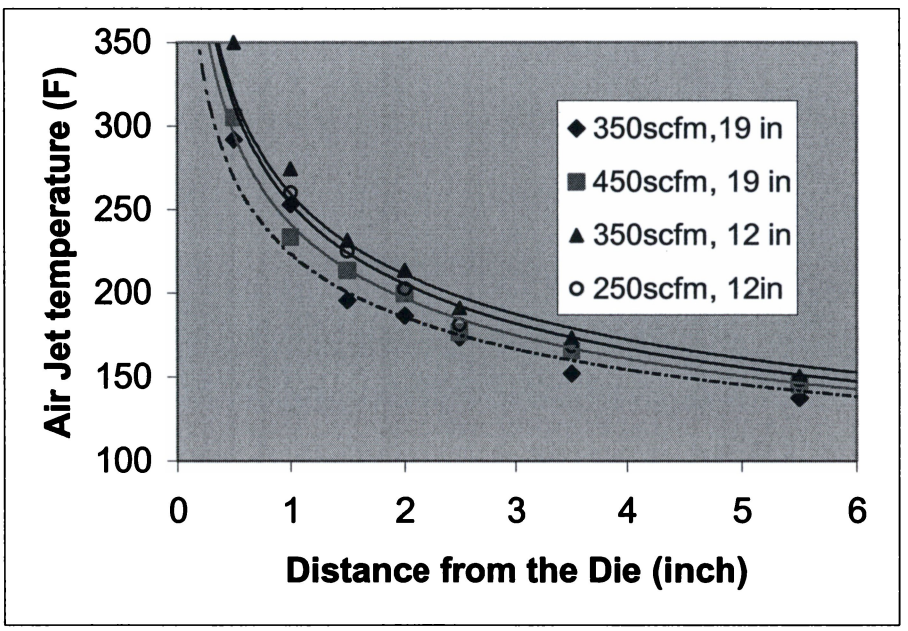

Figure 4.3-3. The effects of airflow rate and DCD on the air temperature (A close-up of Figure 4.3-2)

EXPERIMENTAL. An average of 75 -180 measurements of each location is reported and presented in Figure 4.3-4 and Figure 4.3-5. Figure 4.3-4 compares the fiber attenuation profiles of PP, PET mono-component MB fiber and 75%PP/25%PET bicomponent MB fiber. Figure 4.3-5 compares the fiber attenuation profiles among 75%PP/25%PET, 50%PP/50%PET and 25%PP/75%PET bicomponent MB fibers. All the fibers presented in Figures 4.3-4 and 4.3-5 are produced under the same processing conditions except for the polymer components. The constant conditions are T_d = T_a = 599°F, TP = 15 kg/hr, AR = 450 SCFM, DCD = 19 inch, and BS = 54.13 ft/min.

As shown in Figure 4.3-4, both mono- and bi-component fibers diameter decreased sharply in the first two inches from the die. The filaments of PP attenuated faster than PET filament and the bicomponent filaments attenuated at a medium rate between that of PP and PET. After the first two inches, PP filaments continued decreasing in size at a much slower rate until it reached the solidification point, apparently at 4-5 inches from the die. The decrease of fiber diameter farther away from this point was minimal. The average diameter of PET filament decreased continuously up to 2.5 inches from the die, after which the fiber diameter exhibited an increase and solidified around 8 inches from the die. This result is interesting for melt blowing PET microfibers. Because no dragging device is available to take-up the filaments, MB PET fibers are subjects to shrink when the air drag force becomes very weak during processing. As noted in Figure 4.3- 4, the air jet temperature at 2 inches from the die decreased to about 200°F (93.3°C) from 599°F (315°C) at the die exit, which provides a relatively

rapid quenching effect on the PET filaments resulting in substantially low crystallinity. As shown In Figure 4.2-14, the exothermic peaks are associated with cold crystallization of PET starting at 100°C and the crystallization starting at about 200°C. The heat of fusion contributed by the on-line formed crystalline phase during melt blowing is the difference between the endothermic and exothermic heats, leading to a crystallinity in the range from 5% to 15%. Consequently, the shrinkage of MB PET web is as high as 30-55% [Zhao, 2000]

The 75%PP/25%PET bico MB fiber exhibits a similar attenuation profile. The average diameter of the filaments keeps decreasing slowly after the rapid attenuation. However, the extent is hindered by the PET component compared with single PP filaments. On the other hand, the PP component serves as a heat reservoir to slow down the solidification of the PET part. Therefore, the solidification point of bico fiber moves further down stream of the spinline. Since PET is more thermally conductive than PP (thermal conductivity, J/m/s/°C, PET = 0.29, PP = 0.15 [Rauwendaal, 1986]), it transfers heat more readily than PP. Therefore, it is expected to be affected by the air stream to a higher extent. As the weight percentage of PET increases, the hindering effect becomes more obvious resulting in a fiber diameter profile approaching to that of single PET filaments, as shown in Figure 4.3-5. It is important to see that PP/PET bico filaments generally resulted in a smaller size compared with single PET, which is a great advantage in producing PP/PET bico MB fibers. In addition, their diameter profiles did not have a shrink-induced size increase, even when the

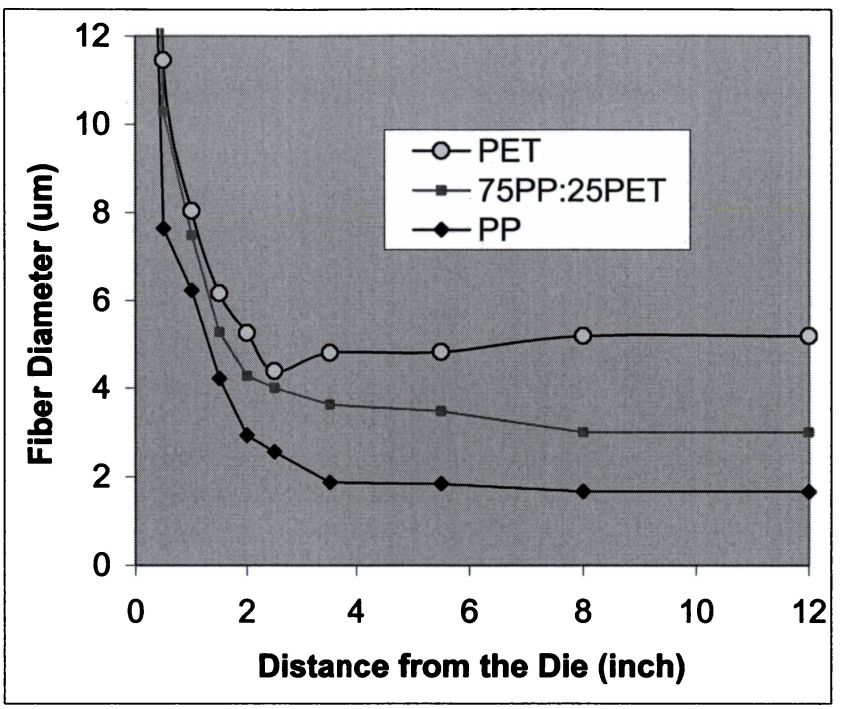

Figure 4.3-4. The Fiber diameter profiles of PP_{35MFR}, PET and PP_{35MFR} /PET bico MB filaments
(T_a= T_d= 599°F, TP =15 kg/hr, AR = 450 SCFM, DCD= 19 inches, and BS = 54.1 ft/min.)

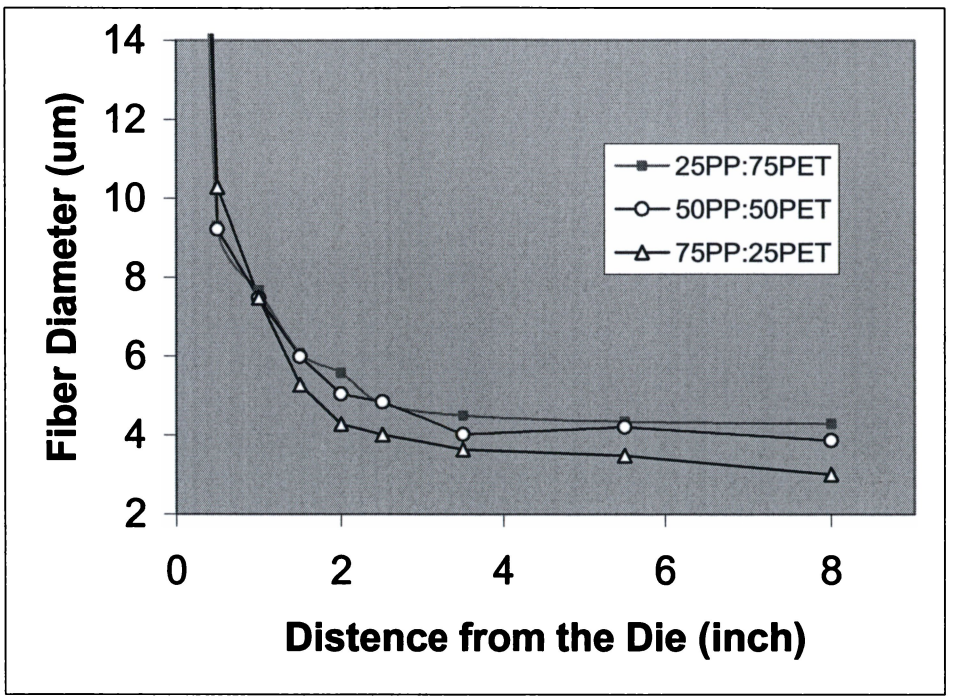

Figure 4.3-5. The Fiber diameter profiles of PP/PET bicomponent MB filaments (T_a= T_d = 599°F, TP =15 kg/hr, AR = 450 SCFM, DCD= 19 inches, and BS = 54.1 ft/min.)

weight percentage of PET was as high as 75%. Apparently, the PP phases in the bico filaments prevented PET from shrinking. This result must relate to the filament temperature and crystallization rates of the two polymers, which will be discussed later in this Chapter.

The Fiber Number Density and Velocity Profile

Determination of fiber velocity is critical in studying the spinline dynamics and understanding the MB process. Yin, Yan and Bresee (1999, 2000) attempted to measure the fiber velocity by using high-speed digital imaging techniques using a 600-hole horizontal MB line. Wu and Shambaugh (1992) measured fiber velocity using laser Doppler velocimetry during concentric, single-hole melt blowing. One of the limitations of these techniques is that only a small mount of fibers can be recorded in the images due to a magnifying lens required. This study tried to avoid the complexity of these techniques, but apply an alternative method to obtain an overall average fiber velocity profile.

Suppose plane 1 and plane 2 are perpendicular to the centerline of the MB filament stream and located arbitrarily between the die and fiber collector. According to the mass conservation principle, in the regular MB process, the polymer mass passing through the two planes at a period of time should keep constant. It is further assumed that each node of the filament and the plane is caused by an individual fiber, and all these fibers are perpendicular to the plane while passing through.

The fibers are collected on a microscope slide, which is attached to a specially designed fast-moving device. This method transports the 3-dimensional filament moving space into a 2-dimensional plane, as shown in Figure 4.3-6. Under microscope, the fibers within a certain length, such as 1- 2 inches, are counted and fiber number density is thus determined. The average of the dada from 3 slides is reported for each position selected in the spinline. Therefore,

$$\left(\frac{d_{f,1}}{2}\right)^2 \pi \cdot V_{f,1} \cdot \rho \cdot N_1 = \left(\frac{d_{f,2}}{2}\right)^2 \pi \cdot V_{f,2} \cdot \rho \cdot N_2 = TP \quad \text{..... (4.3-8)}$$

where: TP: mass flow rate (g/min),

d_f: fiber diameter (cm),

ρ: polymer density (g/cm^3),

V_f: average fiber velocity (cm/min), and

N: total number of fiber past through a plane.

The variables of TP, d_f, and ρ are known. If N is determined, then, V_f can be determined. The subscripts of 1 and 2 represent the different positions along the spinline.

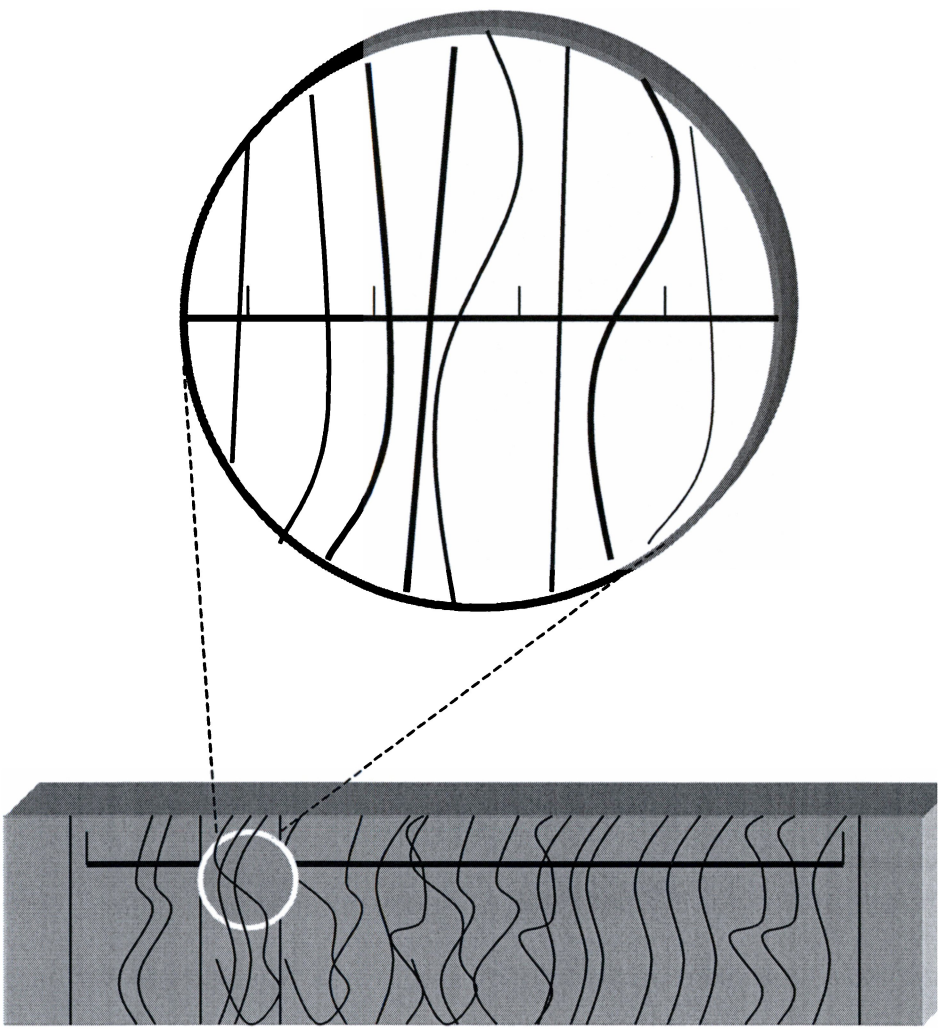

Figure 4.3-6. Measurement of fiber number density under microscope

Figure 4.3-7 shows the relationship between the fiber number density and the distance from the die. It can be seen that the fiber number density generally increases with the DCD except the first inch, which indicates filament entanglement occurs in these regions, The images in Figure 4.3-8 illustrate the entanglement of 75%PP/25%PET bicomponent fibers. There is no doubt that the fibers entangle to a greater extent and fibers form bundles or ropes as they fly a greater distance from the die, The air jet turbulence and fiber jam caused by the velocity reduction are believed to be the two main reasons responsible for this phenomenon, The other important observation from Figure 4.3-8b is fiber breakage at a location near the die, which is normally difficult to detect by direct optical microscopy or SEM examination of the MB webs.

By putting in the results of TP, d_f, ρ, and N (average fiber number density x the die width) of different positions in the spinline into the equation 4.3- 8, the overall average fiber velocity profile can be obtained. Figure 4.3-9 showed the calculated fiber velocity based on the measurement of fiber diameter and fiber number density. The operational conditions were the same as described earlier. For different polymers, the fiber velocity showed different profiles. The filaments of PP exhibited a maximum velocity of 150 m/s at a position as far as 3.5 inches from the die compared with around 70 m/s with PET filaments at 1.5 inches. The maximum velocity of 75%PP:25%PET bicomponent filaments, 90 m/s, were between those of PP and PET single component filaments. After the maximum points, velocity of PP filament decreased slowly, whereas that of PET dropped sharply. The velocity of 75%PP:25%PET bicomponent filament remained

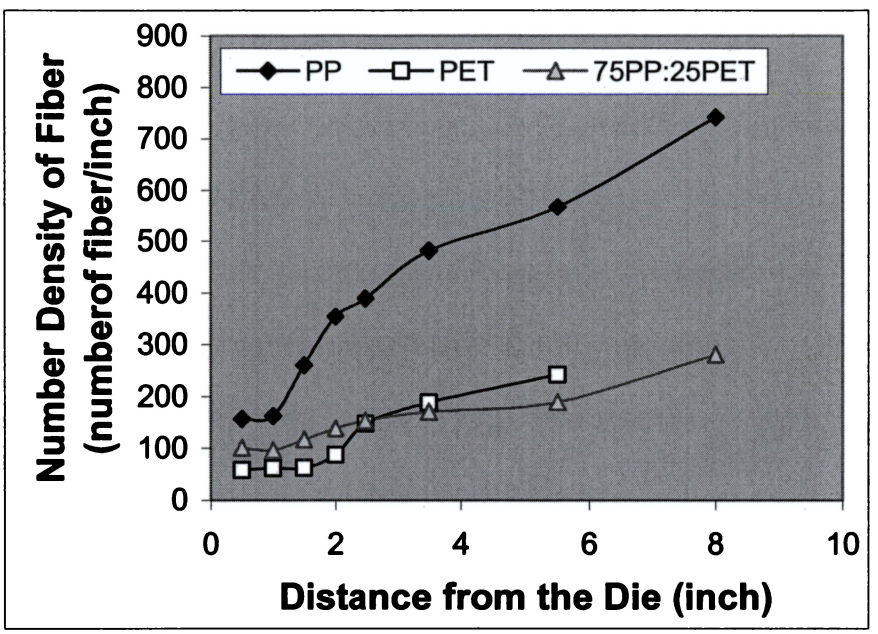

Figure 4.3-7 The fiber number density of PP_{35MFR}, PET and PP_{35MFR} /PET bico MB filaments
(T_d = T_a= 599°F, TP = 15 kg/hr, AR = 450 SCFM, DCD = 19 inch and BS = 54.1 ft/min.)

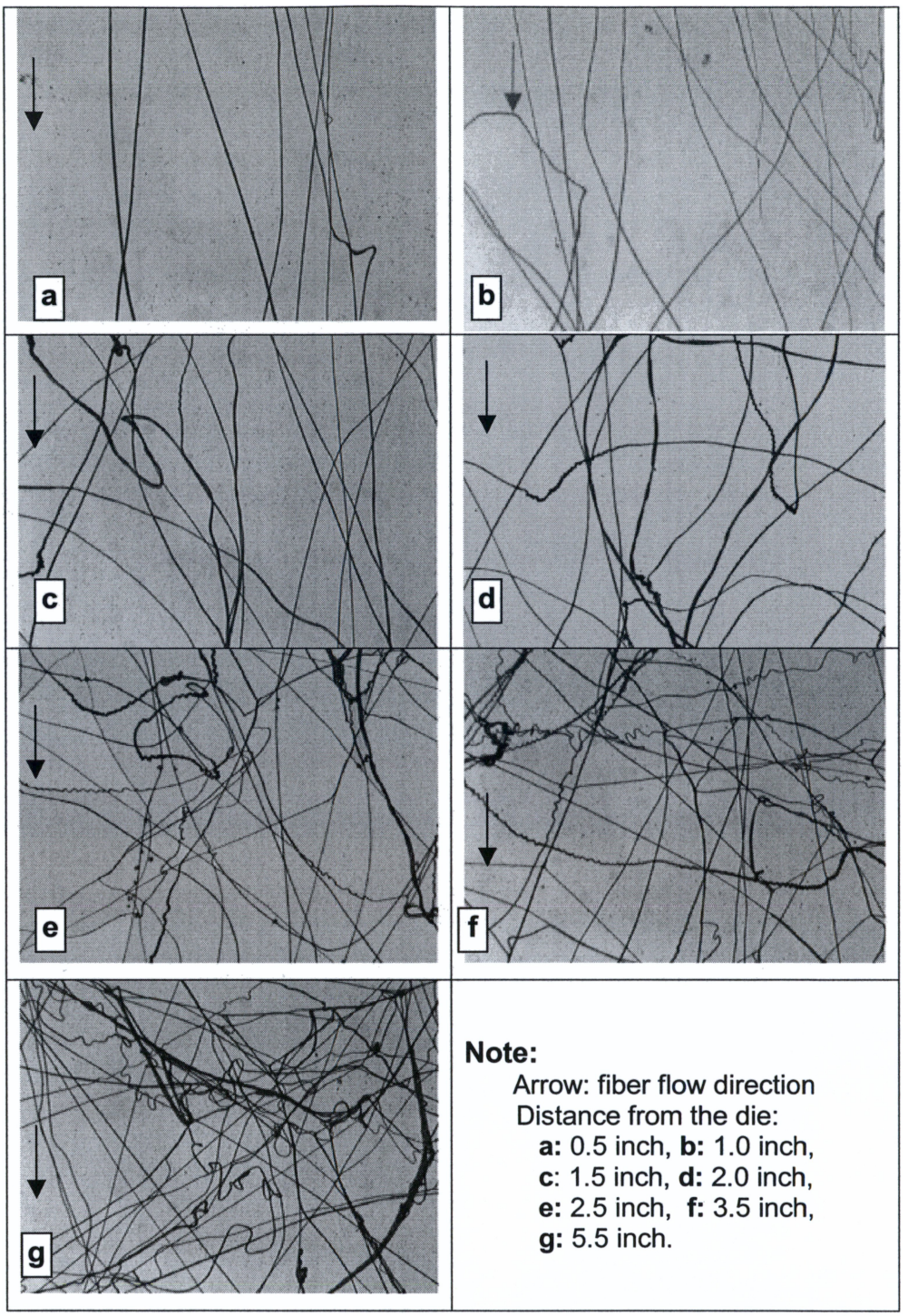

Figure 4.3-8. Optical images of 75%PP_{35MFR} /25%PET bicomponent MB fibers collected at varied positions in the spinline.

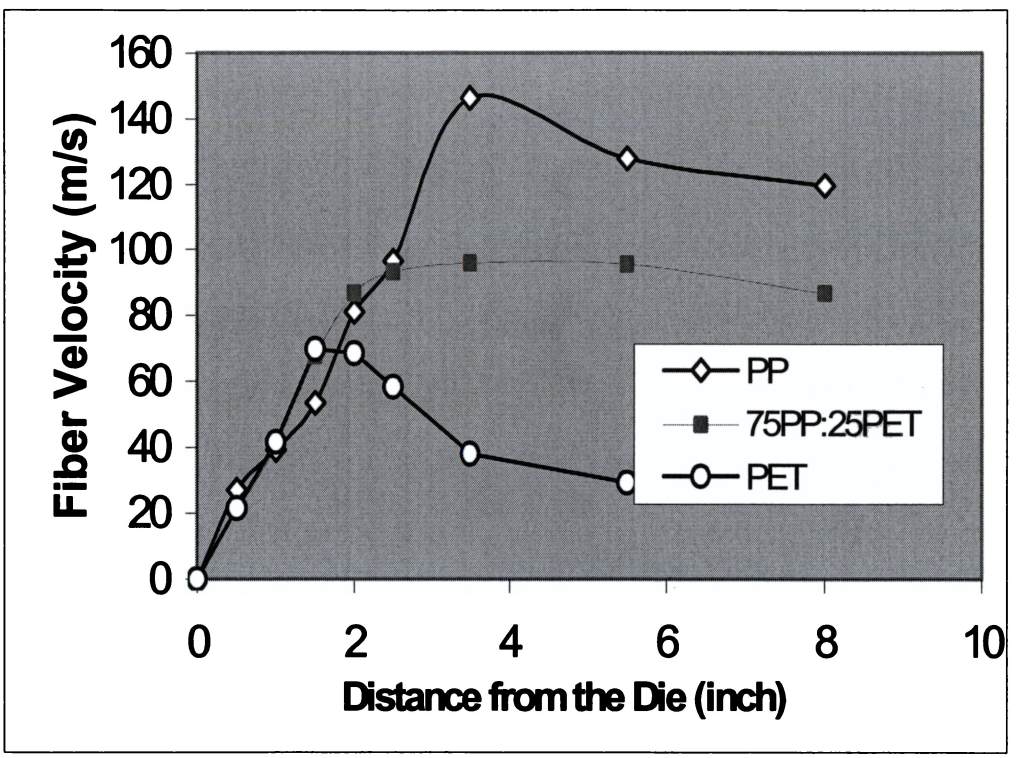

Figure 4.3-9, The fiber velocities of PP_{35MFR}, PET and PP_{35MFR} /PET bico MB filaments

(T_d = T_a= 599°F, TP = 15 kg/hr, AR = 450 SCFM, DCD = 19 inch, and BS = 54.1 ft/min.)

relatively constant and close to that of PP single component filament. These results indicated that the bicomponent filament behaves differently while flying toward the screen collector. Another important observation is that the fiber velocity increases steeply and almost linearly with the distance-from-the-die until reaching the maximum velocity.

Figure 4.3-10 shows the relative fiber velocity (V_{fa}) to the local air jet velocity. The positive V_{fa} indicates the air jet providing drag forces to attenuate the filaments. The negative V_{fa} represents the cases where the fiber moves faster than the surrounding air jet due to the inertia of the denser polymer filament. Therefore, the air jet in these regions provides drag forces in the opposite direction of airflow to stop the filaments. Since the filaments are relatively far from the die, these forces are not really important to the fiber diameter at these regions. Interestingly, experiencing positive air drag along all moving paths does not produce finer PET fiber. This could relate to filament temperature and elongational viscosity, which will be discussed later in this Chapter. It can be seen that the filaments experience most significant air drag force in a short region from the MB die.

Convective heat Transfer Coefficient h

Heat transfer is another critical factor governing filament attenuation. It is even more important in the MB process. Researchers have used Kase and Matsuo's (1985] convection model to analyze high-speed melt spinning (Kikutani, 1996], and melt blowing (Uyttendaele, 1990, Haynes, 1991].

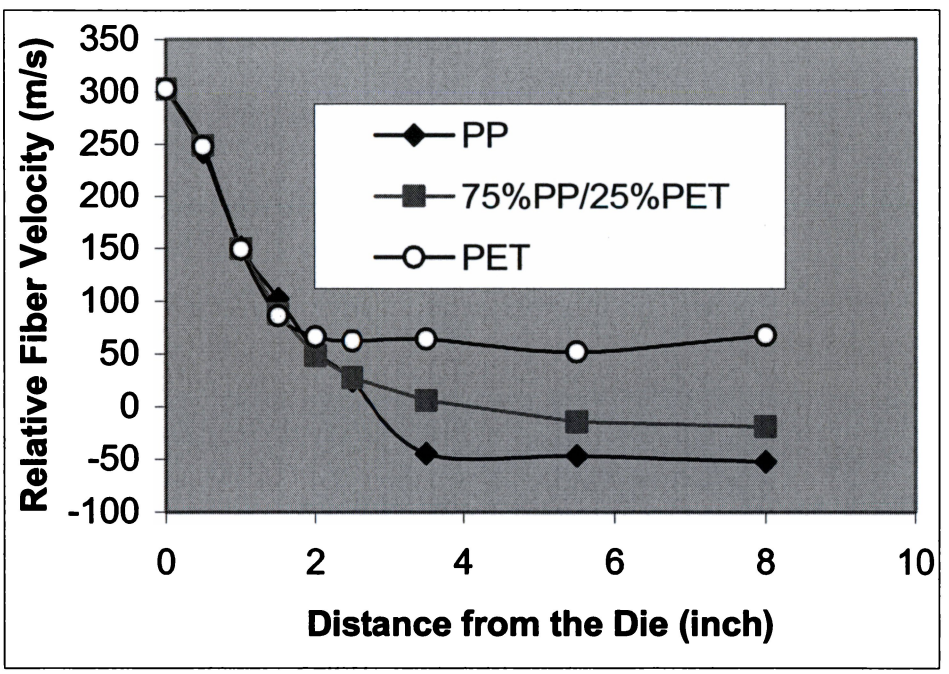

Figure 4.3-10. Fiber velocity relative to the surrounding air jet (T_d = T_a= 599°F, TP = 15 kg/hr, AR = 450 SCFM, DCD = 19 inch, and BS = 54.13 ft/min.)

For the bicomponent melt blowing process, this model may also be valuable. However, the fluid system considered here consists of the filament stream and the air jet stream, which flow in the same direction. When filament is the main concern, the air jet is taken as the environment.

The heat transfer coefficient is given by (Kikutani, 1996]

$$h = \frac{0.42}{d_f} \cdot k_a \cdot \mathrm{Re}^{0.334} \qquad (4.3\text{-}9)$$

where k_a is thermal conductivity of air (cal/cm·s·K), d_f average fiber diameter and Re is Reynolds number. The thermal conductivity of air is a function of temperature T_{fa} (K), described by Southerland equation [Bertin, 1998],

$$k_a = 4.76 \times 10^{-6} \frac{T_{fa}^{1.5}}{T_{fa} + 112} \qquad (4.3-10)$$

In the case of melt blowing, this temperature is the average of the local fiber temperature and the local air jet temperature, which is given by

$$T_{fa} = \frac{T_a + T_f}{2} \qquad (4.3\text{-}11)$$

The Reynolds number in equation 4.3-9 is a measure of the ratio of inertia forces to viscous forces. For melt blowing, it can be expressed as follows,

$$\mathrm{Re} = \frac{d_f \cdot v_{fa} \cdot \rho_a}{\mu_a} = \frac{d_f \cdot v_{fa}}{\nu_a} \qquad (4.3\text{-}12)$$

where, v_{fa} is relative fiber velocity, the difference between the average fiber velocity and the air jet velocity, and v_a kinematic air viscosity, which is defined by the following equation, .

$$\mu_a = 1.458\times10^{-6}\frac{T_{fa}^{1.5}}{T_{fa}+110.4}\ (kg/s\cdot m).....[Bertin, 1998] \qquad (4.3-13)$$

$$\rho_a = \frac{348.324}{T_{fa}}\ (kg/m^3).....[Haynes, 1991] \qquad (4.3-14)$$

$$\upsilon_a = \frac{\mu_a}{\rho_a} = 4.186\times10^{-9}\frac{T_{fa}^{2.5}}{T_{fa}+110.4}\ (m^2/s) \qquad (4.3-15)$$

The Fiber Temperature Profile

Then the fiber temperature profile may be developed through the following energy balance equation [Radhakrishhan, 1997],

$$\frac{dT_f}{dz} = -\frac{\pi d_f h}{W_{pp}\cdot C_p + W_{PET}\cdot C_{p,PET}}\left(T_f - T_a\right) \qquad (4.3\text{-}16)$$

where: T_f; filament temperature, K

T_a: air temperature, K

d_f: fiber diameter, m

h: heat transfer coefficient, j/(m^2·s·K),

W: mass flow rate, g/h/s

C_p: specific heat , J/(g K), [Kikutani, 1996]

$$C_{p,PP} = 2.72 \qquad (4.3\text{-}17)$$

$$C_{p,PET} = 1.25 + 2.5\times10^{-3}\,T \qquad (4.3\text{-}18)$$

By inserting the above formulations, the final energy equation for the melt blown process is given by

$$\frac{dT_f}{dz} = -\frac{1.652\,(d_f \cdot v_{fa})^{0.334}}{W_{pp} \cdot C_p + W_{PET} \cdot C_{p,PET}} \left(\frac{T_a + T_f}{T_a + T_f + 220.8} \right)^{0.6655} \cdot \left(T_f - T_a \right) \qquad (4.3-19)$$

where v_{fa} is the fiber velocity relative to the local air jet velocity with the unit of m/s. This is a first order ordinary differential equation. Providing the following boundary conditions, it can be solved by utilizing the powerful MATLAB ODE solver functions. The corresponding MATLAB codes are listed in the Appendix G, MATLAB Codes.

Boundary conditions for bicomponent the melt blown process:

$T_f = T_{f,0}$ If z = 0 inch, (4.3-20)

$V_f = V_{f,0}$ If z = 0 inch (4.3-21)

$T_a = T_{a,0}$ If z = 0 inch (4.3-22)

$V_a = V_{a,0}$ If z = 0 inch (4.3-23)

$d_f = d_{f,0}$ If z = 0 inch (4.3-24)

As presented earlier, the fiber diameter, air jet temperature and air velocity are a l functions of z, the distance from the die. These profiles are fitted with different equations to best represent the actually measured data. As noticed, the data of each profile are generally fitted with two equations. Each of the equations will be needed at least once during the calculation of filament temperature. As summarized in Table 4.3-1, most of these equations are well fitted R^2 in the range of 0.9000 to 0.9988.

Table 4.3-1. Fitted equations of the profiles of fiber and air jet

	Equations	R^2	Range of z (inch)
PP	$d_f = 5.4827\times10^{-6}\times z^{-0.8372}$ (m)	0.9704	0~5.5
	$d_f = (0.0104\cdot z^2 - 0.2113\cdot z + 2.6868)\times10^{-6}$ (m)	1.0	5.5~10
	$v_f = 40.293\cdot z - 0.0305$ (m/s)	0.9898	0~3.5
	$v_f = 1.9735\times z^{-0.245}$ (m/s)	0.9815	3.5~10
PET	$d_f = 8.786\times10^{-6}\times z^{-0.8436}$ (m)	0.9248	0~2.5
	$d_f = 4.0901\times10^{-6}\times z^{0.1021}$ (m)	0.8626	2.5~10
	$v_f = 44.803 \times z$ (m/s)	0.9936	0~1.5
	$v_f = 104.11 \times z^{-0.7402}$ (m/s)	0.9410	1.5~10
25PP/75PET	$d_f = 8.0697\times10^{-6}\times z^{-0.7114}$ (m)	0.8515	0~2.5
	$d_f = 5.1559\times10^{-6}\times z^{-0.0956}$ (m)	0.8911	2.5~10
	$v_f = -11.293\cdot z^2 + 56.571\cdot z$ (m/s)	0.9836	0~2.5
	$v_f = -0.7469\cdot z^2 + 4.8143\cdot z + 67.655$ (m/s)	0.9385	2.5~10
50PP/50PET	$d_f = 7.8641\times10^{-6}\times z^{-0.7845}$ (m)	0.8578	0~2.0
	$d_f = 5.2916\times10^{-6}\times z^{-0.1539}$ (m)	0.6368	2.0~10
	$v_f = -5.9025\cdot z^2 + 45.31\cdot z$ (m/s)	0.9825	0~3.5
	$v_f = 1.1501\cdot z^2 - 16.218\cdot z + 131.14$ (m/s)	1.0	3.5~10
75PP/25PET	$d_f = 7.22\times10^{-6}\times z^{-0.7942}$ (m)	0.9641	0~2.5
	$d_f = 4.8259\times10^{-6}\times z^{-0.205}$ (m)	0.9503	2.5~10
	$v_f = 40.587 \times z$ (m/s)	0.9825	0~3.5
	$v_f = -0.8192\cdot z^2 + 7.403\cdot z + 79.775$ (m/s)	0.9988	2.5~10
Air Jet	$T_a = T_{a,0}$ (°F)	--	$z \le 3.5w$
	$T_a = 1.79\times(T_{a,0} - T_\infty) \times (w/z)^{0.465} + T_\infty$ (°F)	--	$z > 3.5w$
	$V_a = V_{a,0}$ (m/s)	--	$z \le 8.6w$
	$V_a = 2.92 \times V_{a,0} \times (w/z)^{0.5}$ (m/s)	--	$z > 8.6w$

The calculated fiber temperature profiles are presented in Figure 4.3-11. It can be seen that the fiber temperature decreases dramatically in the first two inches. Compared with the air jet temperature profile, one finds that this is not surprising. Due to higher temperature gradient near the die and a significant amount of secondary air drawn from the ambient, heat radiation and convection are the two main driving mechanisms of the temperature drop of the air jet and the fiber. Interestingly, under the same processing conditions, the temperature profiles of both mono- and bi-component MB fibers appear almost identical, as shown in Figure 4.3-11. However, a closer examination of Figure 4.3-12 reveals that 100% PET filaments exhibit the lowest temperature compared with that of single PP_{35MFR} and PP_{35MFR} /PET bicomponent filaments, due to its relatively higher heat conductivity. The maximum difference for single PP and single PET filaments is between 2°C and 5 °C, which is expected to be even smaller among the filaments with different polymer ratios. This may be balanced by the differences in fiber diameter and fiber velocity of the filaments with different component ratios. For example, PP filament is attenuated to a much lower fiber diameter, which improves the heat transfer from the center to the surface of the fiber, thus, its temperature decreases quicker. On the other hand, the PET filament is less attenuated, which results in larger fiber size and exhibits lowered efficiency of heat loss.

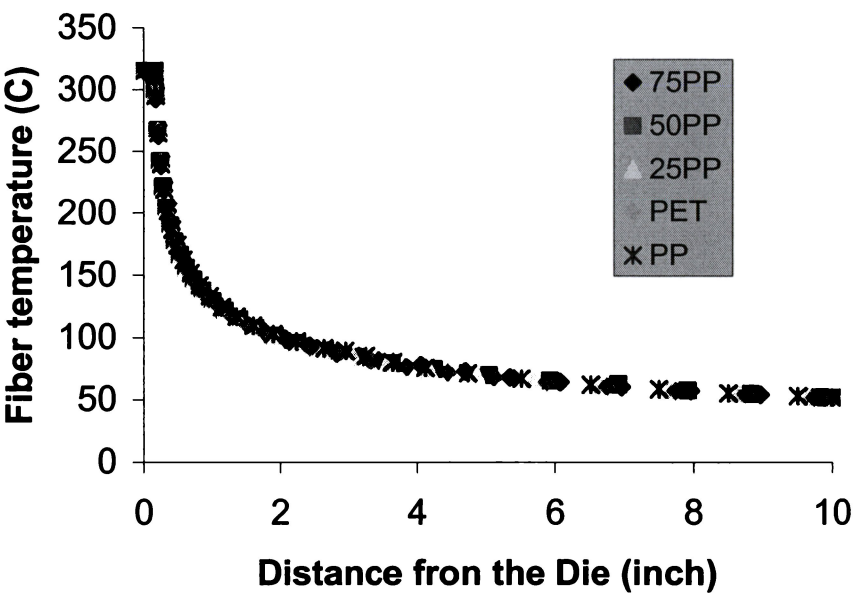

Figure 4.3-11. The fiber temperature profiles of PP_{35MFR}, PET and PP_{35MFR} /PET bico filaments

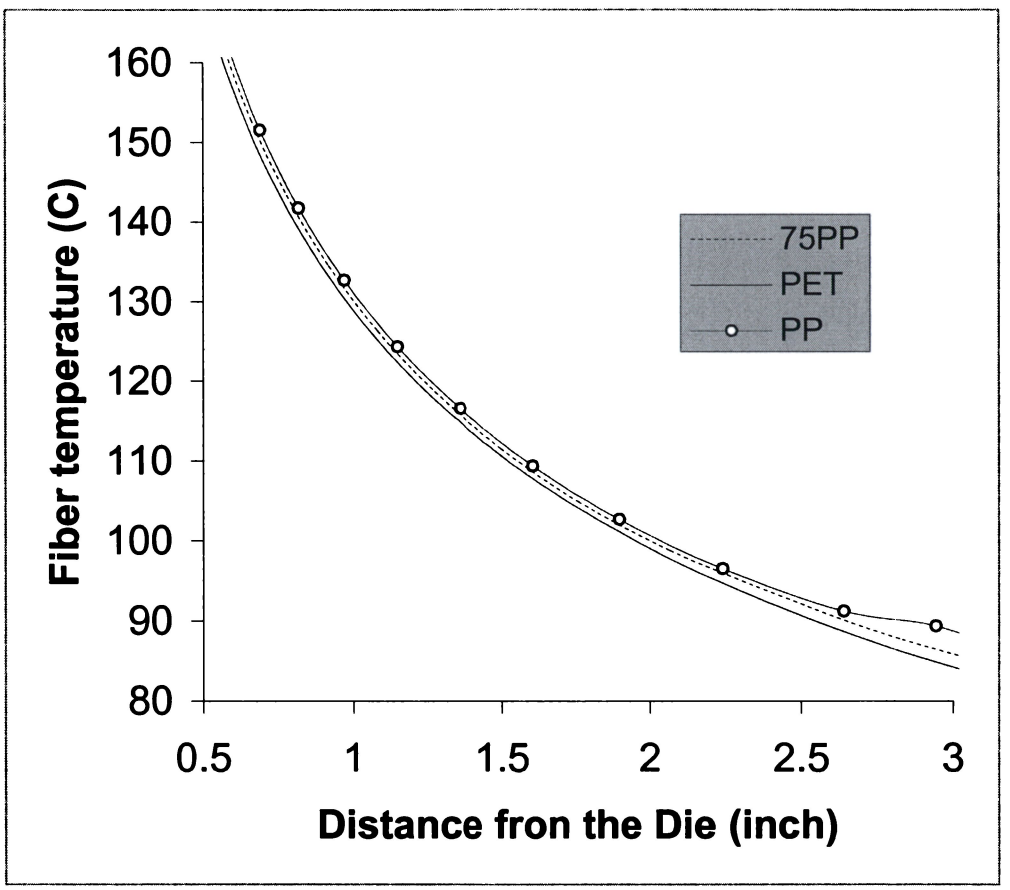

Figure 4.3-12. A close-up of the calculated temperature profiles of PP_{35MFR}, PET and PP_{35MFR} /PET bico filaments

Due to a crystallization temperature around 150 -165 °C, PP phases of the PP/PET bico filaments are expected to start crystallizing at 0.6 inches from the die. The air drag on the filaments could significantly enhance polymer molecular orientation and the crystallization of PP. At a distance of 2.08 inches from the die, the average temperature of 75%PP_{35MFR}/25%PET bico filaments is predicted to be about 99°C. Although PET is the predominant component, the filaments exhibited a smooth attenuation profile without a shrinkage-induced fiber diameter increase as that for single PET filaments. This observation could results partially from the relatively quick crystallization of the PP_{35MFR} phase in the bico filaments.

To provide more supporting data, PP_{35MFR}/PET bico MB webs were treated under heat (90-150°C) for a period of time (1-7min) to investigate their thermal dimensional stability. The treatment conditions and procedures can be found elsewhere [Zhao, 2000]. As shown in Figure 4.3-13, the overall shrinkage of a 25%PP_{35MFR}/75%PET MB web is approximately 2-5%. Comparatively, PET single component MB webs exhibited a shrinkage level up to 25% after exposure to 120°C for 3 minutes. The DSC analysis of the heat treated and untreated samples revealed that PET phase improved its crystallization significantly after the heat treatment, as shown in Figure 4.3-14. The crystallization under heat caused the large degree of shrinkage of the single PET MB web. It is very interesting to note that a small amount of PP (25%) in bico PP_{35MFR}/PET MB web could significantly stabilize the heat shrinkage to approximately 4%, even under 155°C for 5 minutes. Therefore, the PP_{35MFR} phase plays an important role in

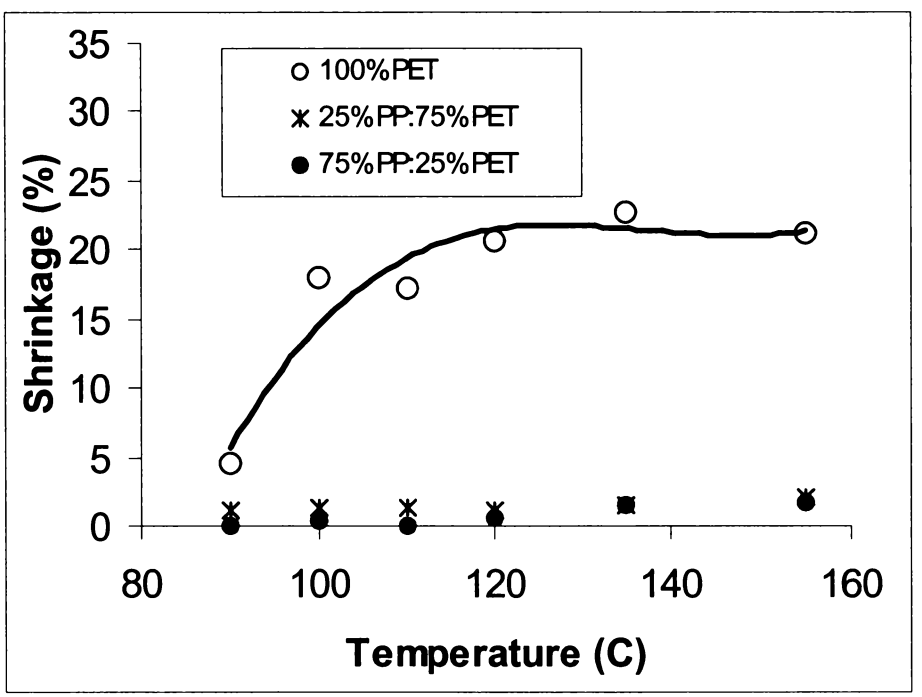

Figure 4.3-13, MB web shrinkage after 3-minute heat treatment at various temperatures

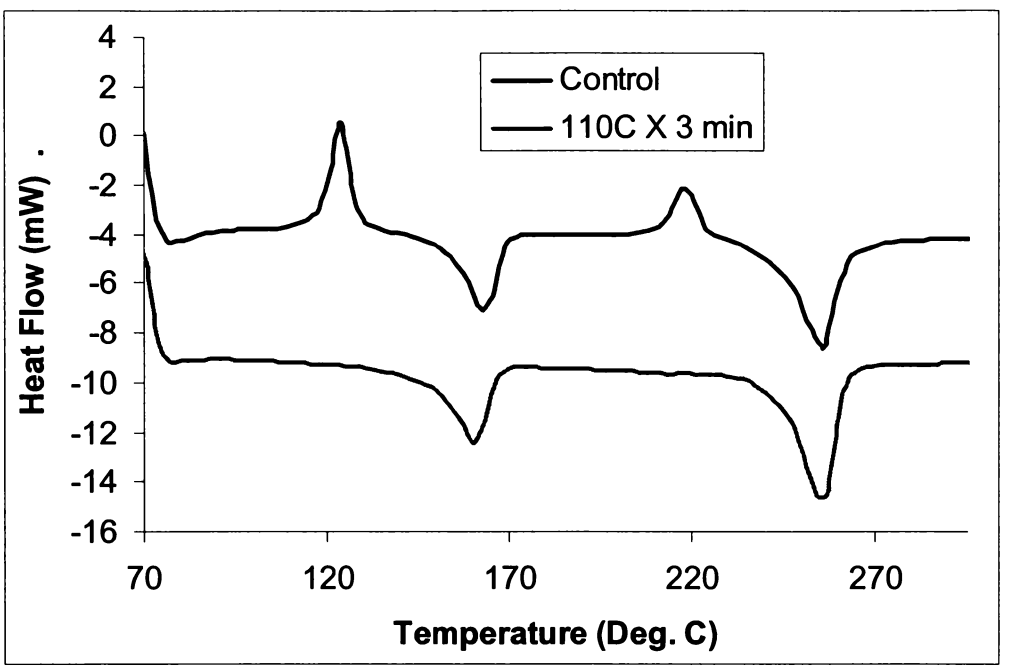

Figure 4.3-14, The DSC curves of 25%PP_{35MFR}/75%PET bicomponent MB Web before and after the heat treatment.

preventing the web shrinkage due to its relatively well-developed crystallization. It may be reasonable to predict that the PP_{35MFR} phase serves the same function during MB process to prevent the filament shrinkage.

The Elongational Viscosity Profile

Melt blowing is a continuous, uniaxial-stretching-like operation, where elongational viscosity (η_e) is a critical property for better understanding the process. Estimating η_e from the Newtonian shear viscosity was first attempted by Trouton (Han, 1976) by giving the following formula,

$$\eta_e = 3\eta_0$$

where η_0 is the zero shear Newtonian viscosity. This relation had been found not to be rigorously correct for many cases [George, 1982]. By assuming a Newtonian flow behavior, Haynes (1991) used the following equation for elongational viscosity of PP in his research of MB process,

$$\eta_e = 2\eta_0 \qquad (4.3\text{-}25)$$

In this study, zero shear viscosities of PP (35MFR) at higher temperatures were determined by extrapolating the viscosity to a rate of zero. These data were combined with Patel's data for a PP of 35 MFR, and the following Arrhenius model of elongational viscosity was then developed and given by

$$\eta_e = 2.56\times10^{-4}\exp\left(\frac{7316}{T+273}\right)(Pa\cdot s) \qquad (4.3-26)$$

The elongational viscosity of PET is a function of temperature and molecular weight, given as follows [Radhakrishnan, 1997]:

$$\eta_e = 0.3 \cdot [I.V.]^{5.1} \exp\left[2.303\left(\frac{3280}{T+273}\right) - 1.54\right] (Pa \cdot s) \qquad (4.3-27)$$

The PET used in this study has an intrinsic viscosity (IV) of 0.645 dl/g. With the result of fiber temperature profile and equations 4.3-26 and 4.3-27, it is not difficult to find the elogational viscosity profiles of PP and PET, as shown in Figure 4.3-15. Under the experimental conditions, the elongation viscosity of PET was determined to be five to ten times higher than that of PP_{35MFR} at all locations in the spinline. This gives a direct explanation of the results observed in Figure 4.3-4. The nature of the polymer determines the elongational viscosity at a given processing condition. Therefore, the higher final fiber diameter of PET is a natural result compared with the much finer fiber size of PP_{35MFR}. If one assumes that the average elonagational viscosity of bico MB filament obeys the simple rule of mixtures, it can be estimated by using the following expression,

$$\eta_{e,bico} = W_{PP}\% \cdot \eta_{e,pp} + W_{PET}\% \cdot \eta_{e,PET}$$

As shown in Figure 4.3-15, the estimated average viscosity of 75%PP_{35MFR}/25%PET bico filament lies between that of PP and PET mono-component filaments. The PET component significantly increased the

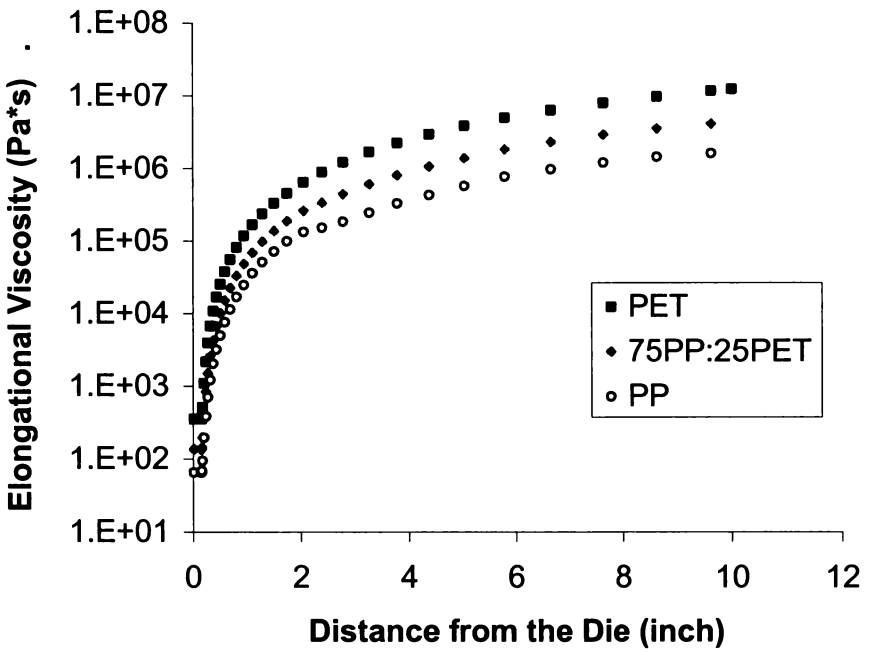

Figure 4.3-15. The elongational viscosity of PP_{35MFR}, PET, and PP_{35MFR} /PET bico MB filaments

($T_a = T_d$ = 315°C, TP = 15 kg/hr, AR = 450 SCFM, DCD= 19 inch)

elongational viscosity of the bico filament, resulting in higher resistance to the attenuation force and higher average final fiber diameter compared with pure PP MB fiber. With more PET in the filament, a higher η_e is expected, and a consequently larger fiber size is not surprising, as observed in Figure 4.3-4

After the polymer melts were extruded from the die, η_e increased dramatically within the first two inches from the die tip. Thereafter, at a certain location in the spinline, η_e reached a level that the local air drag force is no longer strong enough to attenuate the filament. In PET melt spinning with a intermediate take-up speed, its Tg (71°C) was taken as the solidification temperature [George, 1982]. Because no positive drawing device is available in MB processing, the solidification temperature for PET MB filament is of course higher than its Tg. If the transition point in the fiber diameter profile is taken as the solidification point (2.5 inches from the die), the solidification temperature of PET MB filament can be estimated from Figure 4.3-12 about 92°C, which correspondents to an elongational viscosity of about 9.8×10^5 Pa·s. For the PP_{35MFR}/PET bico filaments, it is reasonable to assume that the fiber attenuates continuously until the average η_e reaches this value. Therefore, the solidification point in the spinline for bico filaments lies farther from the MB die, as shown in Figure 4.3-4 and Figure 4.3-5. Compared with PET single component filament, the PP component improved the filament attenuation of the bico filament and increased the bonding property of the web, and thus, enhanced the processability.

CHAPTER 5

CONCLUSIONS AND RECOMMENDATIONS

This chapter presents the conclusions drawn form the experimental study and theoretical predictions. It also includes some recommendations and suggestions for future experimental investigations.

Conclusions:

Phase 1: Preliminary research on PP. PET. and PP/PET bicomponent MB

1. The fiber diameter of $PP_{1200MFR}$ is significantly affected by throughput and airflow rate. Comparatively, the effects of melt temperature, air temperature, and DCD on the $PP_{1200MFR}$ fiber diameter are less significant.
2. To produce smaller diameter fiber, low polymer throughput and high airflow rate are required, when the melt temperature and air temperature are in the range of 230°C to 300°C.
3. The fiber diameter of PET is significantly affected by melt temperature and airflow rate. The effect of throughput is much less important than that for $PP_{1200MFR}$. The effects of air temperature and DCD are minimal.
4. PET and $PP_{1200MFR}$ behave differently. Melt blowing $PP_{1200MFR}$ and PET on the Reicofil® MB pilot line to produce bicomponent microfiber nonwovens requires a careful consideration of the properties of the two polymers.
5. Processing $PP_{1200MFR}$/PET bico MB fiber nonwovens can be performed successfully under different conditions. Their fiber diameters are between

those of $PP_{1200MFR}$ and PET single component MB webs. The processability appears to be improved compared with PET only.

6. The bico filaments possess a side-by-side cross-sectional geometry. The originally expected high crimps of the bicomponent MB fibers were rarely observed.
7. The uniformity of polymer distribution across the web varies with the polymer ratio. When PET is the major component, PP distributes more in the edge areas of the web than in the center area.
8. Thermal analysis and rheological measurements suggest that PP_{35MFR} /PET is a better pair for bicomponent melt blowing.

Phase 2: Research on PP_{3155}/PET bicomponent MB

1. After considering the processability, the thermal stability of the polymer pair and the results in Phase 1, both melt and air temperatures should be set at 599°F (315°C). Throughput, airflow rate, DCD, and weight percentage of PP affected the final fiber diameter; airflow rate was the most significant parameter.
2. In single component MB, higher airflow rate led to smaller fiber diameters. The effect of throughput on the fiber diameter was much less important due to the PET component. The interaction between throughput and airflow rate was minimal.

3. The effect of PP percentage on the fiber diameter of bico filament varied with the airflow rate. This effect was more important at a lower airflow rate, and was minimal as the air rate increased.
4. The effect of DCD on the fiber diameter of the bico filaments depended on the ratio of the two polymers. At a higher percentage of PP, the fiber diameter decreased with an increase of DCD. At a higher percentage of PET, the fiber diameter increased with the DCD.
5. The fiber diameter distribution at different locations in the spinline varied accordingly. It was very broad at a location near the die and became narrower as the position moves further from the die.
6. PP fiber diameter distribution near the die was more uniform at a higher airflow rate. At a position relatively far from the die, the effect of airflow rate on fiber size distribution was not significant.
7. The fiber diameter distribution of bico filaments is broader than that of single PP. Higher airflow rate leads to narrower fiber size distribution for bico filaments.
8. For the polymer pair of PP_{35MFR}/PET, the polymer distribution across the web can be improved by adjusting the die temperature profile, even for the cases with PET as the major component.
9. The ratio of average fiber diameter and the packing density highly correlates to the average circular-capillary-equivalent pore size. As this ratio increases, the average pore size decreases. This ratio also highly

correlates to web performance properties, such as latex filtration efficiency, air permeability and water penetration resistance (HH).

10. The processing conditions that affect the ratio of average fiber diameter and packing density contribute to the construction of MB web structure. Therefore, this ratio is a relative measure of the web structure and is very useful in MB web design for a particular final application.

Phase 3: A study of spin-line dynamics of PP_{35MFR} /PET MB

1. The measured air jet centerline temperatures agree greatly with the predicted data. Therefore, the reported empirical formulation can be used for future studies.
2. Both airflow rate and DCD have an effect on the air jet temperature decay profile. At a constant DCD, higher airflow rate results in slower temperature decay. At a constant airflow rate, temperature decays faster with the increase of DCD.
3. Both mono- and bi-component filaments attenuated from several hundred micrometers to a few micrometers in the first two inches from the die. PP filaments continuously decrease in diameter at a much slower rate. PET filaments shows a slowly increased trend in fiber diameter after reaching the lowest point in the fiber diameter profiles. The diameters of bico MB filaments were between that of 100% PP and 100% PET filaments.

4. As the percentage of PET increases, final fiber diameters are much closer to PET single component filaments. The PET component in the bico filament controls the final fiber diameter.
5. Filaments are aligned with the airflow direction orderly in a short region near the die. Filament entanglement started at about 1 inch from the die and becomes more and more randomly oriented as the distance-from-the-die increases. Fiber breakages were observed at 1 inch from the die.
6. The filaments increased their average velocities almost linearly before they reach a maximum point. Then, their velocities decreased accordingly. Under the same processing condition, 100% PP filaments have a much higher maximum velocity than 100% PET filaments. The maximum velocity of bicomponent filaments lies between that of PP and PET single component filaments.
7. The fiber velocity relative to the surrounding air stream varies with the component and the distance from the die. Within the first two inches, air velocity is greater than that of the filaments. Thereafter, the velocities of PP and bico filaments are close to or greater than air velocity.
8. By taking the high-speed melt spinning model and giving special consideration of the heat transfer coefficient, the filament temperature profile was estimated. It changes dramatically in the first two inches and then decays slowly. The temperature profiles for single component and bicomponent filament are nearly identical in trend. At a certain location in the spin-line, temperature of PP filament was a few degrees centigrade

higher than in PET filament. The temperature profiles of bicomponent filaments were between that of PP and PET.

9. The elongational viscosities of the filaments were estimated based on the calculated filament temperature profile. Under the processing conditions, the elongation viscosity of PET filament was 5 to 10 times higher than that of PP. The elongation viscosity of bicomponent filament was also estimated by using the simple rule of mixtures. These results provide fundamental information to explain the observations of fiber attenuation and web structure development.

Recommendations

The following recommendations are based on the direct observations and the conclusions of this study. This additional study would provide more valuable data for a better understanding of the bicomponent melt blowing process.

1. The effects of air and die temperatures in a suitable range needs to be investigated.
2. The effect of ambient temperature and humidity on the fiber diameter profile should be conducted.
3. Some additives to the polymer pair could provide a proper viscosity match for a relatively easier and more effective improvement in polymer distribution across the web.

4. An improved fiber-collecting device is needed to reduce the data variation. This device should also have the ability to adjust its arm temperature, which is very important during fiber collection.
5. The study on the crystallization of the polymers during the process would generate important additional information for the estimation and simulation of the filament temperature profile. Actual filament temperature profile needs to be measured and compared with the calculated ones.
6. An investigation of the die geometry needs to be conducted to reinforce the validity of the steady-state Newtonian model used in this study.

REFERENCES

1. Baird, D. G. "Polymer Processing" Butterworth-Heinemann, MA, 318 (1995)
2. Bertin, J. J., Smith, M. L. (1998) "Aerodynamics for Engineers (Third Edition)", Prentice Hall, New Jersey.
3. Brandrup, "Polymer Handbook" John Wiley and Sons, New York, 1975
4. Choi, K. Jo, Spruiell, J. E., et. al., (1988) "strength properties of Melt Blown Nonwoven Webs" Polymer Engineering and Science, 28(2): 81-89
5. Collier, R. C., et. al., "Elongational Rheology of Polymer Melts and Solutions" Journal of Applied Polymer Science, 69:2357 -2367
6. George, H. H. "Model of steady-state melt spinning at intermediate take-, up speeds" Polymer Engineering and Science, 22(5): 292-9 (1982)
7. Han, C. D. (1976) " Rheology in Polymer Processing" Academic Press, New York, 198.
8. Han: C.D (1973) "Multiphase Flow in Polymer Processing" Academic Press, NY, 1981.
9. Harding; J. W ., Keller; J. P. ,Buntin; R. R. (1974) "Melt Blowing Die For Producing Nonwoven Mats", US Patent 3,825,380 (07-23-1974)
10. Haynes, B. D. (1991) "An experimental and Analytical Investigation on The production of Microfibers Using a Single Hole Melt Blowing process", Ph.D. Dissertation, The University of Tennessee at Knoxville.

11. Kase, S., and Mastsuo, T, (1965), "Studies on melt spinning: Fundamental Equations on the Dynamics of Melt Spinning", J. Polym. Sci. A-3, 2541.
12. Kayser, J. C. and Shambaugh, R. L. [1990] "The manufacture of Continuous Polymeric Filaments by the Melt Blowing Process", Polymer Engineering and Science, 30(19):1237
13. Khan, A. Y. A, (1993) "A Fundamental Investigation of the effects of Die Geometry and Process Variables on Fiber Diameter and Quality of Melt Blown Polypropylene Webs" Ph.D. Dissertation, The University of Tennessee at Knoxville.
14. Kikutani, T., et. al. (1996) "High-Speed Melt Spinning of Bicomponent Fiber: Mechanism of Fiber Structure Development in Poly(ethylene terephthalate) /Polypropylene System", Journal of Applied Polymer Science, 62:1913-1924
15. Kunze, B. (1998) "SMMS - Any Advantage vs SMS" Book of Papers, 8th TANDEC Conference, Knoxville, Tennessee.
16. Lee, Y., Wadsworth, L. C. (1990), "Structure and Filtration properties of Melt Blown Propylene webs" Polymer Engineering and Science, 30(22): 1413-1419
17. Langmuir, I. (1942) "Report on Smokes and filters," Section 1, U.S. office of scientific research and development, No.865, Part IV.
18. Lohkamp; D. T., Keller; J. P., IIMEL T -BLOWING DIE USING CAPILLARY TUBES" US Patent 3,825,379 (07-23-1974)

19. Malkan, S. R., (1990) "process-Structure-Properties relationships in Different Molecular Weight Polypropylene Webs", Ph.D. Dissertation, The University of Tennessee at Knoxville.

20. Malkan, S. R., and Wadsworth, L. C. (1991) "Process-Structure-Property Relationships in Melt Blowing of Different Molecular Weight Polypropylene Resins: Part I -Physical Properties" INDA Journal of Nonwoven Research, 3(2):21-34

21. Malkan, S. R., and Wadsworth, L. C. (1991) "Process-Structure-Property Relationships in Melt Blowing of Different Molecular Weight Polypropylene Resins: Part II -Morphological and Process Conditions" INDA Journal of Nonwoven Research, 3(3):21-29

22. McCulloch, W. J. G. "The history of the development of Melt blowing Technology", International Nonwovens Journal, 8 (1): 66 (1999)

23. Milligan, M. W., and Haynes, B. D., (1995) "Empirical Models for Melt Blowing", Journal of Applied Polymer Science, 58: 159-163

24. Milligan; M. W. "Multi-hole melt blown die nosepiece" US Patent 6,099,282 (08-08-2000)

25. Patel, R. (1988), "Rheological Properties of Low Molecular Weight: polypropylenes" MS Thesis, University of Tennessee, Knoxville.

26. Radhakrishhan, J, et. al, (1997)" High-Speed Melt Spinning of Sheath-Core Bicomponent Polyester Fibers: high and low Molecular Weight Poly(ethylene Terephthalate) System" Textile Research Journal, 67(9): 684:694

27. Radhakrishhan, J, et. al, (1999)"Enhancement of fiber strauctur formation of a liquid crystalline copolyester (LCP) via Ultra-high Speed Bicomponent Spinning with Poly(ethylene Terephthalate)" Polymer Engineering and Science, 39(1): 89

28. Rauwendaal, C., (1986) "Polymer Extrusion" Hanser Publishers, Munich, 218.

29. Schwarz; E. C. A. "Apparatus and process for melt-blowing a fiber forming thermoplastic polymer and product produced thereby" US Patent 4,380,570 (04-19-1983)

30. Spurr A. R. "A low-viscosity Epoxy Resin embedding Medium for Electron Microscopy" J Ultrastruct. Res 26:31-43 (1969).

31. Staff report," Melt blown technology today" 1989, Miller Freeman Publication, Inc. 500 Howard Street, San Francisco, CA 94105, page 8.

32. Straeffer, G. and Goswami, B. C., (1990) "Mechanics and Structural Properties of Melt Blown Fibers" Book of Papers, INDA- TEC'90, pp 385-419.

33. Sun, C., Zhang, D., Wadsworth, L. C., Zhao, R. (2000), "Processing Development and Investigation of Mono- and Bi-component Fiber Meltblown Nonwovens", Book of Papers, 10th TANDEC Conference, Knoxville, pp 2.4-1

34. Sun, C., Zhang, D. (1998), "Analysis and simulation of Non-Newtonian Flow in the Coat-Hanger Die of a Meltblown Process", Journal of Applied polymer Science, 67 193-200.

35. Uyttendaele, M. A. J, and Shambaugh, R. L. [1990] "Melt Blowing:: General Equation Development and Experimental Verification", AIChE Journal, 36 (2): 175

36. Wadsworth, L. C. and Muschelewicz, A. 0. (1987), Book of Papers. Fourth International Conference on Polypropylene Fibers and Textiles, Nottingham, England, Sept. 23-25,1987, pp 47.11-47.20

37. Wadsworth, L. C., and Hill, G. J. (1985) "Automated Test Apparatus for Rapid Simulation of Bacterial Filtration Efficiency' Book of Papers, INDA 13th Annual Technical Symposium, Boston, MA, June 4-6: 41-54

38. Wu. T.T. and Shambaugh, R.L. Characterization of the Melt Blowing Process with Laser Doppler Velocimetry, *Ind. Eng. Chem. Res.,* 31 (No. 1), 379-389 (1992)

39. Yin, H., Yan, Z. and Bresee, R. R. (1999) "Experimental Study of the Melt Blowing Process", International Nonwovens Journal, 8(1): 60-65

40. Yin, H., Yan, Z., Ko, W. C., and Bresee, R. R. (2000) "Fundamental Description of the Melt Blowing Process", International Nonwovens Journal, 9(4): 25-28

41. Zhang, D., Sun, C., Wadsworth, L. C., Zhao, R. (1999), "Processing and Characterization of Mono- and Bi-component Fiber Meltblown Nonwovens", Book of Papers, 9th TANDEC Conference, Nov. 10-12, Knoxville, TN

42. Zhao, R. Zhang, D., Sun, C., Wadsworth, L. C (2000) "Properties and Characterizations of PBT, PET, Bicomponent PP/PBT and PP/PET Melt

Blown Microfiber Nonwovens after Heat-treatment", Book of Papers, 10th TANDEC Conference, Nov. 7-10, Knoxville, TN

43. Zhao, R. (2000) "Melt blown Die: A Hot Innovation Spot" International Fiber Journal, in press

44. Ziabicki, A., and Kawai, H., (1985), eds., High-speed Fiber Spinning: Science and Engineering Aspects, Wiley, New York.

45. Ziabicki, A., (1976) "Fundamentals of fiber formation", John Wiley & Sons, New York.

APPENDIX

APPENDIX A

SAS Program for PP_{3546G}

```
/* THIS WAS PROGRAMMED ON 4-29-01 FOR THE PHASE-1
PRELIMINARY RESEARCH ON PP-3546G WITH AG/SB=0.8mm/1.0mm
*/

data pp;
input MT TP AT AR DCD Dia @@;

label
        Dia="fiber diameter"
        MT= "Melt Temperature"
        TP= "thruput"
        AT= "Air temperature"
        AR= "Air rate"
        BS= "Belt speed";
datalines;

274   38.7 252   425  10  2.51     274  38.7  252   675   6  1.82
260  29.25 265.5 550  12  1.86     260  29.25 265.5 550   4  2.25
260  29.25 265.5 550   8  1.98     260  29.25 265.5 800   8  1.79
232  29.25 265.5 550   8  2.01     246  19.8  252   425  10  2
246  19.8  252   675   6  1.69     246  19.8  279   425   6  2.15
246  19.8  279   675  10  1.67     246  38.7  252   425   6  1.78
246  38.7  252   675  10  2.02     246  38.7  279   425  10  2.52
246  38.7  279   675   6  2.14     260  10.35 265.5 550   8  1.71
260  29.25 238.5 550   8  1.9      260  29.25 265.5 300   8  2.45
260  29.25 292.5 550   8  1.82     260  48.15 265.5 550   8  2.19
274  19.8  252   425   6  1.92     274  19.8  252   675  10  1.44
274  19.8  279   425  10  1.82     274  19.8  279   675   6  1.79
288  29.25 265.5 550   8  1.49     274   38.7 279   425   6  2.12
274  38.7  279   675  10  1.81

260  25.51 265.5 550  8  1.98     260  29.25 265.5 550  8  1.93
260  29.25 265.5 550  8  1.89     260  29.25 265.5 550  8  1.96
260  29.25 265.5 550  8  1.97

271  11.14 194   220  8  2.80;

proc sort;
by MT TP AR AT DCD;
```

```
run;


proc rsreg data=pp;
model Dia= MT TP AR AT DCD/lackfit;
ridge max;
run;

/*The following is to predict the fiber diameter profile with melt temperature
and throughput. The air temperature is set at 270 degree °C, air rate at
557.5 SCFM, and DCD at 8.63 inch.*/

data grid;
do;
Dia= . ;
AT=270;
AR=557.5;
DCD=8.63;
do MT=230 to 300 by 5;
do TP= 10 to 50 by 2;
output;
end;
end;
end;
data grid;
set pp grid;
run;

proc rsreg data=grid out=predict noprint;
model Dia= MT TP AT AR DCD/predict;
run;

data plot;
set predict;
if AT=270;
AR=557.5;
DCD=8.63;
BS=87.406;
proc g3d data=plot;
plot MT*TP=Dia / rotate=38 tilt=75 xticknum=3 yticknum=3
  zmax=3 zmin=0 ctop=red cbottom=blue caxis=black;
run;

/*This plot is to see the effect of air temperature and rate by comparing
with the previous plot.*/
```

```
data grid1;
do;
Dia= . ;
AT=300;
AR=580.5;
DCD=8.63;
BS=87.406;
do MT=230 to 300 by 5;
do TP= 10 to 50 by 2;
output;
end;
end;
end;
data grid1;
set pp grid1;
run;

proc rsreg data=grid1 out=predict1 noprint;
model Dia= MT TP AT AR DCD/predict;
run;

data plot;
set predict1;
if AT=300;
AR=580.5;
DCD=8.63;
BS=87.406;
proc g3d data=plot;
plot MT*TP=Dia / rotate=38 tilt=75 xticknum=3 yticknum=3
  zmax=3 zmin=0 ctop=red cbottom=blue caxis=black;
run;

**********************************
data grid2;
do;
Dia= . ;
TP=25;
AR=580.5;
DCD=8.63;
BS=87.406;
do MT= 250 to 300 by 5;
do AT=250 to 300 by 5;
output;
end;
```

```
end;
end;


data grid2;
set pp grid2;
run;
proc rsreg data=grid2 out=predict2 noprint;
model Dia= MT TP AT AR DCD/predict;
run;

data plot;
set predict2;
if TP=25;
AR=580;
DCD=8.63;
BS=87.406;
proc g3d data=plot;
plot MT*AT=Dia / rotate=138 tilt=80 xticknum=3 yticknum=3
zmax=3.00 zmin=0 ctop=red cbottom=blue caxis=black;
run;

************************************
data grid3;
do;
Dia= . ;
TP=15;
AR=580.5;
DCD=8.63;
BS=87.406;
do MT= 250 to 300 by 5;
do AT=250 to 300 by 5;
output;
end;
end;
end;
data grid3;
set pp grid3;
run;

proc rsreg data=grid3 out=predict3 noprint;
model Dia= MT TP AT AR DCD/predict;
run;

data plot;
```

```
set predict3;
if TP=15;
AR=580;
DCD=8.63;
BS=87.406;
proc g3d data=plot;
plot MT*AT=Dia / rotate=138 tilt=80 xticknum=3 yticknum=3
  zmax=3.00 zmin=0 ctop=red cbottom=blue caxis=black;
run;

data grid4;
do;
Dia= . ;
MT=270;
AT=270;
AR=580.5;
BS=87.406;
do TP= 10 to 50 by 2;
do DCD=4 to 19 by 1;
output;
end;
end;
end;
data grid4;
set pp grid4;
run;

proc rsreg data=grid4 out=predict4 noprint;
model Dia= MT TP AT AR DCD/predict;
run;

data plot;
set predict4;
if MT=270;
AT=270;
AR=580.5;
BS=87.406;
proc g3d data=plot;
plot DCD*TP=Dia / rotate=138 tilt=80 xticknum=3 yticknum=3
zmax=4.00 zmin=0 ctop=red cbottom=blue caxis=black;
run;
```

APPENDIX B

Output of SAS program in APPENDIX A

The RSREG Procedure

Coding Coefficients for the Independent Variables

Factor	Subtracted off	Divided by
MT	260.000000	28.000000
TP	29.250000	18.900000
AR	550.000000	250.000000
AT	265.500000	27.000000
DCD	8.000000	4.000000

Response Surface for Variable Dia: fiber diameter

Response Mean	1.949375
Root MSE	0.120069
R-Square	0.9205
Coefficient of Variation	6.1593

Regression	*DF*	Type I *Sum of Squares*	*R-Square*	*F Value*	*Pr > F*
Linear	5	1.167797	0.5852	16.20	<.0001
Quadratic	5	0.176459	0.0884	2.45	0.1003
X-product	10	0.492750	0.2469	3.42	0.0278
Total Model	20	1.837006	0.9205	6.37	0.0015

Residual	*DF*	*Sum of Squares*	*Mean Square*	*F Value*	*Pr > F*
Lack of Fit	7	0.153261	0.021894	16.46	0.0084
Pure Error	4	0.005320	0.001330		
Total Error	11	0.158581	0.014416		

Parameter	DF	Estimate	Standard Error	t Value	Pr > |t|	Parameter Estimate from Coded Data
Intercept	1	-58.064294	17.220079	-3.37	0.0062	1.958861
MT	1	0.247178	0.073831	3.35	0.0065	-0.148333
TP	1	-0.085008	0.089218	-0.95	0.3612	0.26424
AR	1	0.003359	0.006793	0.49	0.6307	-0.31333
AT	1	0.188941	0.078150	2.42	0.0341	0.05666
DCD	1	0.927789	0.423506	2.19	0.0509	-0.03333
MT*MT	1	-0.000262	0.000113	-2.32	0.0407	-0.20566
TP*MT	1	0.000161	0.000227	0.71	0.4937	0.08500
TP*TP	1	-0.000011806	0.000250	-0.05	0.9631	-0.00422
AR*MT	1	-0.000020714	0.000017	-1.21	0.2525	-0.14500
AR*TP	1	0.000008466	0.0000254	0.33	0.7453	0.04000
AR*AR	1	0.000002629	0.0000014	1.85	0.0910	0.16434
AT*MT	1	-0.000377	0.000159	-2.37	0.0369	-0.28500
AT*TP	1	0.000039193	0.000235	0.17	0.8707	0.02000
AT*AR	1	0.000001481	0.000018	0.08	0.9351	0.01000
AT*AT	1	-0.000131	0.000122	-1.08	0.3041	-0.09566
DCD*MT	1	-0.001161	0.001072	-1.08	0.3021	-0.13000
DCD*TP	1	0.005357	0.001588	3.37	0.0062	0.40500
DCD*AR	1	-0.000345	0.000120	-2.87	0.0152	-0.34500
DCD*AT	1	-0.002639	0.001112	-2.37	0.0369	-0.28500
DCD*DCD	1	0.006209	0.005545	1.12	0.2867	0.09934

Factor	DF	Sum of Squares	Mean Square	F Value	Pr > F	Label
MT	6	0.335845	0.055974	3.88	0.0250	Melt Temp.
TP	6	0.594515	0.099086	6.87	0.0031	thruput
AR	6	0.780276	0.130046	9.02	0.0010	Air rate
AT	6	0.198974	0.033162	2.30	0.1097	Air Temp
DCD	6	0.405914	0.067652	4.69	0.0132	

Canonical Analysis of Response Surface Based on Coded Data

Critical Value Factor	Coded	Uncoded	Label
MT	-3.553288	160.507938	Melt Temperature
TP	2.123799	69.389798	thruput
AR	-1.093439	276.640153	Air rate
AT	5.816437	422.543788	Air temperature
DCD	-0.041698	7.833207	

Predicted value at stationary point: 2.839792

	Eigenvectors				
Eigenvalues	MT	TP	AR	AT	DCD
0.377912	0.074167	0.346235	-0.567976	-0.233266	0.705415
0.119883	-0.117285	0.572851	0.746986	-0.080789	0.305894
-0.016124	-0.517207	0.204967	-0.181599	0.807433	0.074561
-0.119935	0.540223	0.643960	-0.196499	0.181869	-0.470943
-0.403586	0.649153	-0.308655	0.218691	0.504020	0.425995

Stationary point is a saddle point.

Estimated Ridge of Maximum Response for Variable Dia: fiber diameter

Coded Radius	Estimated Response	Standard Error
0.0	1.958861	0.048170
0.1	2.002963	0.048101
0.2	2.048617	0.047804
0.3	2.097850	0.047572
0.4	2.152142	0.047901
0.5	2.212426	0.049454
0.6	2.279254	0.052931
0.7	2.352955	0.058876
0.8	2.433735	0.067547
0.9	2.521723	0.078942
1.0	2.617008	0.092925

Estimated Ridge of Maximum Response for Variable Dia: fiber diameter

Coded	Uncoded Factor Values				
Radius	MT	TP	AR	AT	DCD
0.0	260.000000	29.250000	550.000000	265.500000	8.000000
0.1	259.211325	30.354753	531.315764	265.872570	8.014914
0.2	258.713113	31.381207	511.522080	266.156500	8.119486
0.3	258.447139	32.320974	491.735043	266.239837	8.295433
0.4	258.339169	33.188309	472.605554	266.130404	8.516566
0.5	258.330373	34.002689	454.277295	265.878490	8.763233
0.6	258.383406	34.779903	436.665196	265.529277	9.024043
0.7	258.476140	35.530924	419.634726	265.113908	9.292889
0.8	258.595401	36.263093	403.063846	264.652556	9.566483
0.9	258.733095	36.981351	386.855430	264.158311	9.842997
1.0	258.884052	37.689093	370.935119	263.639859	10.121372

APPENDIX C

SAS Program for Wellman PET

```
/*THIS WAS PROGRAMMED ON 4-29-01 FOR THE PHASE-1
PRELIMINARY RESEARCH ON WELLMAN PET WITH
AG/SB=0.8mm/1.0mm*/

data pp;
input MT TP AT AR DCD Dia @@;

label

        Dia="fiber diameter"
        MT= "Melt Temperature"
        TP= "thruput"
        AT= "Air temperature"
        AR= "Air rate"
        BS= "Belt speed";
datalines;

 318.0  19.80  324.0  325  10  8.12   318.0  19.80  324.0  575   6  5.74
 318.0  19.80  341.0  325   6  10.2   318.0  19.80  341.0  575  10  6.27
 318.0  39.70  324.0  325   6  13.37  318.0  39.70  324.0  575  10  7.56
 318.0  39.70  341.0  325  10  12.73  318.0  39.70  341.0  575   6  7.84
 335.0  19.80  324.0  325   6  8.38   335.0  19.80  324.0  575  10  4.68
 335.0  19.80  341.0  325  10  7.74   335.0  19.80  341.0  575   6  3.88
 335.0  39.70  324.0  325  10  7.52   335.0  39.70  324.0  575   6  4.18
 335.0  39.70  341.0  325   6  8.68   335.0  39.70  341.0  575  10  5.48
 309.5  29.75  332.5  450   8  18.90  343.5  29.75  332.5  450   8  4.87
 326.5   9.85  332.5  450   8  5.22   326.5  49.65  332.5  450   8  9.60
 326.5  29.75  315.5  450   8  7.20   326.5  29.75  349.5  450   8  6.86
 326.5  29.75  332.5  200   8  17.20  326.5  29.75  332.5  700   8  4.53
 326.5  29.75  332.5  450   4  8.12   326.5  29.75  332.5  450  12  7.97
 326.5  29.75  332.5  450   8  7.49   326.5  29.75  332.5  450   8  6.54
 326.5  29.75  332.5  450   8  8.12   326.5  29.75  332.5  450   8  7.50
 326.5  29.75  332.5  450   8  7.83   326.5  29.75  332.5  450   8  6.93
;

proc sort;
by MT TP AR AT DCD;
run;

proc rsreg data=pp;
model Dia= MT TP AR AT DCD/lackfit;
```

```
ridge max;
run;
/* The following is to predict the fiber diameter profile with melt
temperature and throughput. The air temperature is set at 270 °C,
air rate at 557.5 SCFM, and DCD at 8.63 inches*/



data grid;
do;
Dia= . ;
AT=310;
AR=557.5;
DCD=8.63;
do MT=300 to 340 by 1;
do TP= 10 to 40 by 2;
output;
end;
end;
end;
data grid;
set pp grid;
run;

proc rsreg data=grid out=predict noprint;
model Dia= MT TP AT AR DCD/predict;
run;

data plot; set predict;
if AT=310;
AR=557.5;
DCD=8.63;
BS=87.406;
proc g3d data=plot;
plot MT*TP=Dia / rotate=138 tilt=75 xticknum=3 yticknum=3
  zmax=18 zmin=0 ctop=red cbottom=blue caxis=black;
run;


/* This plot is to see the effect of air temperature and air rate
by comparing with the previous plot.*/

data grid1;
do;
Dia= . ;
```

```
AT=340;
AR=590.5;
DCD=8.63;
BS=87.406;
do MT=300 to 350 by 1;
do TP= 10 to 50 by 2;
output;
end;
end;
end;
data grid1;
set pp grid1;
run;

proc rsreg data=grid1 out=predict1 noprint;
model Dia= MT TP AT AR DCD/predict;
run;

data plot;
set predict1;
if AT=340;
AR=590.5;
DCD=8.63;
BS=87.406;
proc g3d data=plot;
plot MT*TP=Dia / rotate=138 tilt=75 xticknum=3 yticknum=3
  zmax=23 zmin=0 ctop=red cbottom=blue caxis=black;
run;
**************************
data grid2;
do;
Dia= . ;
TP=25;
AT=310;
DCD=8.63;
BS=87.406;
do MT= 300 to 340 by 2;
do AR=450 to 600 by 10;
output;
end;
end;
end;
data grid2;
set pp grid2;
run;
```

```
proc rsreg data=grid2 out=predict2 noprint;
model Dia= MT TP AT AR DCD/predict;
run;

data plot;
set predict2;
if TP=25;
AT=310;
DCD=8.63;
BS=87.406;
proc g3d data=plot;
plot MT*AR=Dia / rotate=138 tilt=80 xticknum=3 yticknum=3
  zmax=16.00 zmin=0 ctop=red cbottom=blue caxis=black;
run;
************************
data grid3;
do;
Dia= . ;
TP=15;
AT=310;
DCD=8.63;
BS=87.406;
do MT= 300 to 340 by 2;
do AR=450 to 600 by 10;
output;
end;
end;
end;
data grid3;
set pp grid3;
run;

proc rsreg data=grid3 out=predict3 noprint;
model Dia= MT TP AT AR DCD/predict;
run;

data plot; set predict3;
if TP=15;
AT=310;
DCD=8.63;
BS=87.406;
proc g3d data=plot;
plot MT*AR=Dia / rotate=138 tilt=80 xticknum=3 yticknum=3
  zmax=15.00 zmin=0 ctop=red cbottom=blue caxis=black;
run;
```

APPENDIX D

Output of the SAS Program in Appendix C

The RSREG Procedure

Coding Coefficients for the Independent Variables

Factor	Subtracted off	Divided by
MT	326.500000	17.000000
TP	29.750000	19.900000
AR	450.000000	250.000000
AT	332.500000	17.000000
DCD	8.000000	4.000000

Response Surface for Variable Dia: fiber diameter

Response Mean	8.039063
Root MSE	2.138140
R-Square	0.8586
Coefficient of Variation	26.5969

Regression	DF	Type I Sum of Squares	R-Square	F Value	Pr > F
Linear	5	253.352754	0.7126	11.08	0.0005
Quadratic	5	38.966195	0.1096	1.70	0.2140
Crossproduct	10	12.933463	0.0364	0.28	0.9718
Total Model	20	305.252411	0.8586	3.34	0.0220

Residual	DF	Sum of Squares	Mean Square	F Value	Pr > F
Lack of Fit	6	48.606177	8.101030	24.08	0.0015
Pure Error	5	1.681883	0.336377		
Total Error	11	50.288061	4.571642		

Parameter

Estimate

Parameter	DF	Estimate	Standard Error	t Value	Pr > |t|	from Coded Data
Intercept	1	535.289834	1201.381618	0.45	0.6646	7.730795
MT	1	-6.982473	4.351430	-1.60	0.1369	-4.112500
TP	1	2.527705	2.969227	0.85	0.4128	1.759167
AR	1	-0.101609	0.236534	-0.43	0.6758	-4.704167
AT	1	4.082309	4.380722	0.93	0.3714	0.215833
DCD	1	-10.146493	14.792065	-0.69	0.5069	-0.205833
MT*MT	1	0.010958	0.005464	2.01	0.0701	3.166818
TP*MT	1	-0.007383	0.006320	-1.17	0.2675	-2.497500
TP*TP	1	-0.003303	0.003988	-0.83	0.4250	-1.308182
AR*MT	1	0.000171	0.000503	0.34	0.7401	0.727500
AR*TP	1	-0.000169	0.000430	-0.39	0.7011	-0.842500
AR*AR	1	0.000034349	0.000025	1.36	0.2012	2.146818
AT*MT	1	-0.001064	0.007398	-0.14	0.8882	-0.30750
AT*TP	1	0.000687	0.006320	0.11	0.9154	0.232500
AT*AR	1	-0.000038	0.000503	-0.08	0.9408	-0.162500
AT*AT	1	-0.005841	0.005464	-1.07	0.3079	-1.688182
DCD*MT	1	0.010184	0.031443	0.32	0.7521	0.692500
DCD*TP	1	0.001916	0.026861	0.07	0.9444	0.152500
DCD*AR	1	0.001718	0.002138	0.80	0.4388	1.717500
DCD*AT	1	0.019890	0.031443	0.63	0.5399	1.352500
DCD*DCD	1	-0.042074	0.098695	-0.43	0.6781	-0.673182

Factor	DF	Sum of Squares	Mean Square	F Value	Pr > F	Label
MT	6	127.202831	21.200472	4.64	0.0137	Melt Temp.
TP	6	28.730085	4.788348	1.05	0.4466	Thruput
AR	6	145.439898	24.239983	5.30	0.0085	Air rate
AT	6	7.508702	1.251450	0.27	0.9378	Air Temp.
DCD	6	6.366898	1.061150	0.23	0.9571	

The RSREG Procedure
Canonical Analysis of Response Surface Based on Coded Data

Factor	Critical Value Coded	Uncoded	Label
MT	0.521755	335.369834	Melt Temperature
TP	0.131560	32.368034	thruput
AR	0.520892	580.222986	Air rate
AT	0.533474	341.569062	Air temperature
DCD	1.330770	13.323081	

Predicted value at stationary point: 5.469086

	Eigenvectors				
Eigenvalues	MT	TP	AR	AT	DCD
3.712022	0.893716	-0.249972	0.348060	-0.019614	0.131356
2.199743	-0.373686	0.031657	0.896574	0.037447	0.232614
-0.474087	0.035089	0.203825	-0.225268	0.486126	0.818633
-1.696316	0.234246	0.940085	0.097523	-0.207356	-0.094135
-2.097270	0.074347	0.105863	0.121460	0.847879	-0.499615

Stationary point is a saddle point.

The RSREG Procedure

Estimated Ridge of Maximum Response for Variable Dia: fiber diameter

Coded Radius	Estimated Response	Standard Error
0.0	7.730795	0.852823
0.1	8.413726	0.850122
0.2	9.163839	0.843743
0.3	9.982279	0.838968
0.4	10.869924	0.844727
0.5	11.827469	0.872892
0.6	12.855479	0.935909
0.7	13.954417	1.043283
0.8	15.124672	1.199324
0.9	16.366570	1.403790
1.0	17.680392	1.654103

Estimated Ridge of Maximum Response for Variable Dia: fiber diameter

Coded	Uncoded Factor Values				
Radius	MT	TP	AR	AT	DCD
0.0	326.500000	29.750000	450.000000	332.500000	8.000000
0.1	325.397345	30.280960	432.242458	332.555930	7.980036
0.2	324.246939	30.800239	415.139911	332.609454	7.948674
0.3	323.056004	31.311992	398.645877	332.659880	7.909428
0.4	321.830321	31.818869	382.711050	332.707329	7.864641
0.5	320.574629	32.322579	367.287422	332.752172	7.815914
0.6	319.292872	32.824239	352.329979	332.794825	7.764361
0.7	317.988369	33.324585	337.797316	332.835670	7.710769
0.8	316.663935	33.824101	323.651736	332.875037	7.655708
0.9	315.321971	34.323112	309.859121	332.913197	7.599591
1.0	313.964536	34.821830	296.388700	332.950375	7.542721

APPENDIX E

SAS Program for PP3155/PET Bicomponent MB

```
/* THIS WAS PROGRAMMED ON 5-16-01 FOR THE PHASE-3 ON
PP3155/PET
WITH AG/SB=0.8mm/1.0mm, The melt and die temp were set at 315°C.*/

data bico;
 input TP AR DCD pp Dia @@;
     label
     Dia="fiber diameter"
     TP= "thruput"
     AR= "Air rate"
      PP="Wt % of PP"
      BS= "Belt speed";
datalines;

/*The first set of data is for the surface response design. The second set is
for the research of spinline dynamics. The third and fourth sets are from
individual experiments. The fifth set is from the duplicative experiments of
the same surface response design. */

 15.0 350.0 11.0  73.01  2.81  10.0  250.0   7.0 52.65 3.81
 20.0 250.0   7.0  52.65  4.20  10.0  450.0   7.0 52.65 2.40
 20.0 450.0   7.0  52.65  2.41  10.0  250.0 15.0 52.65 3.61
 20.0 250.0 15.0  52.65  5.88  10.0  450.0 15.0 52.65 2.47
 20.0 450.0 15.0  52.65  3.74  22.4  350.0 11.0 25.13 3.55
  7.7 350.0 11.0  25.14  2.81  15.0  497.0 11.0 25.13 2.78
 15.0 303.0 11.0  25.14  7.66  15.0  350.0 16.9 25.13 4.70
 15.0 350.0   5.1  25.14  3.69  15.0  350.0 11.0 43.00 2.73

15.0 350.0 19.0 100.0 2.34   15.0 450.0 19.0 100.0 1.7
7.5 450.0 19.0 100.0 1.41

15.0 450.0 19 50.0 3.77    15.0 450.0 19.0 25.0 4.63
15.0 450.0 19.0 75.0 3.0

15.0 350.0 19.0 50.0 4.51    15.0 450.0 19.0  25.0 5.18

19.3 500.0 10.0 47.6 3.08  19.8 500.0 10.0 23.4 2.96  18.8 550.0 14.0
73.1 3.76

19.8  500.0 10.6 23.4 3.12   15.0 497.0 11.0 25.1 2.75
```

```
20.7  500.0 10.0 26.0 2.63

 14.5   349.0   11.0   73.0   2.85   10.0   250.0  7.1   52.7 3.80
 19.8   250.0   7.0   52.6   4.2     10.0   451.0   6.9   52.0   2.40
 20.0   450.0   7.0   52.7 2.46     10.0   250.0  15.0   52.7   3.62
 20.0   251.0 15.0   52.5 5.88     10.0   450.0  15.0   52.7   2.46
 20.0   450.0 15.0   50.2   3.74   22.4   350.0  10.1   25.5   3.55
 7.55   345.0 11.1  25.34  3.21    15.0   497.0  11.0   25.1   2.62
 14.6   203.0 10.5  25.14  7.67    16.0   345.0  16.8   25.4   4.5
 15.0   350.0   5.1  25.13  3.69   15.0   350.0  11.0   43.2   2.72;

proc sort;
by TP AR DCD PP; run;

proc rsquare;
model Dia=TP AR DCD PP;
run;

proc rsreg data=bico;
   model Dia=TP AR DCD PP;
ridge max;
run;

/*The following is to predict the fiber diameter profile with Air rate
and throughput. The air temperature is set at 315°C,PP% at 50%, and
DCD at 12 inches.*/

data grid;
do;
Dia= . ;
PP=50;
DCD=8;
do TP= 10 to 25 by 0.5;
do AR= 200 to 500 by 10;
output;
end;
end;
end;
data grid;
set bico grid;
run;

proc rsreg data=grid out=predict noprint;
model Dia= TP AR DCD PP/predict;
run;
```

```
data plot;
set predict;
if PP=50;
DCD=8;
proc g3d data=plot;
plot AR*TP=Dia / rotate=138 tilt=75 xticknum=3 yticknum=3
  zmax=8 zmin=0 ctop=red cbottom=blue caxis=black;
run;


/* This is to compare with previous plot to see the effect of PP%. */

data grid1;
do;
Dia= . ;
PP=25;
DCD=8;
do TP= 10 to 25 by 0.5;
do AR= 200 to 500 by 10;
output;
end;
end;
end;
data grid1;
set bico grid1;
run;

proc rsreg data=grid1 out=predict1 noprint;
model Dia= TP AR DCD PP/predict;
run;

data plot;
set predict1;
if PP=25;
DCD=8;
proc g3d data=plot;
plot AR*TP=Dia / rotate=138 tilt=75 xticknum=3 yticknum=3
  zmax=8 zmin=0 ctop=red cbottom=blue caxis=black;
run;

/*This is to see the effects of PP% and AR on fiber dia". */
data grid2;
do;
Dia= . ;
```

```
TP=20;
DCD=10;
do PP= 0 to 100 by 2;
do AR=200 to 500 by 10;
output;
end;
end;
end;
data grid2;
set bico grid2;
run;

proc rsreg data=grid2 out=predict2 noprint;
model Dia= TP AR DCD PP/predict;
run;

data plot;
set predict2;
if TP=20;
DCD=10;
proc g3d data=plot;
plot AR*pp=Dia / rotate=138 tilt=80 xticknum=3 yticknum=3
  zmax=9 zmin=0 ctop=red cbottom=blue caxis=black;
run;

/* This is to see the effects of DCD and TP on fiber dia. */

data grid3;
do;
Dia= . ;
AR=450;
PP=50;
do DCD= 4 to 18 by 0.4;
do TP=5 to 25 by 0.3;
output;
end;
end;
end;
data grid3;
set bico grid3;
run;

proc rsreg data=grid3 out=predict3 noprint;
model Dia= TP AR DCD PP/predict;
run;
```

```
data plot;
set predict3;
if AR=450;
PP=50;
proc g3d data=plot;
plot DCD*TP=Dia / rotate=20 tilt=80 xticknum=3 yticknum=3
  zmax=4.5 zmin=0 ctop=red cbottom=blue caxis=black;
run;

/* This is to see the effects of Air rate on fiber dia. */

data grid4;
do;
Dia= . ;
AR=250;
PP=50;
do DCD= 4 to 18 by 1;
do TP=5 to 25 by 0.5;
output;
end;
end;
end;
data grid4;
set bico grid4;
run;

proc rsreg data=grid4 out=predict4 noprint;
model Dia= TP AR DCD PP/predict;
run;

data plot;
set predict4;
if AR=250;
PP=50;
proc g3d data=plot;
plot DCD*TP=Dia / rotate=20 tilt=80 xticknum=3 yticknum=3
  zmax=8.5 zmin=0 ctop=red cbottom=blue caxis=black;
run;

/*This is to see the effect of PPxDCD. */

data grid5;
do;
Dia= . ;
```

```
AR=450;
TP=15;
do DCD= 4 to 19 by 1;
do pp=0 to 100 by 2;
output;
end;
end;
end;
data grid5;
set bico grid5;
run;

proc rsreg data=grid5 out=predict5 noprint;
model Dia= TP AR DCD PP/predict;
run;

data plot;
set predict5;
if AR=450;
TP=15;
proc g3d data=plot;
plot PP*DCD=Dia / rotate=138 tilt=80 xticknum=3 yticknum=3
  zmax=5.5 zmin=1 ctop=red cbottom=blue caxis=black;
run;
```

APPENDIX F

Output of the SAS Program in Appendix E

The RSREG Procedure

Coding Coefficients for the Independent Variables

Factor	Subtracted off	Divided by
TP	14.950000	7.450000
AR	376.500000	173.500000
DCD	12.060000	6.940000
PP	50.000000	50.000000

Response Surface for Variable Dia: fiber diameter

Response Mean	3.552596
Root MSE	0.384155
R-Square	0.9406
Coefficient of Variation	10.8134

Regression	DF	Type I Sum of Squares	R-Square	F Value	Pr > F
Linear	4	52.150792	0.6769	88.35	<.0001
Quadratic	4	13.292060	0.1725	22.52	<.0001
Crossproduct	6	7.030309	0.0912	7.94	<.0001
Total Model	14	72.473161	0.9406	35.08	<.0001

Residual	DF	Sum of Squares	Mean Square
Total Error	31	4.574818	0.147575

The RSREG Procedure

Parameter	DF	Estimate	Standard Error	t Value	Pr > |t|	Parameter Estimate from Coded Data
Intercept	1	16.338173	2.177629	7.50	<.0001	2.823702
TP	1	0.206285	0.148501	1.39	0.1747	0.620426
AR	1	-0.057843	0.005926	-9.76	<.0001	-1.170099
DCD	1	-0.235295	0.134344	-1.75	0.0898	0.601988
pp	1	-0.078829	0.022928	-3.44	0.0017	-1.307751
TP*TP	1	-0.005620	0.003783	-1.49	0.1475	-0.311948
AR*TP	1	-0.000353	0.000167	-2.11	0.0426	-0.456430
AR*AR	1	0.00006514	0.000008	8.01	<.0001	1.960778
DCD*TP	1	0.014843	0.004490	3.31	0.0024	0.767410
DCD*AR	1	-0.000206	0.000205	-1.01	0.3219	-0.248246
DCD*DCD	1	0.011635	0.004240	2.74	0.0100	0.560403
pp*TP	1	-0.0000202	0.000859	-0.02	0.9814	-0.007523
pp*AR	1	0.000196	0.000038	5.13	<.0001	1.703137
pp*DCD	1	-0.002058	0.000756	-2.72	0.0106	-0.714016
pp*pp	1	0.0000387	0.000115	0.34	0.7394	0.096870

Factor	DF	Sum of Squares	Sum of Mean Square	F Value	Pr > F	Label
TP	5	7.444684	1.488937	10.09	<.0001	thruput
AR	5	47.946692	9.589338	64.98	<.0001	Air rate
DCD	5	10.461346	2.092269	14.18	<.0001	
pp	5	17.467771	3.493554	23.67	<.0001	PP% wt

The RSREG Procedure
Canonical Analysis of Response Surface Based on Coded Data

Factor	Critical Value Coded	Uncoded	Label
TP	-0.279809	12.865420	thruput
AR	0.555206	472.828275	Air rate
DCD	-0.713282	7.109820	
pp	-0.770318	11.484108	Wt % of PP

Predicted value at stationary point: 2.701077

	Eigenvectors			
Eigenvalues	TP	AR	DCD	pp
2.352764	-0.101261	0.910321	-0.158184	0.368836
0.711948	0.283177	0.258421	0.907668	-0.170786
-0.192223	0.571010	-0.246542	0.039200	0.782066
-0.566386	0.763874	0.209170	-0.386755	-0.472403

Stationary point is a saddle point.

Estimated Ridge of Maximum Response for Variable Dia: fiber diameter

Coded Radius	Estimated Response	Standard Error	Uncoded Factor Values TP	AR	DCD	pp
0.0	2.823702	0.165726	14.95	376.50	12.06	50.00
0.1	3.038270	0.163831	15.16	364.97	12.27	46.89
0.2	3.293443	0.161081	15.33	351.84	12.48	44.16
0.3	3.591792	0.157379	15.47	337.81	12.66	41.66
0.4	3.934716	0.153387	15.60	323.23	12.84	39.32
0.5	4.323022	0.150467	15.71	308.32	13.00	37.08
0.6	4.757203	0.150633	15.82	293.19	13.16	34.93
0.7	5.237577	0.156273	15.92	277.92	13.30	32.82
0.8	5.764357	0.169498	16.02	262.53	13.45	30.77
0.9	6.337691	0.191479	16.11	247.07	13.59	28.74
1.0	6.957686	0.222314	16.20	231.55	13.720	26.74

APPENDIX G

The MATLAB Progam
for Filament Temperature Simulation of PP_{35MFR}

This is an example for solving the filament energy balance equation 4.3-19 for PP_{3155} in this dissertation. To get the temperature profile for other polymers or other processing conditions, different profile equations of fiber diameter, air temperature, air velocity and heat capacity should be obtained accordingly

This following part was written in June 18, 2001 in the MATLAB Editor window and saved as an M-file in the MATLAB folder.

```
function dTpp=bicombpp(zpp,Tpp);
%---------- fiber diameter, m
if zpp<5.5
  df=5.4827*zpp^(-0.8372)*10^(-6);
else
  df=(0.0104*zpp^2-0.2113*zpp+2.6868)*10^(-6);
end
%----------fiber velocity,m/s
if zpp<3.5
  vf=40.293*zpp-0.0305;
else
  vf=197.35*zpp^(-0.245);
end
%----------air velocity, m/s
if zpp<0.4
  va=303;
else
```

```
  va=190.56*zpp^(-0.5);
end
%-------------Air jet temperature, K
if zpp<0.16
  Ta=588; %588K=599F=315C
else
  Ta=(255.15*zpp^(-0.3156)-32)/1.8+273;
end

%------------Cp of PET, j/g/K
vfa=abs(va-vf);
Cp=2.72;
Wpp=4.167/601;  % mass flow rate: g/s/h
dfp=df.^0.334;
vfap=vfa.^0.334;
vfp=vf.^0.334;
dTpp=((-1.652*(dfp.*vfap))/
        (Wpp*Cp))*(((Ta+Tpp)/(Ta+Tpp+220.8))^0.6655)*(Tpp-Ta);
```

****** The following commands need to be written in the command window.

```
>>zppspan = [0.001, 10]; % specify the range of simulation
>>Tpp0 = 588;           % the initial value of filament temperature
>>[zpp, Tpp] = ode23('bicombpp', zppspan, Tpp0);
>>Tppc=Tpp-273;         % convert °K to °C
>>plot (zpp,Tppc)
>>xlable('distance from the die (in)'),ylabel('fiber temperature (°C)')
```

VITA

Mr. Rongguo Zhao was born in a farmland in HeBei province of China. He received the best education affordable to his family. After graduated from graduate school with a Master of Science degree in chemistry, he worked as a researcher for a few years in both Beijing Institute of Chemical Fiber Technology and China Textile Academy. In 1996, He attended the University of Tennessee, Knoxville (UTK) to pursue his doctoral degree.

Before his Ph.D. program in polymer and nonwovens, he took advantage of the variety of courses available at UTK in chemistry, polymer materials and engineering, and built up a solid foundation for his future career in research, product development, and teaching.

He was a winner of Outstanding in Graduate Research of 1998/1999 school year at UTK, an Ida A. Anders Scholarship holder from 1998 to 2001. He is an active member of Fiber Society, American Association of Textile Chemists and Colorists (AATCC), and KAPPA OMICRON NU, National Honor Society. He is expecting to join Sigma XI, the Scientific Research Society in the near future.

He is very interested in the development of microfibers in sub-micrometer and nanometer scale from melt blown technology, the structure/property relationship of micro-fiber nonwovens, and their applications in filtration, absorbent, and protective clothing.